

Development of a coupled blowing snow-atmospheric model and its applications

By

Jing Yang

Department of Atmospheric and Oceanic Sciences
McGill University
Montréal, Canada

June, 2010

A thesis submitted to the
Graduate and Postdoctoral Studies Office
in partial fulfillment of the requirements for the degree of
Doctor of Philosophy

© Jing Yang 2010

Abstract

Blowing snow can occur over snow-covered surface in association with strong winds. Snow particles are lifted into the boundary layer where they are subject to sublimation and horizontal transport over long distances. The snow transport and in-transit sublimation processes affect the moisture and the snow mass budgets. The cooling effect of sublimation also affects the temperature in the boundary layer and thus may play a role in the dynamics of both the boundary layer and the larger scale synoptic flow. In this thesis, a coupled blowing snow-atmospheric model is developed to study the effects of blowing snow on the winter season Northern Hemisphere snow mass budget and anticyclonogenesis.

We first extended a one-dimensional double-moment blowing snow model (PIEKTUK-D) to a triple-moment version (PIEKTUK-T). The procedure is to formulate predictive equations for three moments of an assumed Gamma particle size distribution for blowing snow. The three moments are the total number concentration, the total mass mixing ratio, and the total radar reflectivity. The results of idealized experiments and real case simulations indicated that PIEKTUK-T predicts well the number concentration, mixing ratio, the shape parameter, and visibility in blowing snow. The model also simulated a power law relationship between the radar reflectivity factor and the particle extinction coefficient consistent with observations in snow storms. However, PIEKTUK-T cannot treat horizontal advection, lateral entrainment, and the interaction between blowing snow and the atmospheric boundary layer. To allow for the consideration of these effects, we next coupled PIEKTUK-T to an atmospheric mesoscale model (MC2).

The coupled modeling system is applied to study the relative roles of blowing snow sublimation and transport, and surface sublimation on the snow mass budget. Over the three winter months in 2006-2007 in the northern hemisphere, blowing snow sublimation was found to return up to 50 mm Snow Water Equivalent (SWE) back to the atmosphere over the Arctic Ocean. On the other hand, the divergence of blowing snow transport typically accounts for only a few mm SWE in the snow mass budget. When the results are averaged over 10 degree latitudinal bands, the surface sublimation tends to decrease with latitude, while blowing snow sublimation behaves in the opposite direction. Sublimation from surface and blowing snow processes together can return 23% to 52% of winter precipitation back to the atmosphere over the three month winter season.

As a second application, we simulated an observed anticyclogenesis event over the Arctic Ocean. Three experiments were performed. Experiment STD was run without blowing snow. Experiment CPL and CPL2 were conducted with the coupled modeling system but any supersaturation with respect to ice in the blowing snow module was removed in the CPL run. The results indicated colder low level temperatures in CPL in regions where blowing snow occurred. This cooling extended throughout the boundary layer. In addition to air being cooled near the surface by sublimation there is also enhanced downward turbulent heat flux transport which leads to cooling in the boundary layer. The net result is a rise in sea level pressure compared to the STD simulation. A potential vorticity (PV) inversion technique was then applied to quantify how this cooling affects the geopotential height and balanced wind fields. Surface potential temperature differences between the CPL and STD runs were used as the lower boundary conditions for the inversion. The results indicate that the cooling effect induced positive geopotential height and anticyclonic flow perturbations extending up to 500 mb over the

regions of cooling. In the low level, the strong inverted anticyclonic flow and geopotential height perturbations at 1000 mb around the anticyclone suggest that near surface cooling can play a role in anticyclogenesis. Finally, moisture in the atmosphere affects the amount of blowing snow sublimation cooling as the temperature differences between the CPL2 and STD experiments are much reduced.

Résumé

La poudrerie est un phénomène observé sur les surfaces couvertes de neige lorsque le vent est fort. Les particules de neige sont soulevées dans la couche limite où elles peuvent sublimer ou être transportées sur de longues distances. Le transport de la neige et la sublimation affectent l'humidité de l'air et la quantité de neige au sol. L'effet refroidissant de la sublimation affecte aussi la température de la couche limite et peut ainsi modifier la dynamique de l'atmosphère non seulement localement mais aussi à grande échelle. Dans cette thèse, un modèle couplé d'atmosphère et de poudrerie a été développé afin d'étudier l'effet de la poudrerie sur la génèse d'anticyclones et sur le bilan total de neige de l'hémisphère nord en hiver.

Dans un premier temps, on prolonge le modèle unidimensionnel de poudrerie PIEKTUK d'un schéma à double moments (PIEKTUK-D) à un schéma de triple moments (PIEKTUK-T). La procédure utilisée consiste à formuler des équations pour trois moments d'une distribution gamma de dimensions de particules. Ces trois moments sont: la concentration de particules totale, le ratio de mélange total et la réflectivité radar totale. Les résultats d'expériences effectuées dans un contexte idéalisé et réaliste suggèrent que PIEKTUK-T reproduit bien la concentration, le ratio de mélange, le paramètre de forme des particules et la visibilité. Le modèle reproduit aussi une loi de puissance entre la réflectivité radar et le coefficient d'extinction issue d'observations durant les tempêtes de neige. Par contre, PIEKTUK-T n'a pu reproduire l'advection horizontale, l'entraînement latéral et l'interaction entre la poudrerie et la couche limite. Afin de mieux représenter ces effets, on a ensuite couplé le modèle PIEKTUK-T au modèle atmosphérique MC2.

Le modèle couplé a été utilisé pour étudier l'importance relative de la sublimation et du transport de poudrerie ainsi que la sublimation de surface sur le budget total de neige au sol. Durant les trois mois d'hiver 2006-2007, un retour à l'atmosphère de 50 mm d'équivalent eau-neige (<<Snow Water Equivalent>>) a été imputable à la sublimation de la poudrerie au dessus de l'océan Arctique. Par ailleurs, la divergence de transport de poudrerie est typiquement responsable seulement d'une faible quantité d'équivalent eau-neige dans le bilan total. Lorsque les résultats sont moyennés sur des bandes de 10 degrés de latitude, la sublimation de surface tend à décroître en fonction de la latitude, alors que la sublimation de la poudrerie évolue de manière inverse. La sublimation totale de la surface et de la poudrerie combinés retourne à l'atmosphère de 23% à 52% de la précipitation hivernale sur les trois mois considérés.

La deuxième application du modèle couplé consiste à simuler une genèse d'anticyclone sur l'océan Arctique en utilisant des données d'analyses comme conditions initiales. Trois expériences ont été effectuées: 1. l'expérience STD, sans poudrerie, 2. l'expérience CPL avec poudrerie mais sans supersaturation associée à la poudrerie et 3. l'expérience CPL2 avec le modèle couplé complet. Un anticyclone plus froid est observé avec CPL dans les régions où il y a présence de poudrerie. Ce refroidissement était étendu à toute l'épaisseur de la couche limite. En plus de ce refroidissement d'air associé à la sublimation près de la surface, un flux turbulent de chaleur vers le sol a aussi été observé. En conséquence, un refroidissement de la couche limite et une augmentation de la pression au niveau de la mer a été observé par rapport à l'expérience STD. Par la suite, une technique d'inversion de vorticit  potentielle a été utilis e pour quantifier comment ce refroidissement affecte les courbes d' paisseur g opotentielle et les vents. La diff rence entre la temp rature potentielle de surface des exp riences CPL et STD a  t  utilis e comme condition de

frontière du niveau inférieur pour effectuer l'inversion. Les résultats indiquent que le refroidissement induit une augmentation des courbes d'épaisseur géopotentielle et une perturbation anticyclonique des vents jusqu'à 500mb. Au niveau inférieur, ce fort vent anticyclonique et cette perturbation des courbes géopotentielle à 1000mb suggèrent que le refroidissement près de la surface peut jouer un rôle dans la genèse d'anticyclone. Finalement, l'humidité de l'atmosphère affecte l'amplitude du refroidissement associé à la sublimation de la poudrière puisque les différences de températures entre les expériences CPL2 et STD sont grandement réduites.

Statement of Originality

The main original contributions and findings of this thesis are as follows:

- Development of a new triple-moment blowing snow model PIEKTUK-T.
- Validation of this new blowing snow model with observation data at three different sites.
- Development of a coupled triple-moment blowing snow-atmospheric model.
- A seasonal simulation with the coupled modeling system over the entire Northern Hemisphere.
- Computation of the seasonal blowing snow transport and sublimation, and surface sublimation over the Northern Hemisphere using the coupled modeling system.
- Analysis of the seasonal winter snow mass budget.
- Application of the PV inversion technique to quantify the effects of blowing snow on anticyclogenesis.

Acknowledgments

I would first like to thank Prof. M.K.(Peter)Yau, my supervisor, for all his assistance in this research. Over the years at McGill, he has given me continuous help and instruction. I sincerely appreciated his patience, suggestions, and guidance in the supervision of my Ph.D. work.

I am grateful to my McGill colleagues, specifically Lei Wen, Kao-shen Chung, Xiaoli Li, Ruben Santos, Yosvany Martinez, Lily Ioannidou, Xingbao Wang, Barbara Winter, Bruno Tremblay, David Straub and everyone else who have helped me throughout the years. In particular, I am indebted to Dr. Nagarajan Badrinath, who helped me a lot not only in the aspect of numerical modeling, but also taught me how to become a cautious researcher. Discussion with him greatly encouraged me to continue my research.

I would also like to thank Michael Havas, our computer system administrator, for his patience and fast response on many occasions when I had computer problems. The administrative support from Karin Braidwood, Ornella Cavaliere, Anna Cerrone and Vaughn Thomassin are also much appreciated. Special thanks go to Vaughn Thomassin who passed away in November 2009. His kind help and cheerful personality smoothed out many administrative glitches along the way!

Thanks to Mr. Louis-Philippe Nadeau for his help in translating the abstract into French, as well as for some nice meals! I really appreciate my friends Jun Liu, David Hogarth, Ryoko Hashizume, Larry Lessard and Michelle Seymour for lots of nice weekend meals and friendship. The memories I have of spending time with you in Montréal are memories I will keep for a lifetime.

I want to thank my parents, although not college-educated themselves, for their understanding and support all these years of my study. They always have more confidence in me than I have in myself. My elder brother is sort of my mental tutor in my life. Each time when I was depressed, he always gave me the confidence and courage I needed to overcome various hurdles. Like he said, no matter how difficult the past, you can always begin again today!

Finally, but most importantly, a very special thanks to my fiancé, Ergou. Thank you for doing all the arduous housework and cooking so that I had extra time to work on this project. Without your love and support, I would never have made it so far.

Co-authored Manuscripts

Chapter 2 and 4 of this thesis are in the form of articles published in *Boundary Layer Meteorology*, submitted to *Hydrological Earth System Sciences* and the *Journal of Geophysical Research*. The results presented in these manuscripts originated from the research I conducted within the context of my Ph.D. studies. The co-author of these three papers, Dr. M. K. Yau provided normal supervision of the research project as well as text editing. The other two co-authors of the paper in Chapter 3, Dr. J.W. Pomeroy and Xing Fang, provided the field data for verification of the model results. Dr. J.W. Pomeroy also contributed to the editing of the manuscript in Chapter 3.

Table of Contents

Abstract.....	i
Résumé	iv
Statement of Originality	vii
Acknowledgments.....	viii
Co-authored Manuscripts	x
Table of Contents	xi
List of Figures	xiii
List of Tables	xviii
Chapter 1 Introduction	1
1 Background and motivation	1
2 Review of blowing snow modeling literature	4
3 Objective and outline of the thesis	8
Chapter 2 A triple-moment blowing snow model	13
1 Introduction	14
2 Model Formulation	18
3 An Idealized Experiment	20
4 Comparison with Observations	23
4.1 Byrd station	23
4.2 Wyoming observations.....	26
4.3 Halley station.....	29
5 Discussion and Conclusions.....	30
Appendix A Radar reflectivity change rate due to sublimation S_z	34
Appendix B Derivation of radar reflectivity factor Z	36
Chapter 3 A triple-moment blowing snow-atmospheric model and its application in computing the seasonal wintertime snow mass budget	51
1 Introduction.....	54
2 Modeling system	60
2.1 MC2 model.....	61

2.2 Blowing snow model	61
2.3 Coupling strategy	63
2.4 Experimental design.....	65
3 Results of Simulation 1	66
4 Results of Simulation 2.....	68
4.1 Comparison with surface measurements.....	68
4.2 Results of water mass budget	71
4.2.1 Blowing snow transport.....	71
4.2.2 Blowing snow sublimation	73
4.2.3 Surface sublimation.....	75
4.2.4 Distribution over latitude bands.....	77
5 Comparison with empirical formula.....	78
6 Discussion	82
7 Conclusions	83
Chapter 4 Blowing snow cooling effects on anticyclogenesis	103
1 Introduction	105
2 Case description.....	108
3 Model description and setup of experiment.....	110
4 Simulation results	113
4.1 Simulation CPL	113
4.2 Comparison between the CPL and STD simulations.....	116
5 PV inversion.....	118
5.1 Basis for PV diagnostics of the effects of blowing snow sublimation	118
5.2 Diagnostic results.....	120
6 Discussion and concluding remarks	121
Appendix 1 Potential vorticity inversion diagnostic equations	124
Chapter 5 Summary and conclusion.....	141
1 Summary	141
2 Suggestions for future work.....	146
References.....	149

List of Figures

Chapter 1

1 Migrating snow waves moving about 5 m h^{-1} with a wind speed of 40 km h^{-1} . View is facing wind (Tabler, 1986)	11
2 Drifting snow trajectories. Wind speeds are 1 m height level, and the field is 25 cm. (Photographed by D. Kobayashi, 1972).....	11
3 Schematic of blowing snow transport (Takeuchi 1984)....	12

Chapter 2

1 (a) Particle size distribution at $z=0.1\text{m}$ and $z=2.4\text{m}$ predicted by the double-moment model and the triple-moment model. Thick solid and dashed lines are results at $z = 0.1 \text{ m}$, and thin solid and dashed lines are results at $z = 2.4 \text{ m}$. (b) Profiles of parameter a predicted by the double- and triple-moment models after 1min and 10 min of simulation in the idealized case.	40
2 Vertical profiles of (a) number concentration, (b) blowing snow mixing ratio, (c) total radar reflectivity and (d) mean particle radius predicted by the double-moment and triple-moment models 10 min after initialization for the idealized experiment.....	41
3 (a) Particle size distribution $F(r)$ at $z = 57.5 \text{ m}$. Contribution to (b) first moment of size distribution $rF(r)$, (c) third moment of size distribution $r^3F(r)$ and (d) sixth moment of size distribution $r^6F(r)$ predicted by the double-moment and triple-moment models 10 minutes after initialization in the idealized case.....	42
4 Observed and simulated particle size distributions at five heights 10 min after initialization for the Byrd station runs.....	43

5 Vertical profiles of (a) mean particle radius, (b) shape parameter α , (c) blowing snow mixing ratio, and (d) scale parameter β from observations and model simulations 10 min after initialization for the Byrd station runs.....	44
6 Calculated extinction coefficient versus predicted radar reflectivity factor at different levels from PIEKTUK-T for the Byrd station runs (solid curve). Dashed-dotted line is the best fit.....	45
7 Vertical profiles of (a) number concentration, (b) mixing ratio, (c) radar reflectivity and (d) mean particle radius from observations and simulations 10 min after initialization for the Wyoming site.....	46
8 Vertical profiles of (a) parameter a and (b) parameter b from the observations and simulations 10 min after initialization for the Wyoming site... ..	47
9 Particle size distribution from observations and simulations at six vertical levels 10 min after initialization for the Wyoming site.....	48
10 Vertical profiles of (a) number concentration, (b) mixing ratio, (c) radar reflectivity and (d) mean particle radius from observations and simulations 10 min after initialization for the Halley station.....	49
11 Particle size distribution from observations and simulations 10 min after initialization for the Halley station.....	50

Chapter 3

1 Hourly observations of air temperature (a), relative humidity with respect to ice (b), wind speed (c), and snow rate (d) from 31 October 2005 to 30 April 2006 over SDNWA, Saskatchewan, Canada.....	89
2 Comparison of blowing snow sublimation from stand-alone blowing snow model (PIEKTUK-T) and coupled model (CPL) from 31 October 2005 to 30 April 2006 over SDNWA. Units in mm SWE.....	90

3 Comparison of the evolution of observed and simulated pre-melt snow accumulation from January 2005 to April 2006 over SDNWA. The solid line represents the observation. The simulated pre-melt SWE is obtained by interpolating the grid point values to the station site.....	91
4 Comparison of observed and simulated air temperature (a), surface pressure (b), wind speed (c) and relative humidity with respect to ice (d) at Baker Lake (64.3° N, 96.08° W) from December 2006 to February 2007....	92
5 Same as Fig. 4, but for Rankin Inlet (62.82° N, 92.12° W).....	93
6 Winter season blowing snow transport from coupled model over DJF 2006/2007. The arrows denote the transport vectors. Units in Mg m^{-1}	94
7 Winter season divergence of blowing snow transport from the coupled model over DJF 2006/2007. Units in mm SWE.....	95
8 Winter season blowing snow sublimation from the coupled model over DJF 2006/2007. Units in mm SWE.....	96
9 Spatial distributions of different vegetation types: (a) mixed wood forests, (b) evergreen needle-leaf trees, (c) deciduous needle-leaf trees (units in fraction), and (d) roughness length (units in m).....	97
10 Winter season surface sublimation from the coupled model over DJF 2006/2007. Units in mm SWE.....	98
11 Time evolution of surface sublimation (a) and blowing snow sublimation (b) averaged over latitudinal bands. Units in mm SWE.....	99
12 Winter season blowing snow sublimation from empirical formula over DJF 2006/2007. Units in mm SWE.....	100
13 Comparison of blowing snow sublimation from PIEKTUK-T, the empirical formula and observation over the Wyoming site. Units in mm h^{-1}	101

14 Winter season surface sublimation from empirical formula over DJF 2006/2007. Units in mm SWE.....	102
--	-----

Chapter 4

1 (a) Sea level pressure (solid contours every 8 mb below 1018 mb and every 4 mb above 1018 mb), (b) 850-mb temperature (solid contours every 4 °C) and wind speed (unit: knots), (c) 250-mb geopotential height (solid contours every 4 dam) and temperature (blue dashed contours every 4 °C), and (d) 850-500 mb thickness (solid contours every 4 dam) at 1200 UTC Nov 25 2005 from CMC analysis data.	126
2 Sea level pressure (black solid contours every 6 mb) and 850-mb temperature (blue dashed contours every 6 °C) from 0000 UTC 26 Nov 2005 to 1200 UTC 28 Nov at 12 h intervals (a-f) from CMC data.....	127
3 Comparison of observed and simulated (a)air temperature (unit: °C), (b)wind speed (unit: ms ⁻¹) and (c) relative humidity with respect to ice at Coral Harbour station (64.19° N , -83.36° W) from 1200 UTC 25 November to 29 November....	129
4 Sea level pressure (solid contours every 8 mb) and surface wind vectors (unit: knots) at $t=12, 24, 36, 48, 60$ and 72 h (a-f) from the CPL run.....	130
5 Blowing snow mixing ratio q_b at 12 m (a, c and e in the left panel, unit: 10 ⁻⁵ kgkg ⁻¹), and 3-hour accumulated blowing snow sublimation (b, d and f in the right panel, unit: mm SWE) at $t=24, 48$ and 72 h from the CPL run.	132
6 Temperature differences (unit: °C) at 12 m between the CPL and STD runs at $t=12, 24, 36, 48, 60$ and 72 h (a-f).....	133
7 (a) Vertical cross section of temperature differences (unit: °C), and (b) 72-hr accumulated blowing snow sublimation (unit: mm SWE)....	134
8 Sea level pressure differences (unit: mb) between the CPL and STD runs at $t=12, 24, 36, 48, 60$ and 72 h (a-f).....	135

9 Potential temperature θ differences (color shading, unit: K) between the CPL and STD runs and the inverted 850-mb geopotential height (red solid contours every 2 dam) at $t=12, 24, 36, 48, 60$ and 72 h (a-f).....	136
10 Vertical profiles of inverted geopotential height (unit: dam) averaged over the areal extent of the anticyclone at $t=24, 48$ and 72 h (a-c).....	137
11 850-mb potential temperature θ (color shading, unit: K) and balanced velocity (vector, unit: knots) at $t=12, 24, 36, 48, 60$ and 72 h (a-f).....	138
12 Temperature differences (unit: K) at $z=12$ m between the CPL2 and STD runs at $t=12, 24, 36, 48, 60$ and 72 h (a-f).....	139

List of Tables

Chapter 2

- 1 The blowing snow transport rate (Q_t) and sublimation rate (Q_s), the time integrated values of transport (QT_t) and sublimation (QT_s) over 10 min for 3 real cases predicted by the PIEKTUK-D and PIEKTUK-T models.37
- 2 The blowing snow number concentration (N), mean particle radius (r_m), shape parameter (a) at the height of 2 m, and the visibility (V) for 3 real cases predicted by the PIEKTUK-D and PIEKTUK-T models.38
- 3 The corrected (C) and uncorrected (U) parameters α , β , the mean particle diameter D_m , and the number concentration N at 6 heights for the Wyoming experiments.39

Chapter 3

- 1 Observed snow density, snow depth and Snow Water Equivalent (SWE) averaged over four transects within SNDWA, Saskatchewan, Canada (52.03° N, 106.1° W)....86
- 2 Comparison of observed and simulated surface variables at Baker Lake and Rankin Inlet, Nunavut, Canada. The relative humidity is with respect to ice. R is the correlation coefficient.87
- 3 Seasonal average surface sublimation (Q_{surf}), blowing snow sublimation (Q_s), divergence of blowing snow transport (Div) and precipitation amount over latitudinal bands in units of mm SWE. Sum denotes the sum of surface sublimation, blowing snow sublimation and divergence of transport, and Percentage is defined as the ratio of Sum to the solid precipitation (Precip.).88

Chapter 1

Introduction

1 Background and motivation

In high latitude countries such as Canada winters are long and snow cover can persist over many months. Snow covered days account for over six months of the year in continental regions north of 60°N and as much as 10 months over most of the Arctic Ocean. In addition to other forms of severe winter weather (blizzards, mountain-induced storms, ice storms) strong winds can bring blowing snow to these snow covered regions.

Blowing snow is defined by the Meteorological Service of Canada (MSC) as ‘snow particles raised by the wind to sufficient heights above the ground to reduce the horizontal visibility at eye level to 9.7 km or less’. Wind speed is one of the important factors in determining the occurrence and movement of blowing snow. Depending on wind speed, there are three types of blowing snow movement: surface creep, saltation, and suspension. When the wind speed surpasses a threshold, wind stress will overcome the inertia and cohesive forces between snow particles at the snow surface. Particles start to roll over the surface, but remain in contact with it. This movement is known as surface creep and usually forms snow waves, also called snow dunes (Fig. 1). If the wind is somewhat stronger, the snow particles will be lifted up from the loose snow surface and

accelerated horizontally by the wind before falling back to the ground due to gravity (Fig. 2). They may rebound from the surface, or may eject more particles from the surface through momentum exchanges. As they continuously bombard the snow surface, abrasion results in the snow particles losing their crystalline structure, so that they come to resemble spheroids of ice. The density of blowing snow particles is thus much greater than that of fresh snow, being instead comparable to that of ice, e.g., as large as 900 kg m^{-3} . Such particles are called saltated particles and the saltation layer is a few cm thick. Within this layer, one can think of the particles as jumping or dancing along the surface. In fact, the term saltation derives from the Latin 'saltare', meaning to dance. If the turbulent energy of the flow field is sufficiently large, turbulent eddies near the saltation layer will pick up snow particles and suspend them in the atmospheric boundary layer. These suspended particles can reach to heights of several hundred meters, with gravitational sedimentation balanced by turbulent diffusion. A schematic showing these three blowing snow transport processes is presented in Fig. 3.

Blowing snow occurrence depends not only on wind speed, but also on surface conditions such as snow age, snow hardness and temperature. Observations in the Antarctic (Budd et al., 1966) suggest high threshold wind speeds for saltation at extremely cold temperatures. Pomeroy et al. (1993) gave typical values for the threshold friction velocity which vary from 0.15 to 0.25 ms^{-1} for fresh, loose, dry snow, and from 0.25 to 1.0 ms^{-1} for older, wind-hardened, wet snow. Li and Pomeroy (1997) demonstrated that favorable temperature for blowing snow transport ranges between -25°C and -10°C . If the surface temperature is too cold, cohesion associated with

strengthening elastic and frictional forces reduces the wind's capacity to displace snow from the surface. On the other hand, if the temperature is too warm, some of the melted snow water will increase the cohesive bonding forces among the particles, and a high wind threshold is needed to eject snow particles.

Due to the large amounts of transported particles in the air during a blowing snow event, the visibility is therefore reduced greatly. More than 80% of the reported Arctic blowing snow is associated with visibility of less than 5 km and 30% to 40% of those have visibility less than 800 m (Hanesiak et al., 2004). This reduced visibility can be a serious hazard to the traffic/transport and public safety. For example, on March 17, 1992, low visibility associated with blowing snow in Chitose City, Hokkaido (Japan) resulted in a multi-car accident in which two people died and 70 people were injured (Matsuzawa et al., 2005). To mitigate this sort of hazard, it is necessary to have the accurate prediction of blowing snow events.

Fortunately, most blowing snow events occur in sparsely populated areas. There are, however, other reasons one might be concerned with predicting and modeling this phenomenon. Blowing snow plays a role in the surface water mass budget through mass transport and in-transit sublimation. Snow erosion usually occurs over open areas with low roughness, whereas deposition occurs in regions with high roughness length where the wind decelerates. Understanding snow accumulation will be important to assessing changes in the hydrological cycle. Therefore, accumulation can in some cases be critically dependent on blowing snow. As such, blowing snow has the potential to affect

i) Arctic sea ice cover and freshwater (salinity) budgets, ii) land ice accumulation or erosion and iii) the mass budgets of drainage basins. For example, blowing snow over Greenland is likely to represent an effective sink of ice mass when loss of snow blowing from the ice sheet into the open water is taken into account. At small spatial scales, divergence of blowing snow can affect net accumulation rates and can potentially redistribute mass enough to have a significant impact on the flux through a drainage basin. For example, in the Canadian prairies, up to 75% of the annual snowfall over a one kilometer fallow field was shown to be removed by blowing snow, with half of this amount sublimating into the air (Pomeroy and Gray, 1995). All of this suggests that the transport and sublimation of blowing snow are factors that should be considered in the wintertime water budgets. Past studies in surface mass budgets have included blowing snow related processes (Schmidt, 1982; Bintanja, 1998; Pomeroy and Essery, 1999; King et al., 2001). However, these results are either limited to localized station sites or cover only a very short time span. Such studies are of limited use in understanding how blowing snow affects hemispheric mass budgets. There is a need to know more about the distribution of individual terms in surface snow mass budget over larger spatial and temporal scales. This thesis addresses this need. The following sections give a review of the blowing snow literature, state our objectives and give an outline of the remainder of the thesis.

2 Review of blowing snow modeling literature

Studies on blowing snow have their roots in the study of sand saltation transport, dating to the 1940s (Bagnold, 1941). Bagnold assumed that the upward momentum of sand

ejected by the shear stress exerted on the surface balances that of sand falling to the surface under gravity. Such a balance yields a parameterization of saltation transport. Bagnold's concept was then developed by Dyunin (1954; 1967) and applied to blowing snow. Shiotani and Arai (1953) and Loewe (1956) proposed the suspension theory, i.e., that snow particles are in a vertical balance between the upward turbulent flux of snow particles and a downward sedimentation flux. Mellor and Radok (1960) then derived the drift density profile $h_z = h_r \left(\frac{z}{z_r}\right)^{-w_f / ku_*}$ for drifting snow as the steady-state solution for the balance of turbulent mixing and gravitational sedimentation assuming uniform constant fall velocity w_f of all the particles. Here, η_r is the drift density at reference height z_r , w_f is the particle fall speed, k is the von Kármán constant and u_* is the friction velocity. This expression is somewhat artificial because the fall velocity for a volume of drifting snow is not a constant. At higher levels the mean particle radius is smaller and thus the average fall velocity will also be less. Therefore, the fall velocity should decrease with height. Pomeroy (1988) gives an empirical expression derived from experimental data for the settling velocity as function of particle radius, r . More specifically, he finds $w_f(r) = 1.1 \times 10^7 r^{1.8}$, where r is mean particle radius (m) and w_f is in ms^{-1} . Given the particle size distribution, a bulk moment-weighted terminal velocity was derived by Déry and Yau (1998). This takes into account size sorting effects and gives mass-weighted and number-weighted fall velocities. The distinction between these two sedimentation velocities represents a realistic gravitational size sorting mechanism, which will be useful when deriving our triple moment scheme.

Schmidt (1972) was the first to address blowing snow sublimation, i.e., that blowing snow particles would sublime in air undersaturated with respect to ice. Subsequent studies paid attention to the role of blowing snow sublimation in the hydrological cycle. There has been some disagreement as to the importance of blowing snow sublimation. Calculations at Halley Station suggested it to be small in wintertime (King et al., 1996). However, other studies (Tabler, 1975; Schmidt, 1982; Berg, 1986; Pomeroy et al., 1993; Pomeroy et al., 1997; Déry and Yau, 2001a) suggest that blowing snow sublimation does make significant contribution to the surface mass budget.

These theories, together with field experiment results, provided the basis for blowing snow models development (Pomeroy, 1988; Pomeroy et al., 1993; Liston and Sturm, 1998; Déry et al., 1998; Bintanja, 2000a; Bintanja, 2000b). Essentially, these models include the saltation and suspension transport processes as well as the blowing snow sublimation, and are used to study the interaction of blowing snow with boundary-layer processes. Most of the models ignored the feedback of blowing snow sublimation on the atmosphere. One of the few exceptions is the PIEKTUK model (Déry et al., 1998), which considered a feedback whereby blowing snow sublimation increases relative humidity and decreases temperature. This, in turn, changes the sublimation rate. This model is a spectral model, which treated blowing snow particles explicitly in 64 size classes to calculate the total blowing snow suspension and sublimation rates. The model can provide detailed information of particle size distribution. However, it is computationally expensive.

To increase the computational efficiency, Déry and Yau (1999, 2001a) proposed a bulk scheme to solve the equations for blowing snow number concentration and mixing ratio, as well as the temperature and humidity. The bulk model assumes that particles follow a gamma size distribution $F(r) = N \frac{r^{a-1} e^{-r/b}}{b^a \Gamma(a)}$. Here N is the total number concentration (m^{-3}), α is a dimensionless shape parameter, β is a scale parameter with a length dimension (m), and r is the particle radius (m). This distribution was proposed by Budd (1966) from field observation at an Antarctic site and was also verified by subsequent researchers (Kobayashi, 1972; Schmidt 1982; Pomeroy, 1988; Dover, 1993). Given the three parameters, it is straightforward to calculate the various moments of the size distribution. The zeroth and third moments correspond to N and q_b (mixing ratio), respectively. In Déry and Yau's paper, α is held fixed and predictive equations for N and q_b are used to determine the size distribution. Note, however, that both field experiments and spectral model calculations indicate that the shape parameter α is not a constant; it usually increases with height. Moreover, Pomeroy and Male (1988) demonstrated that the α parameter, as well as the mean particle radius of the size distribution, are very important in visibility modeling.

Blowing snow sublimation not only contributes to the mass budget, but also affects the boundary layer conditions by cooling and moistening the environmental air during the phase changes. In a study of an Arctic blizzard, Déry and Yau (2001b) found blowing snow related cooling effects to lead to an increase in sea level pressure (SLP). Specifically, they found SLP higher relative to a simulation without blowing snow in

regions where cooling occurred. It is possible that this mechanism may contribute to anticyclonogenesis. Note, however, that their regions where cooling (relative to the reference simulation without blowing snow) were displaced somewhat from where blowing snow occurs. This suggests that the possible connection between blowing snow and anticyclonogenesis may be more involved than a simple microphysical process.

3 Objective and outline of the thesis

Blowing snow is a complicated phenomenon which is the result of the interaction of mesoscale dynamics, boundary layer processes and microphysical processes. Past studies have shown that blowing snow effects on visibility, snow cover redistribution are evident, and blowing snow may contribute to anticyclonogenesis. To better simulate the blowing snow size distribution, and all the related physical processes, it is important to have a more sophisticated yet efficient blowing snow model. Moreover, the entrainment process and the horizontal advection effects should also be considered to yield more realistic results. The goal of this thesis is to develop a coupled blowing snow–atmospheric model, and to use this coupled model to study blowing snow effects on the hydrological cycle and on anticyclonogenesis. The thesis is organized as a series of three papers focused on the following questions: Can we improve the blowing snow model to better represent the particle size distribution and, if so, does this lead to an improved prediction of visibility? What is the contribution of blowing snow to the water mass budget over large temporal and spatial scales? What are the impacts of the blowing snow on anticyclone development? Is the contribution solely from blowing snow sublimation, or from any other processes related to blowing snow? To what extent does the blowing snow cooling

effect contribute to anticyclogenesis? Specifically, our objectives are proposed as the following:

1. To extend the double moment blowing snow model PIEKTUK-D to a triple moment scheme PIEKTUK-T, and to validate this model with field observation data;
2. To couple this one-dimensional model with an atmospheric mesoscale model MC2;
3. To compute water mass budgets over the Northern Hemisphere, and quantify the contribution of blowing snow on the seasonal water mass budget;
4. To carry out sensitivity experiments with and without blowing snow to isolate its cooling effect;
5. To study and quantify the contribution of blowing snow to the dynamics of anticyclogenesis.

An outline of the remainder of the thesis is as follows. In Chapter 2, an additional predicted equation for radar reflectivity, which is the sixth moment of particle size distribution, was proposed to relax the limitation of a fixed α . The detailed particle size distribution at different heights is thus predicted in the one-dimensional blowing snow model PIEKTUK-T. This model is then validated by field observation data.

In Chapter 3, PIEKTUK-T is coupled to MC2 (V4.9.8) in order to provide an interactive platform involving atmospheric and surface processes to study the water budget over Northern Hemisphere. By conducting the simulations as a sequence of 54-h integrations, a time series for the entire three winter months is constructed. The spatial patterns of blowing snow sublimation, blowing snow transport and surface sublimation

are presented. The results were further stratified in 10 degree latitudinal bands to examine how these terms vary with latitudes.

In Chapter 4, we simulated an anticyclogenesis event over the Arctic Ocean. Comparing the temperature fields and sea level pressure fields from coupled and uncoupled runs, the blowing snow cooling effects was thus isolated. A potential vorticity (PV) inversion diagnostic system was then applied to further analyze and quantify the blowing snow cooling effects on the anticyclogenesis.

A summary and conclusions are given in Chapter 5.

Chapters 2 to 4 are presented in the form of papers published in *Boundary layer meteorology*, submitted for publication to *Hydrological Earth System Sciences* (published in *Hydrological Earth System Sciences Discussion*), and submitted for publication in *Journal of Geophysical Research*. The text of the papers is meant to be self-contained, which leads to unavoidable overlaps.



Figure 1: Migrating snow waves moving about 5 m h^{-1} with a wind speed of 40 km h^{-1} . View is facing wind (Tabler, 1986).

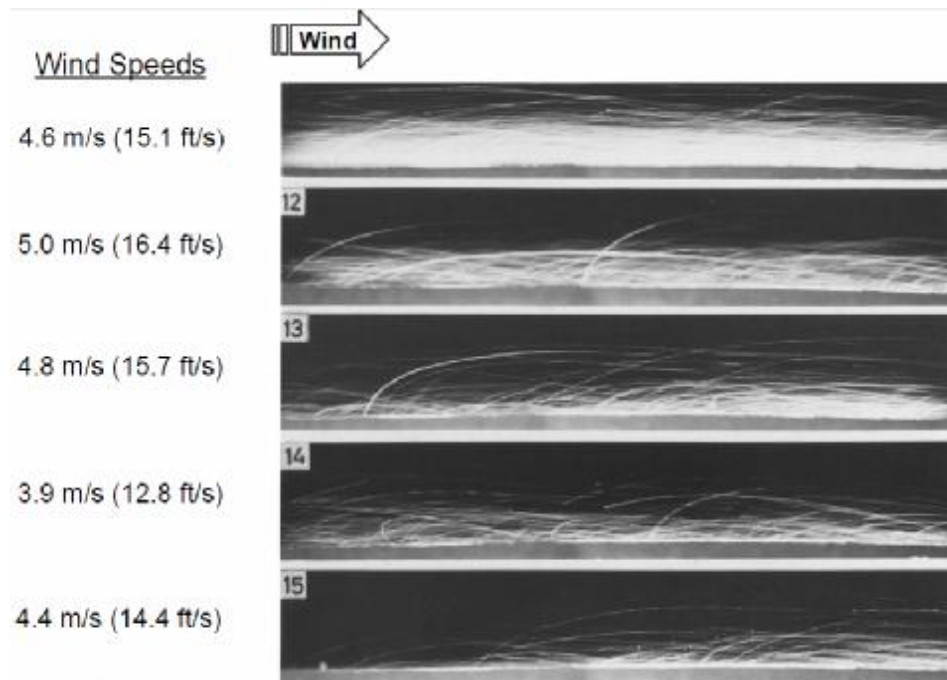


Figure 2: Drifting snow trajectories. Wind speeds are 1 m height level, and the field is 25 cm (Photographed by D. Kobayashi, 1972).

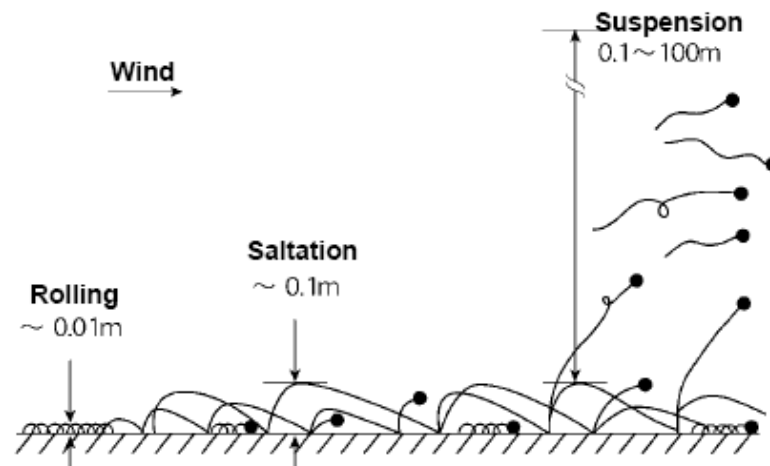


Figure 3: Schematic of blowing snow transport (Takeuchi 1984).

Chapter 2

A new triple-moment blowing snow model

To model blowing snow occurrence and especially the particle size distribution, the one-dimensional double moment blowing snow model PIEKTUK-D was extended to a triple moment blowing snow model, PIEKTUK-T. It produced better vertical profiles of number concentration and mixing ratio of blowing snow particles, as was verified against available observations. The improved model also yields particle size distributions which compare favourably with more complicated spectral models, but with much less computational costs. This makes feasible the coupling to an atmospheric mesoscale model.

This chapter is based on the following published paper:

Yang, J. and M.K. Yau (2008) A new triple-moment blowing snow model. *Boundary-Layer Meteorology*, 126: 137-155. DOI 10.1007/s10546-007-9215-4.

Reproduced with kind permission from Kluwer Academic Publishers.

A new triple-moment blowing snow model

Jing Yang and M. K. Yau

Department of Atmospheric and Oceanic Sciences, McGill University

Montréal, Quebec, H3A 2K6, Canada

Abstract This paper presents a new triple-moment blowing snow model PIEKTUK-T by including predictive equations for three moments of the gamma size distribution. Specifically, predictive equations for the total number concentration, total mass mixing ratio, and total radar reflectivity for blowing snow are included. Tests in the context of idealized experiments and observed case studies demonstrated that the triple-moment model performs better than the double-moment model PIEKTUK-D in predicting the evolution of the number concentration, mixing ratio, shape parameter, and visibility in blowing snow, provided that the fall velocities for the total number concentration, mass mixing ratio, and radar reflectivity are weighted by the same order of the respective moments in both models. The power law relationship between the radar reflectivity factor and particle extinction coefficient found in PIEKTUK-T is consistent with one observed in snow storms. Coupling of the triple-moment blowing snow model to an atmospheric model would allow realistic studies of the effect of blowing snow on weather and climate.

Keywords Blowing snow, Double-moment, Gamma distribution, Triple-moment.

1. Introduction

Blowing snow is a common phenomenon occurring in high latitudes where the surface is snow covered, the temperature is below zero, and the wind speed is strong. When the wind speed exceeds a threshold value, snow particles start to bounce in a series of leaps at the surface and the saltation layer is formed. With stronger winds, turbulent eddies can diffuse the saltated particles upwards and they can become suspended in the atmosphere as the result of the balance of turbulent diffusion and sedimentation. Sublimation of blowing snow particles then result. Blowing snow can decrease the visibility and redistribute the mass and water in a given area. Déry and Yau (2002) studied the role of blowing snow transport and sublimation in affecting the global surface mass and water balance. They found that surface sublimation and blowing snow sublimation can erode about 20% of the annual precipitation over Antarctic, while the mass transport exceeds $100 \text{ Mg m}^{-1} \text{ year}^{-1}$.

Budd (1966) was among the first to propose that blowing snow particles follow a gamma size distribution. He used the maximum likelihood method to fit the observed blowing snow size spectra in the Byrd snow drift experiment. The fitted gamma distribution is of the form

$$F(r) = \frac{Nr^{a-1}}{b^a \Gamma(a)} e^{-r/b} \quad (1)$$

where $F(r)$ ($\text{m}^{-3} \text{ m}^{-1}$) is the particle number concentration of radius r (m), a and b (m) are respectively the dimensionless shape parameter and the scale parameter of the distribution, and N (m^{-3}) is the total number concentration defined by

$$N = \int_0^{\infty} F(r) dr. \quad (2)$$

Other field experiments and theoretical studies have also tested the goodness of fit of the

gamma distribution (Kobayashi, 1972; Schmidt, 1982; Pomeroy, 1988; Dover, 1993) with good results.

A number of blowing snow models have been developed to study the interaction of blowing snow with boundary-layer processes. There are two methods to represent the particle size distribution in these models: the spectral method and the bulk method. In the former case, the particle size range is discretized into a finite number of size bins, and the particles in each bin have to satisfy the governing diffusion-sedimentation-sublimation equation. The solution to the system of equations then yields the evolution of the particle size distribution (e.g., Pomeroy et al., 1993, 1997; Mann, 1998; Déry et al., 1998; Bintanja, 2000a, 2000b). While spectral models can provide detailed information for all sizes, they are computationally expensive. As a simplification, Déry and Yau (1999) proposed the bulk method which typically employs an analytic function, like the gamma function, to represent the size distribution. Since the gamma distribution in (1) is governed by 3 parameters (N , a , and b), the evolution of the size spectrum can be obtained by predicting the evolution of three moments of the distribution. Alternatively, if one or more of the parameters are specified, the number of predicted moment equations can be reduced. For example, in the bulk PIEKTUK-B model (Déry and Yau, 1999), two parameters are held fixed and the predicted variable is the mixing ratio q_b (kg kg^{-1}) of blowing snow, which is related to the third moment of the size distribution as

$$q_b = \frac{4\rho r_{ice}}{3\rho} \int_0^{\infty} r^3 F(r) dr \quad (3)$$

where r_{ice} (kg m^{-3}) and ρ (kg m^{-3}) are the densities of ice crystals and air respectively. In (3), blowing snow particles are assumed spherical in shape for simplicity. Déry and

Yau (1999) showed that PIEKTUK-B can predict the sublimation and transport rate of blowing snow as well as the spectral model, but not the variation of the number concentration with height (Xiao et al., 2000).

Déry and Yau (2001) introduced a two-moment version of PIEKTUK, so called PIEKTUK-D, where both the total number N and the mixing ratio of blowing snow particles are predicted. The parameter a is still held fixed. While PIEKTUK-D represents an improvement over PIEKTUK-B, observations and spectral model calculations do indicate that the a parameter is not a constant and normally increases with height.

To overcome this shortcoming, it is the purpose of this paper to introduce a three-moment version of PIEKTUK (PIEKTUK-T). In addition to predictive equations for N (the zeroth moment of the size distribution) and q_b (related to the third moment), a new predictive equation for radar reflectivity of blowing snow is formulated. The radar reflectivity Z is defined as the sixth moment of the particle size distribution, with the form

$$Z = \int_0^{\infty} (2r)^6 F(r) dr, \quad (4)$$

where r is the radius of blowing snow particles. With three predictive moment equations, the three parameters in (1) can be determined completely without arbitrary assumptions. In principle, any three moment equations can determine the three parameters in the size distribution function to close the system. We choose radar reflectivity as one of the predicted moments for two reasons: First, radar reflectivity is often a measured variable in field experiments. Second, Z has been found to relate monotonically to the extinction

coefficient of blowing snow particles (Muench and Brown, 1977; Dixon et al., 2004) and hence can be used to calculate the visibility. We will compare the two- and three- moment versions of PIEKTUK with each other and with field measurements. It will be shown that the three-moment PIEKTUK-T model is superior in predicting the evolution of the blowing snow particle size distribution as verified against available observations.

2. Model Formulation

The governing equations for PIEKTUK-T include those for atmospheric temperature T_a (K), water vapor mixing ratio q_v (kg kg^{-1}), blowing snow mixing ratio q_b (kg kg^{-1}), blowing snow number concentration N (m^{-3}), and blowing snow radar reflectivity Z ($\text{m}^6 \text{m}^{-3}$)

$$\frac{\partial T_a}{\partial t} = \frac{\partial}{\partial z} \left(K_h \frac{\partial T_a}{\partial z} \right) + \frac{S_b L_s}{c_p} \quad (5)$$

$$\frac{\partial q_v}{\partial t} = \frac{\partial}{\partial z} \left(K_v \frac{\partial q_v}{\partial z} \right) - S_b \quad (6)$$

$$\frac{\partial q_b}{\partial t} = \frac{\partial}{\partial z} \left(K_b \frac{\partial q_b}{\partial z} + v_b q_b \right) + S_b \quad (7)$$

$$\frac{\partial N}{\partial t} = \frac{\partial}{\partial z} \left(K_N \frac{\partial N}{\partial z} + v_N N \right) + S_N \quad (8)$$

and

$$\frac{\partial Z}{\partial t} = \frac{\partial}{\partial z} \left(K_z \frac{\partial Z}{\partial z} + v_z Z \right) + S_z \quad (9)$$

The first term on the right-hand side of each equation represents vertical turbulent eddy diffusion where K_h , K_v , K_b , K_N and K_z ($\text{m}^2 \text{s}^{-1}$) are the eddy diffusion coefficient for

heat, moisture, and the mixing ratio, number concentration and radar reflectivity for blowing snow particles respectively. For simplicity, the coefficients are assumed given by the eddy diffusion coefficient for momentum which is related to the product of the mixing length and the friction velocity in near-neutral conditions.

The second terms on the right in the last three equations indicate sedimentation of blowing snow mixing ratio, total number concentration, and reflectivity. The sedimentation velocities for the different variables $v_{N,b,Z}$ are weighted by the order of the respective moments

$$v_{N,b,Z} = \frac{\int_0^{\infty} v(r) r^{0.3,6} F(r) dr}{\int_0^{\infty} r^{0.3,6} F(r) dr} \quad (10)$$

where $v(r)$ is the terminal velocity of blowing snow particles in still air. The last term in each equation denotes the source/sink term arising from sublimation with L_s (J kg⁻¹) and c_p (J kg⁻¹ K⁻¹) being respectively the latent heat of sublimation and the specific heat of air at constant pressure.

The bulk mixing ratio sublimation rate S_b (kg kg⁻¹ s⁻¹) and the accompanying rate of change in number concentration S_N (m⁻³ s⁻¹) follow those in Déry and Yau (1999, 2001), of the form

$$S_b = \frac{q_b Nu (q_v / q_{is} - 1)}{2 r_{ice} r_m^2 (F_K + F_D)} \quad (11)$$

$$S_N = \frac{S_b}{q_b} N \quad (12)$$

where Nu is the Nusselt number representing ventilation effects, q_{is} (kg kg⁻¹) is the

saturation water vapor mixing ratio with respect to ice, F_K (m s kg^{-1}) and F_D (m s kg^{-1}) indicate thermal conduction and water vapor diffusion terms respectively, and r_m (m) is the mean particle radius. The rate of change in radar reflectivity S_Z ($\text{m}^6 \text{m}^{-3} \text{s}^{-1}$) can be derived (see Appendix A for details) following Harrington et al. (1995) as

$$S_Z = 384r_m^2 b^4 \frac{\Gamma(a+4)}{\Gamma(a)} S_N. \quad (13)$$

Following Milbrandt and Yau (2005), a relation for the parameter a in terms of the three moments N , q_b and Z can be obtained (see Appendix B for details)

$$G(a) = \frac{\Gamma(a)\Gamma(a+6)}{\Gamma(a+3)\Gamma(a+3)} = NZ \left(\frac{pr_{ice}}{6rq_b} \right)^2. \quad (14)$$

At each time step, T_a , q_v , N , q_b and Z are predicted. The parameter a can then be calculated from (14). The parameter b is obtained following Déry and Yau (2001) as

$$b = \left[\frac{3rq_b\Gamma(a)}{4pr_{ice}\Gamma(a+3)N} \right]^{\frac{1}{3}}. \quad (15)$$

With N , a , and b determined, the size distribution (1) is completely defined.

3. An Idealized Experiment

Before comparing with observations, we compare the three-moment PIEKTUK-T and the two-moment PIEKTUK-D in the context of an idealized experiment reported in Déry and Yau (2001). For the initial conditions, we assume that the wind is given by a logarithmic profile in near-neutral conditions (Pomeroy et al., 1993) with the 10-m height wind speed $U_{10} = 15 \text{ m s}^{-1}$. The initial temperature is constant at -10°C in the atmospheric boundary

layer. The initial relative humidity with respect to ice is set to $RH_i = 0.7$ at and above 100 m, and below $z = 100$ m, the humidity is calculated following Garratt (1992) as

$$q_v = q_{is} + \frac{q^*}{k} \ln\left(\frac{z + z_0}{z_0}\right) \quad (16)$$

with q_v equals to its saturation value (q_{is}) with respect to ice at $z = 0$ m. Here, z_0 (m) denotes the roughness length and q^* (kg kg^{-1}) is the humidity scale. The specification of blowing snow at the saltation level follows Déry and Yau (2001), with mean particle radius $r_m = 100 \mu\text{m}$ and $a = 2$. The PIEKTUK model has 30 vertical levels, spaced equidistantly on a logarithmic scale. The experiment was run for 10 min until a steady state is reached. For PIEKTUK-D, $a = 2$ at all levels throughout the experiment.

Figure 1a shows the spectrum of particle size distribution 10 minutes subsequent to the initiation of the models at two different levels. The vertical profile of the shape parameter a is plotted in Fig. 1b at two times. In the double-moment model, the shape parameter has a constant value of 2. In the triple-moment version, a increases with height (Fig. 1b). Since the shape parameter in the two models has similar values at $z = 0.1$ m, the size distributions are almost the same at this height at 10 min (Fig. 1a). However, higher up at $z = 2.4$ m, the triple-moment model indicates a larger value of $a = 4.05$ (Fig. 1b). It can be shown readily from (1) that the radius at which the particle number is at a maximum is given by $r_{max} = (\alpha - 1) \beta$. As α is larger in PIEKTUK-T than in PIEKTUK-D higher up, consequently the spectrum (Fig. 1a) predicted by the triple-moment model shifts to the right of the double-moment model.

Figure 2 depicts the number concentration, mixing ratio, radar reflectivity and mean particle radius. In general, the plotted values are smaller in the double-moment run at any

height. The vertical profiles of total number concentration and radar reflectivity are closer between the double and the triple moment versions than the blowing snow mixing ratio and mean radius. Specifically, q_b in PIEKTUK-D is $\approx 50\%$ of that in PIEKTUK-T from 0.5 m to 100 m in altitude while the ratio for N is $\approx 70\%$ (Figs. 2a, 2b). It can be shown that the ratio of q_b to N is related to the product of the third power of the mean radius r_m and an inverse function of the shape parameter as

$$\frac{q_b}{N} = \frac{4pr_{ice}}{3r} b^3 \frac{\Gamma(a+3)}{\Gamma(a)} = \frac{4pr_{ice}}{3r} r_m^3 \left(1 + \frac{1}{a}\right) \left(1 + \frac{2}{a}\right). \quad (17)$$

Since the predicted ratio of q_b/N for PIEKTUK-D and PIEKTUK-T is ≈ 0.7 , and $a = 2$ for PIEKTUK-D but varies from 2.2 to around 5 in PIEKTUK-T (Fig. 1b), the application of (17) indicates that the mean radius for PIEKTUK-D is $\approx 70-85\%$ of that for PIEKTUK-T, in agreement with the results depicted in Fig. 2d.

The smaller difference in N and Z relative to that for q_b between the double and triple moment runs in Fig. 2 can also be accounted for from a plot of the contribution of different radii to the zeroth, first, third and sixth moments of the size distribution at $z = 57.5$ m (Fig. 3). The contribution to the zeroth moment is larger in the triple-moment model from 10 -70 μm (Fig. 3a). This leads to a larger mixing ratio in PIEKTUK-T depicted in Fig. 2d. Although the contribution to the zeroth moment is larger in PIEKTUK-D for radii larger than 70 μm , the number concentration becomes too low to make a significant difference in the mixing ratio. However, the effect of the tail becomes progressively more important at higher moments (Fig. 3d). As a result, the relative difference in the field of radar reflectivity becomes negligible (Fig. 2c).

4. Comparison with Observations

Measurements obtained in three experiments, from two Antarctic stations and from the Great Plains over Wyoming, will be used for model comparison.

4.1. Byrd station

This experiment was carried out at the Byrd station (80°01' S, 119°32' W) over the Antarctic during 1962-1963. Detailed information on meteorological conditions, drift snow concentration, and the shape and size of blowing snow particles are available from Budd et al. (1966). Although there were 129 individual case runs, the number of samples of observed particles in each case was small. To obtain a realistic distribution, we averaged the number density, friction velocity and roughness length as a function of height in all the runs. Budd et al. (1966) determined the particle sizes through Formvar technique from 133 slides obtained during the whole experiment and very small particles with effective diameter smaller than 20 μm were neglected. However, their plotted frequency distribution of snow particles (see also Fig. 4) indicates that the frequency of these very small particles is insignificant and their neglect would not change the analyzed size distribution.

The first observational level, at $z = 0.03$ m, is chosen to be the saltation level. The observed mean diameter, drift density (ρq_b) and a at this level are used as the boundary conditions. Unfortunately, there are no humidity measurements. We therefore assume that the relative humidity follows a logarithmic profile from the lowest level (assumed saturated with respect to ice) to a height of 100 m. Above 100 m, the relative humidity is set at 80%. Sensitivity tests with various humidity profiles have been performed, and

though some sensitivity was found but the major conclusions were not affected.

Comparisons with observations were made when the models reached their steady state 10 minutes after the initiation of blowing snow. Figure 4 depicts the observed histogram and the simulated size distributions at heights of 0.125 m, 0.25 m, 0.5 m, 1 m and 2 m. As indicated, there is good agreement between the triple-moment model size distributions and the observed distributions except for a slight shift at the height of 0.125 m. In contrast, the size distributions predicted by the double-moment model generally shift to the right of the observed at all levels. This spectral shift is consistent with the profile of mean particle radius in Fig. 5a, with the triple-moment model showing better agreement with the measurements. The triple-moment results also revealed a better performance in predicting the shape parameter (Fig. 5b) and the blowing snow mixing ratio (Fig. 5c), whereas the double-moment simulation underpredicted these quantities throughout the column. The agreement between the simulated and observed scale parameter is reasonable for both models (Fig. 5d).

Transport and sublimation are two important quantities determining the surface snow mass redistribution; the integrated expression for the rate of transport Q_t ($\text{kg m}^{-1} \text{s}^{-1}$) and sublimation Q_s (mm day^{-1}) are given by

$$Q_t = r \int_{z_{lb}}^{z_{ub}} q_b U dz \quad (18)$$

and

$$Q_s = -r' \int_{z_{lb}}^{z_{ub}} S_b dz, \quad (19)$$

where U represents the wind speed. The coefficient $-r'$ is used to convert the negative sublimation rate in units of ms^{-1} to the positive value in units of mm day^{-1} snow water

equivalent. Table 1 shows that the transport rate for PIEKTUK-T is $0.26 \text{ kg m}^{-1} \text{ s}^{-1}$, around 2.5 times of that in PIEKTUK-D. This difference is attributed to the underpredicted mixing ratio of the PIEKTUK-D run, and the difference in q_b also leads to about a four times larger sublimation rate Q_s for PIEKTUK-T. Similar results also apply to the time integrated transport (QT_t) and time integrated sublimation (QT_s).

The visual visibility (Vis) is another important parameter in blowing snow. Usually with an increase in particle size and number concentration, the extinction of visible light by blowing snow particles will decrease the meteorological visual range. For a distribution of particle sizes, the extinction coefficient $E \text{ (m}^{-1}\text{)}$ for visible light can be written as

$$E = \int F(r)pr^2Q_{ext}(r)dr \quad (20)$$

with $Q_{ext}(r)$ being the individual particle extinction efficiency for the wavelength range of visible light. Using regression analysis, Pomeroy and Male (1988) found that the mean extinction efficiency $\overline{Q_{ext}}$ over the whole size spectrum is a function of the mean particle radius $r_m \text{ (m)}$, of the form

$$\overline{Q_{ext}} = 1.82r_m^{-0.011} \quad (21)$$

By calculating E exactly using (20) for a specific $F(r)$ and comparing the result with an approximation using (21) in (20), they found that the difference is less than 0.3%. We therefore adopt the same simplification. Using (1) and (21), (20) can be integrated to yield

$$E = pNa(a+1)b^2\overline{Q_{ext}} \quad (22)$$

Following Middleton (1952), the meteorological visibility $V \text{ (m)}$ can be related inversely

to the extinction coefficient E as

$$V = 3.912 / E \quad (23)$$

Instead of calculating E from (22), it is possible to relate E to the radar reflectivity factor Z empirically as follows. Using the output of the PIEKTUK-T model for the Byrd station runs, we first calculate E using (21) and (22), and then plot E against Z at 15 different model levels from the lowest level to the height of 4.7m. The results in Fig. 6 indicate that E is a power function of Z and can be fitted by the least square method to give $E = 0.0065Z^{0.8194}$, with Z measured in unit of mm^6m^{-3} . This monotonically increasing relationship is similar to the expression $E = 0.07Z^{0.39}$ obtained from observations during snowstorms (Muench and Brown, 1977).

Information on visibility was available for the Byrd station. Budd et al. (1966) fitted an empirical relationship between the ensemble average of the observed mean visibility and the mean drift density at 2m height for different wind speeds. With the average observed drift density of 0.83 g m^{-3} at 2 m height, the mean visibility was found to be 121 meter. To compare with the PIEKTUK-T results, we used the model predicted 2 m height blowing snow mixing ratio and number concentration of 0.67 g kg^{-1} and $2.23 \times 10^6 \text{ m}^{-3}$ respectively, the shape parameter of 14.23, the mean particle radius of $45 \text{ }\mu\text{m}$ (Table 2) and calculated an extinction coefficient $E = 0.0315 \text{ m}^{-1}$. Using (23), the model predicted visibility $V=124 \text{ m}$, close to the result of 121 m from Budd et al. (1966).

4.2. Wyoming observations

Schmidt (1982) reported on blowing snow measurements carried out in southeastern Wyoming from April 4 to April 5, 1974 under different meteorological conditions. Wind

speed at 10-m (U_{10}), temperature and humidity as a function of height, and blowing snow density at 6 levels were obtained. There are ten continuous observations, referred to as Runs 1-10. We selected the Run 1 case for comparison because of the availability of observed particle size distributions and because the run started at 2100 local time on April 4 with no complication from the effect of short wave radiation. Schmidt (1982) presented a detailed analysis of the size distribution and evaluated the shape parameter a at six levels. At each level, the total number of blowing snow particles measured was converted to the drift flux of snow particles by taking into consideration the instrument sampling area of about 100 mm^2 and a measuring time of 10 min. The number concentration N_0 at a given height is then obtained by dividing the drift flux by the wind speed at that level. However, the snow particle counters used were not able to detect particles smaller than $40 \text{ }\mu\text{m}$ in diameter. Indeed Fig. 6 in Schmidt (1982) shows that the relative frequency in the smallest measured diameter interval usually exhibits an absolute maximum indicating that the number of particles smaller than $40 \text{ }\mu\text{m}$ in diameter is probably not negligible. We therefore corrected the measured number concentration N_0 and the measured mean particle diameter D_{m0} at each height by considering the truncation effects at the small-diameter end with the incomplete gamma function. The corrected expressions are

$$D_m = D_{m0} \frac{Q(a+1, D_t / b)}{Q(a, D_t / b)} \quad (24)$$

$$N = N_0 Q(a, D_t / b) \quad (25)$$

where $Q(a, x) = \frac{1}{\Gamma(a)} \int_x^\infty e^{-t} t^{a-1} dt$ is the incomplete gamma function, and D_t (m) is the

truncated diameter with a value of $60 \text{ }\mu\text{m}$. Table 3 gives the corrected and the

uncorrected values for a , b , the mean particle diameter, and the number concentration at the six observational heights. As shown, the corrected values for b and N are generally larger than the uncorrected ones. On the other hand, the corrected D_m and a are smaller.

Using as initial conditions the observed temperature $T = -5.5^\circ\text{C}$, wind speed at 10 m height $U_{10} = 14.8 \text{ m s}^{-1}$, a logarithmic profile for relative humidity, a calculated $a = 3.2$ at the first level ($z = 0.05 \text{ m}$) based on the size distribution, the measured number concentration N , and the measured mean particle radius r_m , we ran the double- and triple-moment models for 10 min. Figure 7 shows that the vertical profiles of mixing ratio q_b (Fig. 7b), reflectivity Z (Fig. 7c), and mean particle radius r_m (Fig. 7d) for the triple-moment model are closer to the observations than the double-moment model. The mixing ratio in PIEKTUK-T is in general 2.6 – 2.9 times larger than that in the double-moment run. Although both models over-predict the number concentration N above the height of 0.6m (Fig. 7a), the value of N in PIEKTUK-T is much closer to the observations at the lower levels. The profiles of a and b also agree well with the measurements in the triple-moment run (Fig. 8). In particular, b decreases with height similar to that in the idealized experiment (not shown). In comparison to the Byrd experiment, the number concentration and the mean radius are smaller in Wyoming blowing snow, so the visibility is therefore larger (Table 2).

Figure 9 is a plot of the size distribution at $z = 0.05 \text{ m}$, 0.10 m , 0.20 m , 0.35 m , 0.50 m and 1 m levels. The simulated size distributions from the triple-moment model are quite similar to the observation. As for the double-moment run, the simulated spectra shifted to

smaller sizes because of the smaller simulated mean radius.

Table 1 also contains the vertically integrated transport rate Q_t . The values in PIEKTUK-T and PIEKTUK-D are $0.098 \text{ kg m}^{-1} \text{ s}^{-1}$ and $0.078 \text{ kg m}^{-1} \text{ s}^{-1}$ respectively. The observed value for Run 1 is $0.096 \text{ kg m}^{-1} \text{ s}^{-1}$ (Schmidt, 1982), much closer to the triple-moment run. The smaller Q_t in PIEKTUK-D can be explained by the smaller predicted mixing ratio of blowing snow (Fig. 7b).

4.3. Halley station

The STABLE2 experiment was carried out by the British Antarctic Survey in 1991. Halley station (75.6° S , 26.7° W) is located in the Antarctic with typical ice shelf conditions (Mann, 1998). Blowing snow occurs frequently at Halley station because of the strong katabatic winds (King, 1989). There was a 30 m high meteorological mast with instruments mounted at different heights. The particle number flux was measured by snow particle counters at heights of 0.1, 1.17, 1.67, 2.95, 5.61 and 10.87 m (Mann et al., 2000). The number concentration of blowing snow particles can be obtained by dividing the number flux by the wind speed. Snow particle collectors sampled particles and pictures were taken of the shape and size of the particles in slides, and for the whole experiment, there were 99 slides recording the information on blowing snow particles. Due to contamination and testing using the ratio of chemical solutions, most slides were discarded and only 22 slides were analyzed (Dover, 1993). We selected the data on May 23, 1991 for our comparison. The size distribution reported by Dover on that day followed well the gamma distribution; however, the observed mean particle radius in this experiment are somewhat larger than other experiments. It is known that for particles

with a Reynolds number above the Stokes range, the particle settling velocity in turbulent flow is reduced (Sommerfeld and Businger, 1965). Since model results are very sensitive to the sedimentation velocity (Déry and Yau 1999; Xiao et al. 2000), a number of tests were performed to find a multiplication factor that would improve the comparison of model results with observations. From trial and error, a multiplication factor to the sedimentation velocity with a value of 0.55 was found. This factor was applied both in PIEKTUK-D and in PIEKTUK-T.

The slide records were available from 1233 to 1254 local time on 23 May 1991, and the appropriate initial condition for that time are $U_{10} = 15.46 \text{ m s}^{-1}$, $T = -6.8^\circ\text{C}$, and $RH_i = 98.21\%$. There are 30 levels in the model with the lowest level at $z = 0.1 \text{ m}$ and the highest level at $z = 1000 \text{ m}$. The observed profiles of number concentration, mean particle radius, and shape parameter were used to compare with model results.

Figure 10 shows that there is good agreement between the observations and the triple-moment results in the profile of number concentration (Fig. 10a). The simulated mean particle radius (Fig. 10d) is smaller than the measurement, and the mixing ratio and reflectivity are also smaller (Fig. 10b, 10c). Nevertheless, the triple-moment profiles are better than the double-moment ones. Figure 11 depicts the simulated and observed size distributions at four different levels, and again, the profiles from the triple-moment model agree with the observations very well. The spectrum becomes narrower and more symmetric with height indicating an increase in the shape parameter a when the height increases.

5. Discussion and Conclusions

We have developed a triple-moment blowing snow model PIEKTUK-T and validated it using idealized experiments and comparison with observations. The main results are as follows:

(1) Blowing snow particles can be well represented by a three parameter gamma size distribution. The shape parameter a usually increases with height both in the triple-moment model and the observations except for the very low levels. On the other hand, the scale parameter β always decreases with height in all the cases examined. Correspondingly, the size distribution for blowing snow particles becomes narrower with height, particularly at higher levels. It was also noted that in the idealized case and over the Wyoming site, the vertical variation of the shape parameter is positive. However, over Byrd station, a decreases with altitude in the lowest levels. This difference can be explained by the fact that the mean radius (r_m) always decreases with height because there is a net diffusion of smaller particles upward as larger particles undergo sedimentation (settle downwards) against the turbulence diffusion. It can be shown readily that $r_m = a \beta$, and

$$\frac{\partial \ln r_m}{\partial z} = \frac{\partial \ln a}{\partial z} + \frac{\partial \ln b}{\partial z}. \quad (26)$$

Since the left-hand side of (26) and the second term on the right are always negative, for

a given $\frac{\partial \ln r_m}{\partial z}$, $\frac{\partial \ln a}{\partial z}$ can be either positive or negative depending on how negative

$\frac{\partial \ln b}{\partial z}$ is. Comparing Figs. 5d and 8b, it is clear that $\frac{\partial \ln b}{\partial z}$ at the low levels over the

Byrd station is much less negative than over the Wyoming site, thus $\frac{\partial \ln a}{\partial z}$ needs to be

negative at the low levels over the Byrd station to ensure a decrease of the mean radius with height.

(2) The triple-moment PIEKTUK-T model represents an improvement over the double-moment PIEKTUK-D. Specifically, the simulated profiles of number concentration, mixing ratio, and mean particle radius are in better agreement with observations, so is the visibility over the Byrd station. When the fall velocities for N , q_b and Z , weighted by the order of the respective moments as in (10), are applied to both the double and triple moment versions of PIEKTUK, the results in Table 1 indicated that the values of blowing snow sublimation and transport can differ up to a factor of 4 between PIEKTUK-D and PIEKTUK-T. Similar conclusions can also be drawn regarding the number concentration, mean particle radius, and visibility tabulated in Table 2. We emphasize that this remark on the difference between the results of the double and triple moment versions of the blowing snow model is valid if (10) is used in both models. On the other hand, the fall velocities for N and q_b can be adjusted in PIEKTUK-D to give better results. Specifically, Déry and Yau (1999) weighted the fall velocity of q_b by the fifth moment so that the predicted profile of q_b in a single-moment version of PIEKTUK agrees with that from a spectral model. Déry and Yau (2001) weighted the fall velocity of N by the second moment so that the predicted results from PIEKTUK-D is close to an analytic solution when blowing snow sublimation is inactive. Despite the fact that the double-moment blowing snow model can be improved by tuning the fall velocities, no such adjustment is needed for the triple-moment PIEKTUK-T and this represents a distinct advantage.

(3) PIEKTUK-T performs as well as the spectral model in simulating the evolution

of the blowing snow sublimation rate and the details of the blowing snow size spectrum.

The power law relationship between the radar reflectivity factor and extinction coefficient in PIEKTUK-T is quite similar to one observed in snowstorms. The predicted radar reflectivity can be used to forecast the visibility and is therefore a valuable predicted variable. Our bulk triple-moment blowing snow model is much less costly in terms of computational resources and is ideal for coupling to an atmospheric model to simulate the effect of blowing snow in weather and climate predictions.

Acknowledgements We would like to express our great thanks to Dr. Stephen Déry who wrote the original source code of the blowing snow model and provided us with help and suggestions. We also appreciate the help from Dr. Graham Mann and Dr. P.S. Anderson for their generosity in providing the observation data of STALBE2 as well as constructive suggestions.

Appendix A: Radar reflectivity change rate due to sublimation S_Z

The mass change rate due to sublimation is expressed by (Thorpe and Mason, 1966)

$$\frac{dm}{dt} = \frac{2prNu(q_v / q_{is} - 1)}{F_K + F_D}. \quad (27)$$

Assuming that blowing snow particles are spherical, the rate of change of radius can be written as

$$\frac{dr}{dt} = \frac{Nu(q_v / q_{is} - 1)}{2r_{ice}r(F_K + F_D)}. \quad (28)$$

Differentiating Eq. (4) with respect to time gives

$$\frac{dZ}{dt} = 2^6 \int_0^\infty \frac{d}{dt} (r^6 F(r)) dr = 2^6 \int_0^\infty \left(6r^5 F(r) \frac{\partial r}{\partial t} + r^6 \frac{\partial F(r)}{\partial t} \right) dr \quad (29)$$

The first term on the right hand side of Eq. 29 is zero, and the second term is related to the spectrum shift. Since

$$\frac{\partial F(r)}{\partial t} = -\frac{\partial}{\partial r} \left(F(r) \frac{dr}{dt} \right), \quad (30)$$

we can write

$$\begin{aligned} \int_0^\infty \left(r^6 \frac{\partial F(r)}{\partial t} \right) dr &= -\int_0^\infty \left\{ r^6 \frac{\partial}{\partial r} \left(F(r) \frac{dr}{dt} \right) \right\} dr \\ &= -\int_0^\infty \frac{\partial}{\partial r} \left(r^6 F(r) \frac{dr}{dt} \right) dr + \int_0^\infty \left(F(r) \frac{dr}{dt} \frac{\partial r^6}{\partial r} \right) dr \quad (31) \end{aligned}$$

By using Eqs. 1 and 28 we obtain

$$r^6 F(r) \frac{dr}{dt} = \frac{Nu(q_v / q_{is} - 1) N r^{a+4}}{2r_{ice}(F_K + F_D) b^a \Gamma(a)} \exp(-r/b). \quad (32)$$

Since (32) vanishes when r tends to 0 and infinity, the first integral on the right of (31) is zero. Using the gamma size distribution and Eq. 28, the second term on the right of Eq. 31 is calculated as

$$\int_0^\infty \left(F(r) \frac{dr}{dt} \frac{\partial r^6}{\partial r} \right) dr = \frac{6Nu(q_v / q_{is} - 1) \Gamma(a+4) b^4 N}{2r_{ice}(F_K + F_D) \Gamma(a)}, \quad (33)$$

and Eq. 29 becomes

$$\frac{dZ}{dt} = S_z = \frac{384Nu(q_v / q_{is} - 1) \Gamma(a+4) b^4 N}{2r_{ice}(F_K + F_D) \Gamma(a)}. \quad (34)$$

Finally, using Eqs. 11 and 12, 34 can be put in the form

$$S_z = 384r_m^2 b^4 \frac{\Gamma(a+4)}{\Gamma(a)} S_N. \quad (35)$$

Appendix B: Derivation of radar reflectivity factor Z

From the particle size distribution $F(r) = \frac{Nr^{(a-1)}}{b^a \Gamma(a)} e^{-r/b}$, the p^{th} moment is given by

$$M(p) = \int_0^{\infty} r^p F(r) dr = Nb^p \frac{\Gamma(a+p)}{\Gamma(a)}. \quad (36)$$

Using (36) and $p=3$ and $p=6$, we obtain

$$q_b = \frac{4pr_{ice}}{3r} Nb^3 \frac{\Gamma(a+3)}{\Gamma(a)} \quad (37)$$

$$Z = 2^6 Nb^6 \frac{\Gamma(a+6)}{\Gamma(a)}. \quad (38)$$

With Eq. 37, b can be solved in terms of N , q_b and a as

$$b = \left(\frac{3rq_b \Gamma(a)}{4pr_{ice} N \Gamma(a+3)} \right)^{1/3}. \quad (39)$$

Substituting Eq. 39 into Eq. 38 allows Z to be written in the following form:

$$Z = \frac{1}{N} \left(\frac{6rq_b}{pr_{ice}} \right)^2 \frac{\Gamma(a)\Gamma(a+6)}{\Gamma(a+3)^2}. \quad (40)$$

The shape parameter a can thus be calculated if q_b , N , and Z are known.

Variables	Model	Q_s	QT_s	Q_t	QT_t
Stations	version	(mm d ⁻¹ swe)	(mm swe)	(kg m ⁻¹ s ⁻¹)	(kg m ⁻¹)
Byrd	D	0.1221	0.000753	0.1096	58.93
	T	0.4615	0.003201	0.2588	125.1
Wyoming	D	0.5999	0.0043	0.0781	46.40
	T	1.4352	0.0108	0.0982	57.48
Halley	D	0.6392	0.004024	1.570	604.9
	T	0.2522	0.001410	0.3464	186.8

Table 1: The blowing snow transport rate (Q_t) and sublimation rate (Q_s), the time integrated values of transport (QT_t) and sublimation (QT_s) over the 10 min for three real cases predicted by PIEKTUK-D and PIEKTUK-T models.

Variables	Model	N	r_m	a	V
Stations	version	(m^{-3})	(10^{-6} m)		(m)
Byrd	D	568060	48.73	14.50	425
	T	2234103	45.43	14.23	124
Wyoming	D	755840	23.85	3.20	1079
	T	844120	36.51	7.61	480
Halley	D	2864300	44.00	1.81	71.2
	T	1038100	37.81	2.33	288

Table 2: The blowing snow number concentration (N) and mean particle radius (r_m), shape parameter (a) at the height of 2 m, and the visibility (V) for three real cases predicted by PIEKTUK-D and PIEKTUK-T models.

Variables	C/U	0.05 m	0.1 m	0.2 m	0.35 m	0.50 m	1.0 m
D_m (mm)	C	166	155	105	101	94	78
	U	181	173	136	121	115	87
a	C	3.2	3.7	4.2	5.1	5.9	7.2
	U	5.1	5.3	5.3	8.4	10.2	14.0
b (mm)	C	51.87	41.89	25.00	19.80	15.93	10.83
	U	35.49	32.64	25.66	14.40	11.27	6.21
N (m ⁻³)	C	18106000	9586000	5408000	2284000	1553000	576000
	U	16536000	8806000	4383000	1881000	1254000	367000

Table 3: Corrected (C) and uncorrected (U) parameters a , b , mean particle diameter D_m , and number concentration N at six heights for Wyoming experiments.

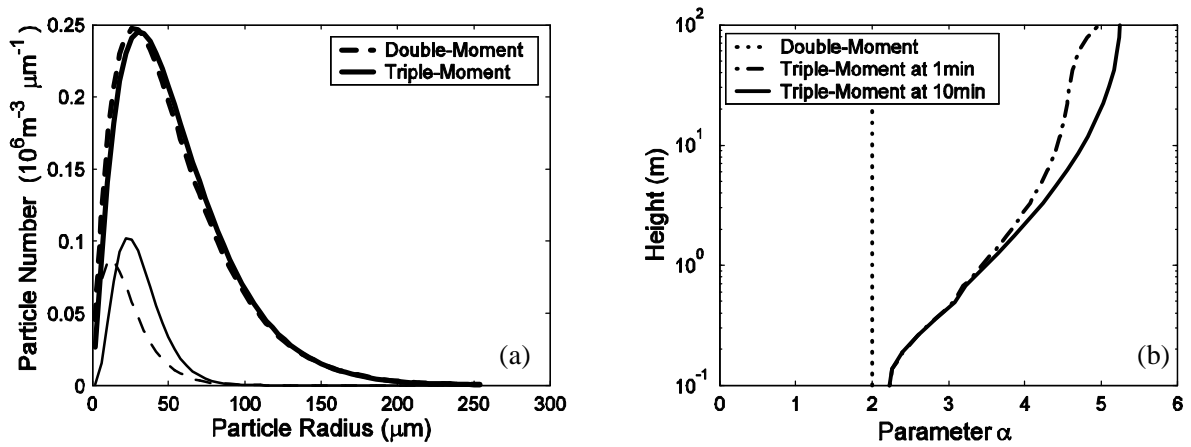


Figure 1: (a) Particle size distribution at $z = 0.1 \text{ m}$ and $z = 2.4 \text{ m}$ predicted by the double-moment model and the triple-moment model. Thick solid and dashed lines are results at $z = 0.1 \text{ m}$, and thin solid and dashed lines are results at $z = 2.4 \text{ m}$. (b) Profiles of parameter α predicted by the double- and triple-moment models after 1 min and 10 min of simulation in the idealized case.

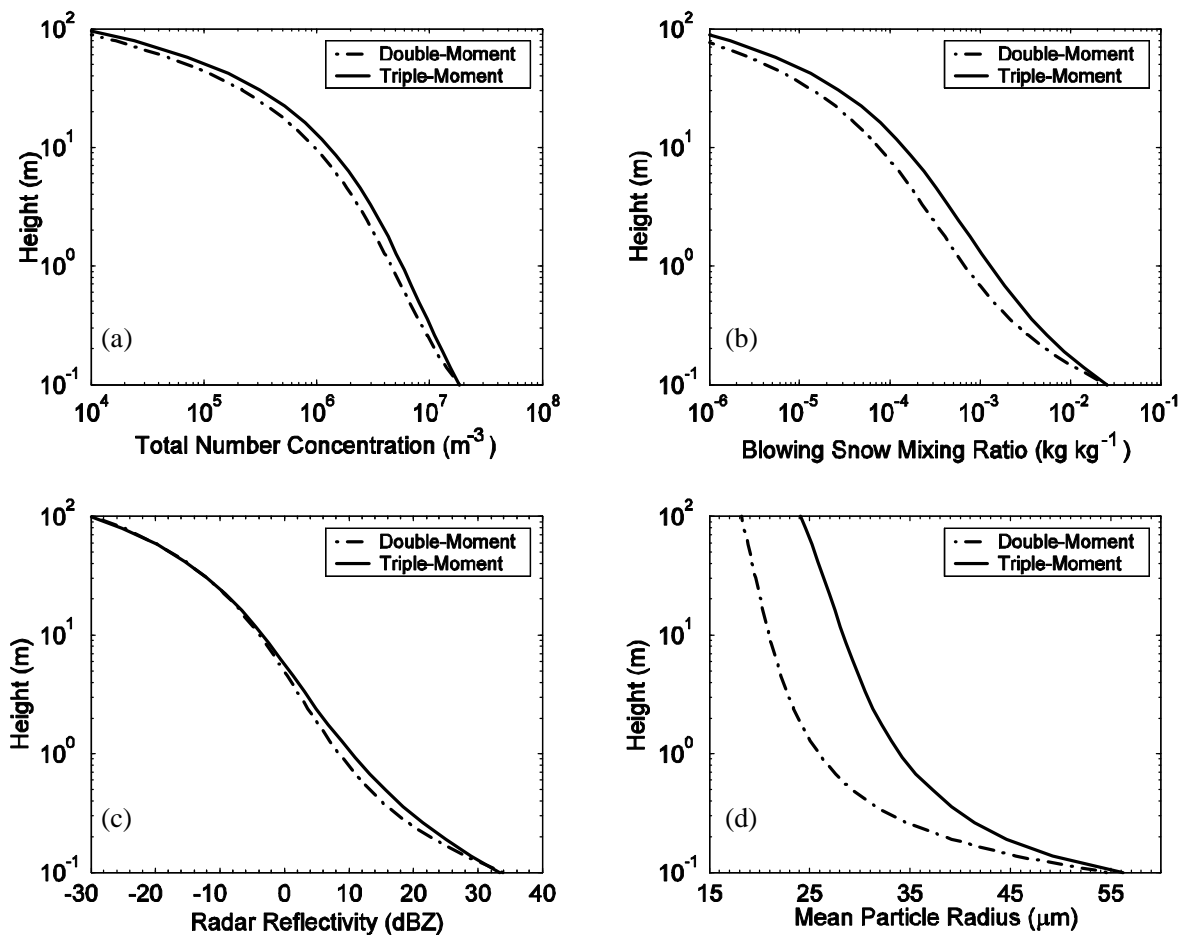


Figure 2: Vertical profiles of (a) number concentration, (b) blowing snow mixing ratio, (c) total radar reflectivity and (d) mean particle radius predicted by the double-moment and triple-moment models 10 min after initialization for the idealized experiment.

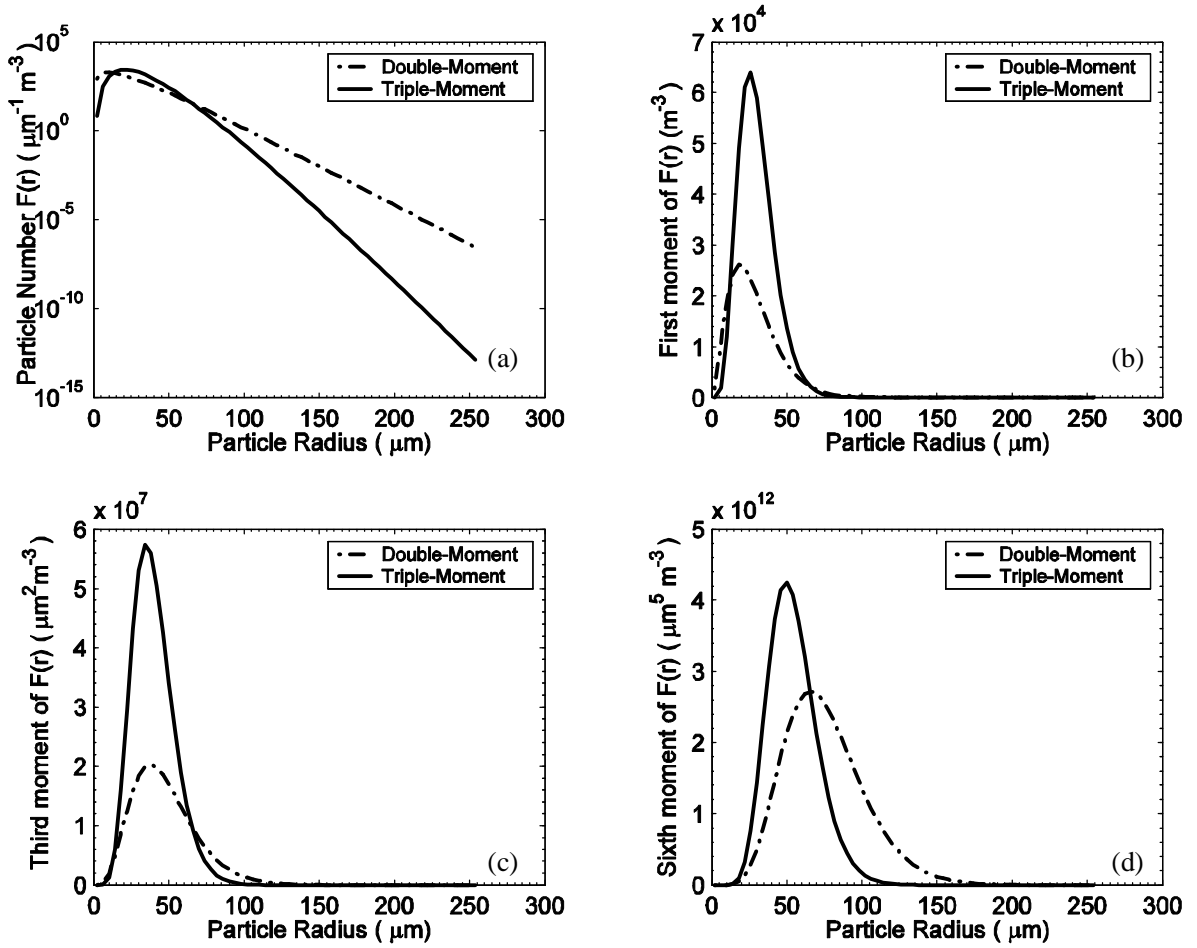


Figure 3: (a) Particle size distribution $F(r)$ at $z = 57.5$ m. Contribution to (b) first moment of size distribution $rF(r)$, (c) third moment of size distribution $r^3F(r)$ and (d) sixth moment of size distribution $r^6F(r)$ predicted by the double-moment and triple-moment models 10 minutes after initialization in the idealized case.

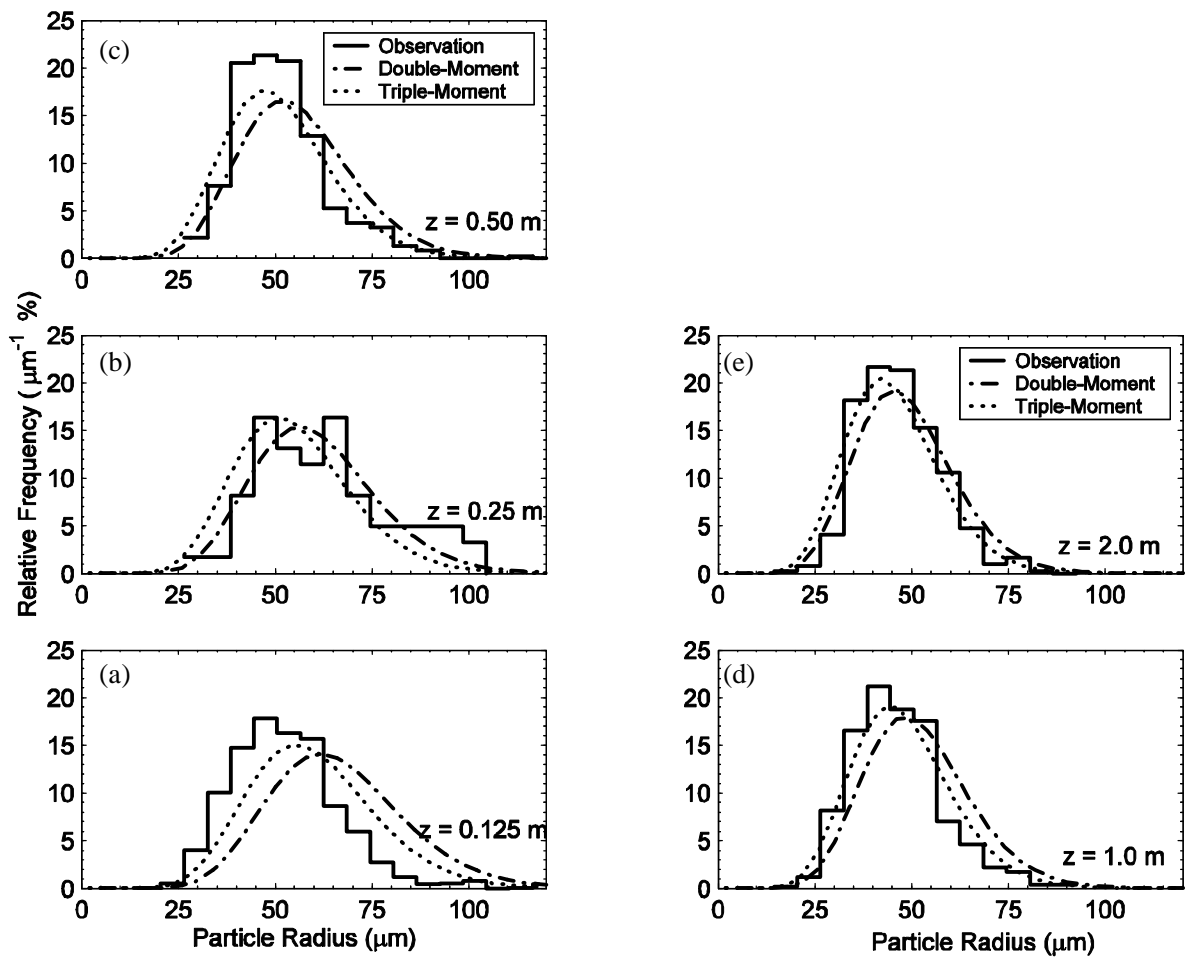


Figure 4: Observed and simulated particle size distributions at five heights 10 min after initialization for the Byrd station runs.

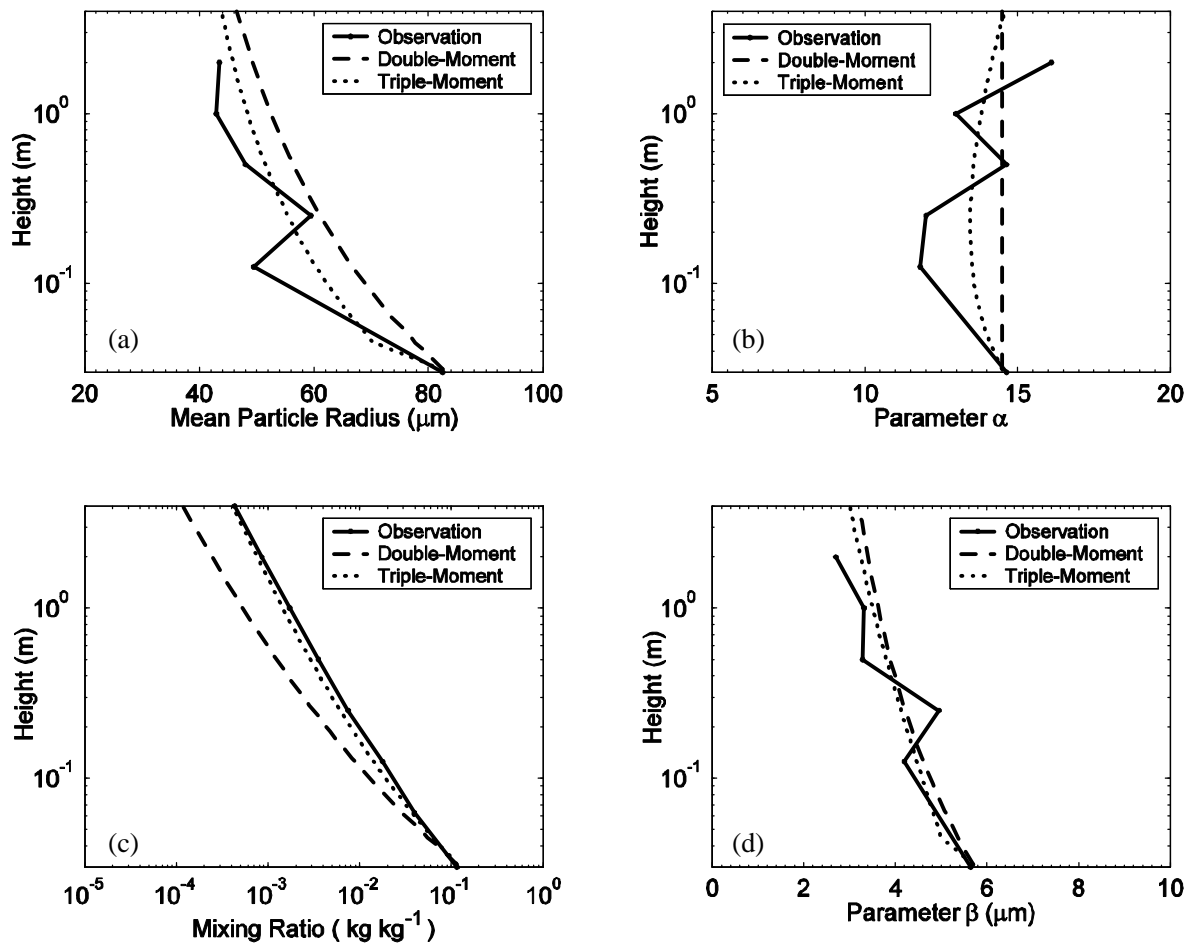


Figure 5: Vertical profiles of (a) mean particle radius, (b) shape parameter a , (c) blowing snow mixing ratio, and (d) scale parameter b from observations and model simulations 10 min after initialization for the Byrd station runs.

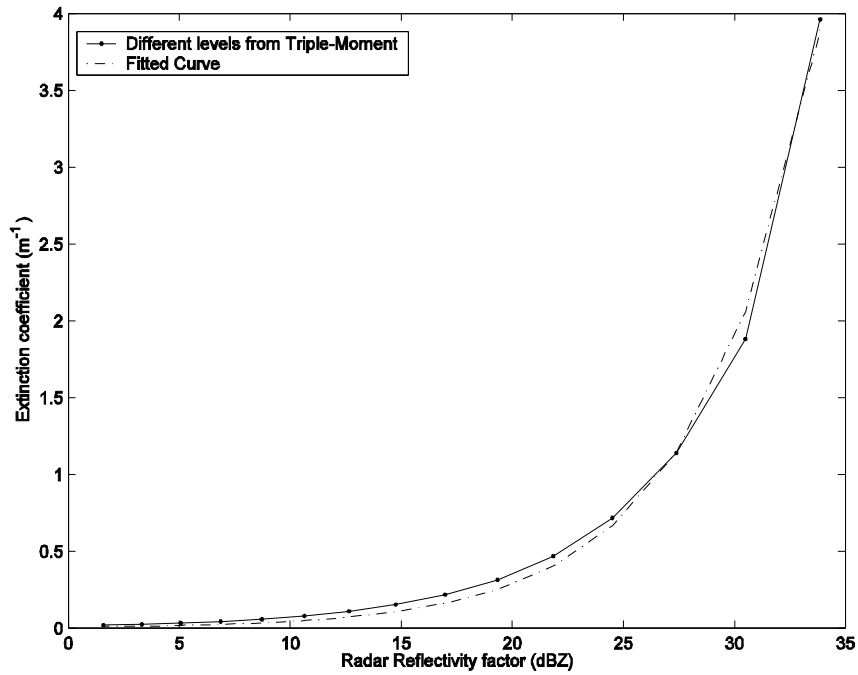


Figure 6: Calculated extinction coefficient versus predicted radar reflectivity factor at different levels from PIEKTUK-T for the Byrd station runs (*solid curve*). *Dashed-dotted* line is the best fit.

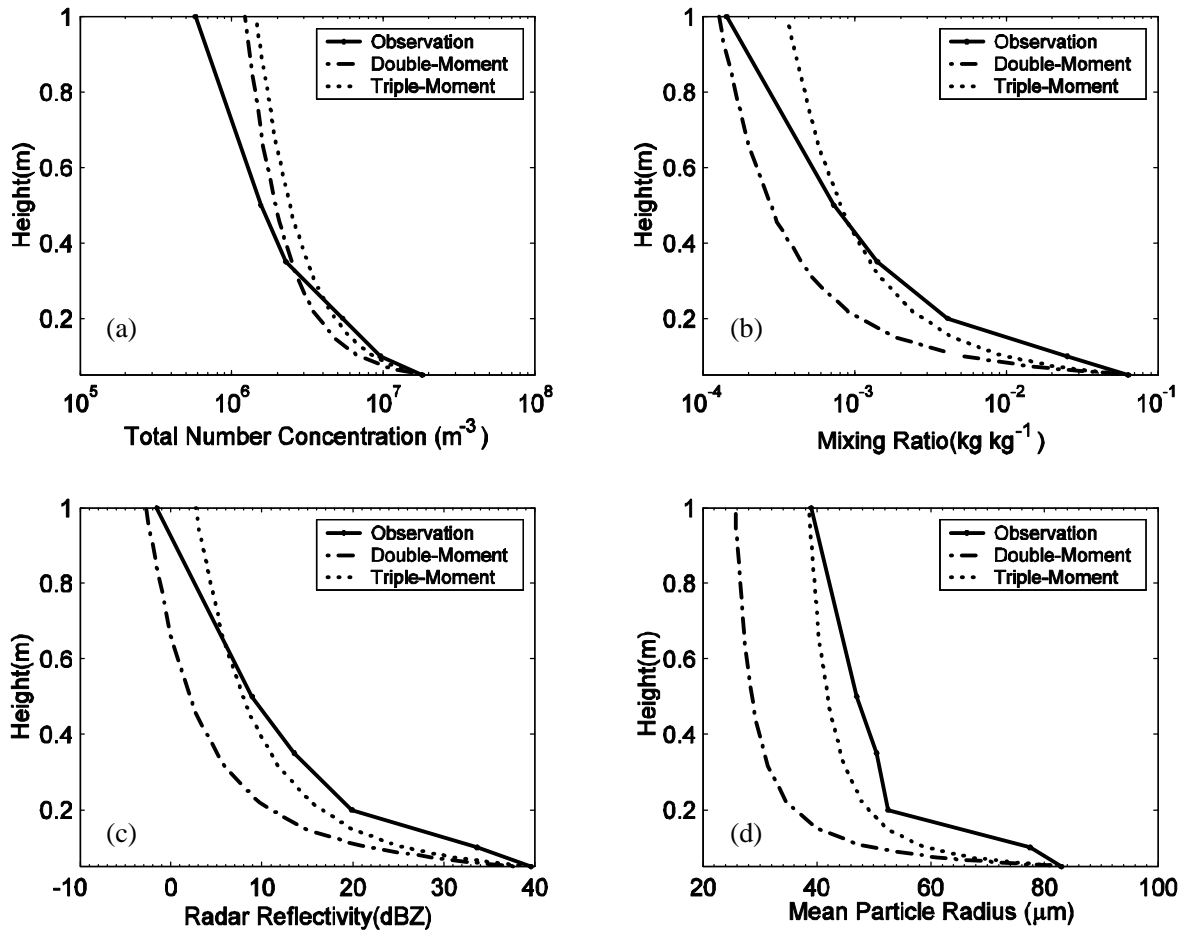


Figure 7: Vertical profiles of (a) number concentration, (b) mixing ratio, (c) radar reflectivity and (d) mean particle radius from observations and simulations 10 min after initialization for the Wyoming site.

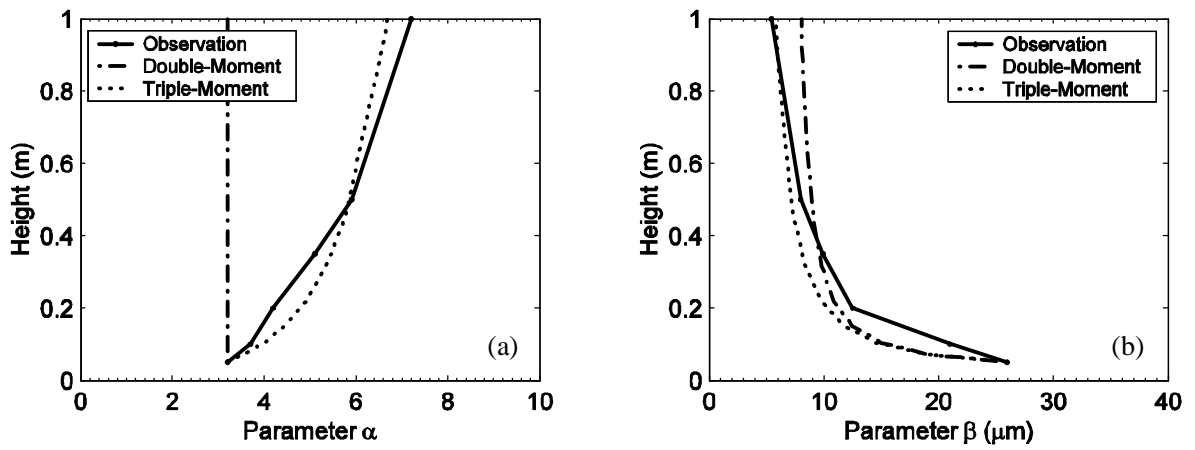


Figure 8: Vertical profiles of (a) parameter a and (b) parameter b from the observations and simulations 10 min after initialization for the Wyoming site.

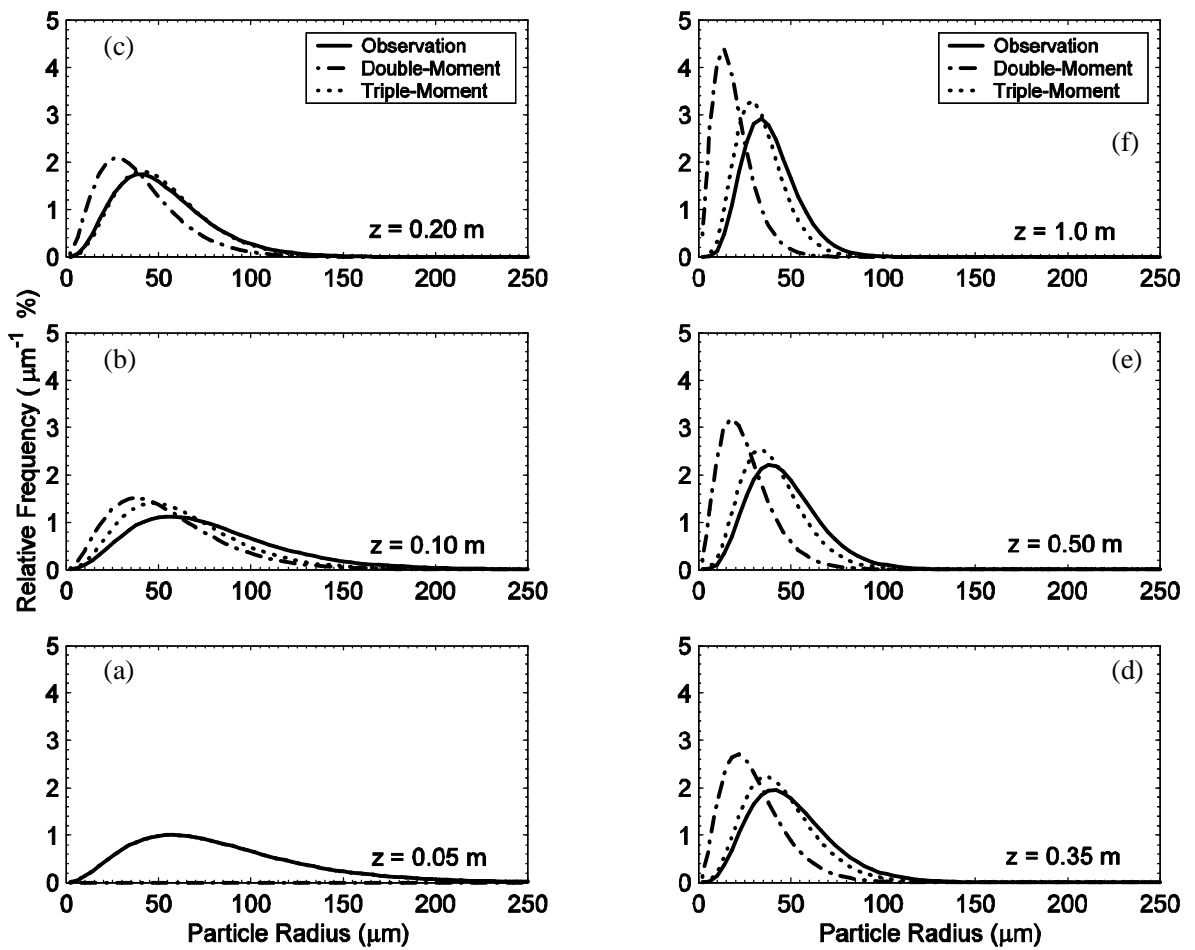


Figure 9: Particle size distribution from observations and simulations at six vertical levels 10 min after initialization for the Wyoming site.

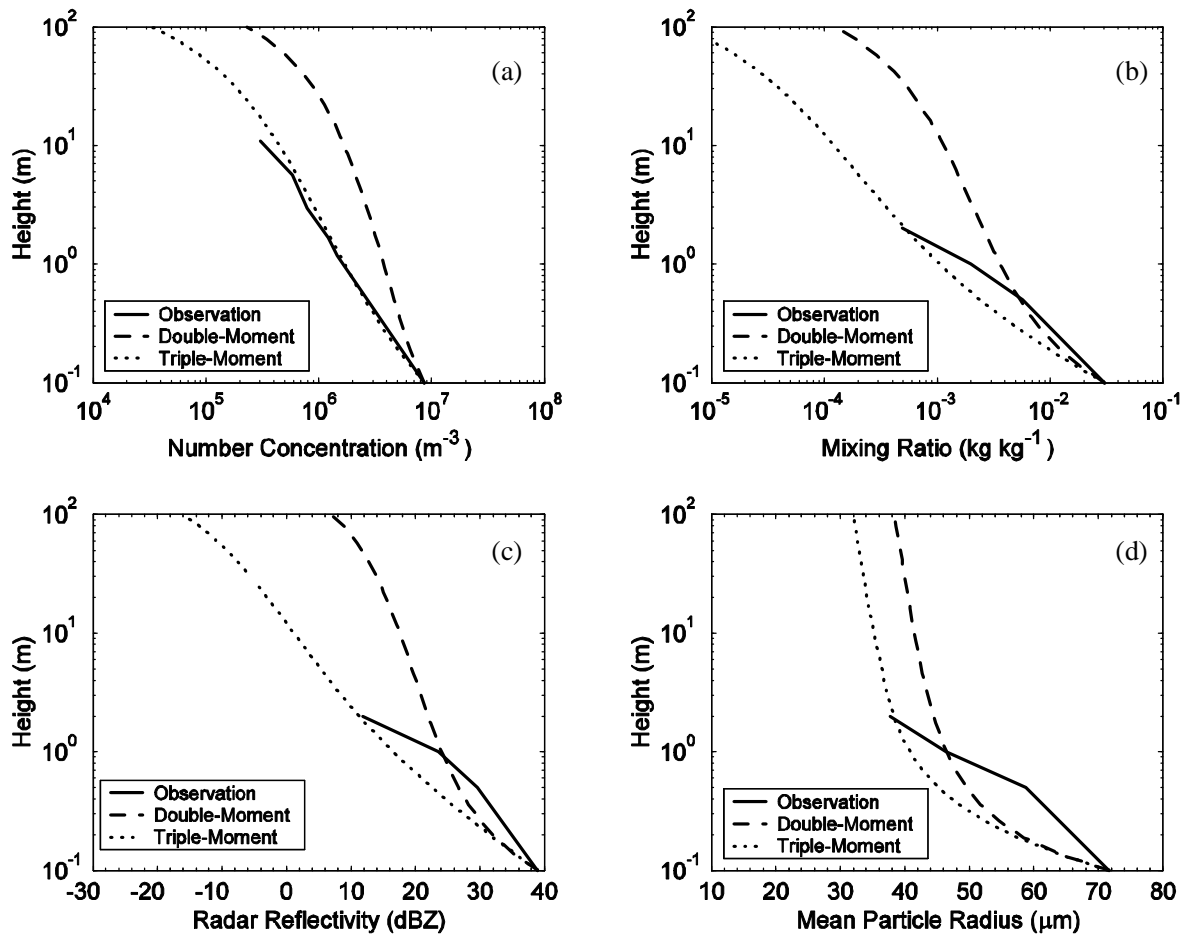


Figure 10: Vertical profiles of (a) number concentration, (b) mixing ratio, (c) radar reflectivity and (d) mean particle radius from observations and simulations 10 min after initialization for the Halley station.

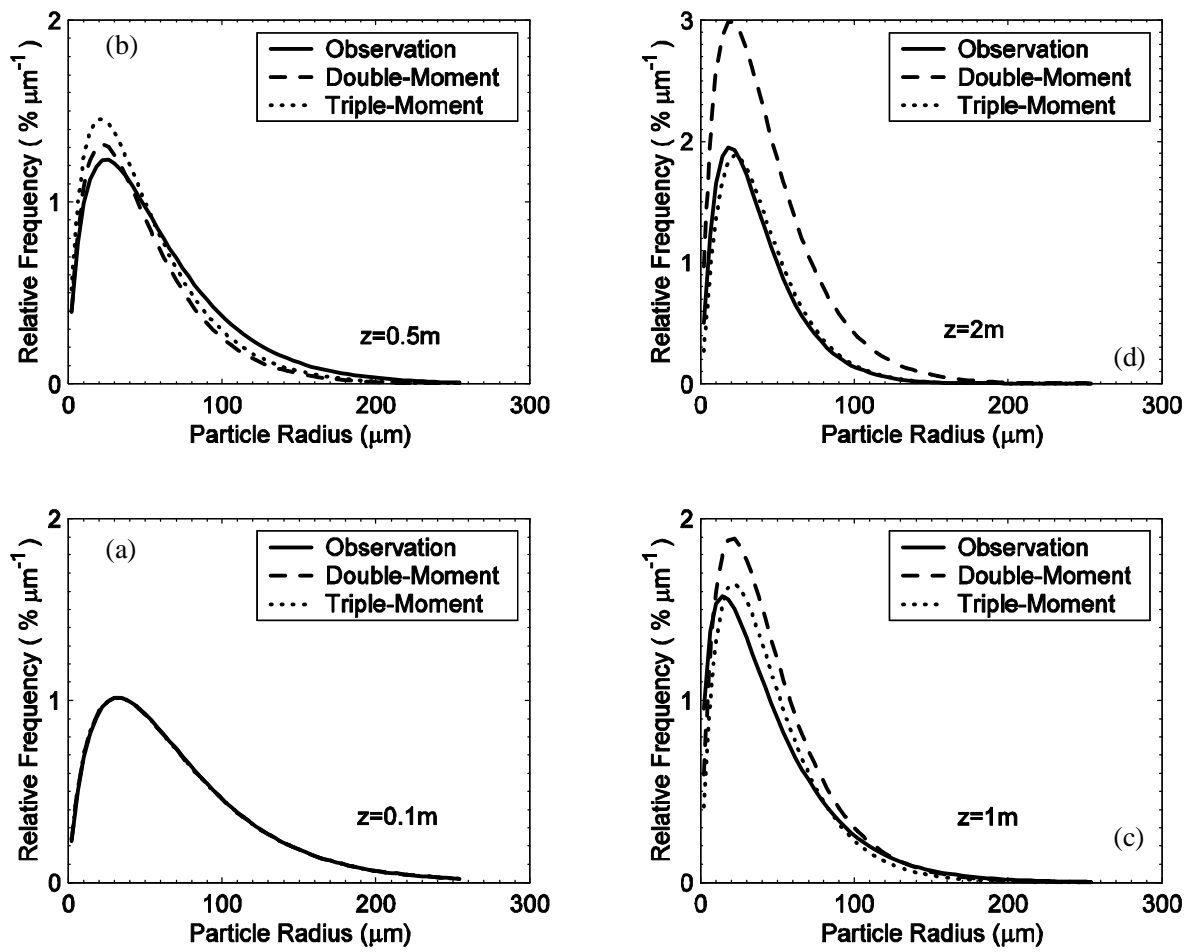


Figure 11: Particle size distribution from observations and simulations 10 min after initialization for the Halley station.

Chapter 3

A triple-moment blowing snow-atmospheric model and its application in computing the seasonal wintertime snow mass budget

The previous chapter described a stand-alone triple-moment blowing snow model, PIEKTUK-T. In order to study blowing snow contributions to the snow mass budget over large temporal and spatial scales, we will couple this one-dimensional model to the atmospheric mesoscale model, MC2. We will be especially interested in a) the interaction between the snow particles and environmental air, b) the horizontal advection and c) entrainment processes. With this coupled model system, it is possible to explore blowing snow transport and sublimation contributions to the snow mass budget over the entire Northern Hemisphere.

This chapter is based on the following submitted/published paper:

Yang, J., M.K. Yau, X. Fang and J.W. Pomeroy, 2010: A triple-moment blowing snow-atmospheric model and its application in computing the seasonal wintertime snow mass budget. *Hydrology and Earth System Sciences Discussion*, **7**, 929-970.

One of the co-author is my supervisor, Dr. M.K. Yau, who provided the normal supervision and contributed to the manuscript editing. The other two co-authors, Xing Fang and Dr. J.W. Pomeroy provided the field data at SNDWA site to verify the simulated snow mass budget. Dr. J.W. Pomeroy also contributed to the manuscript editing.

**A triple-moment blowing snow-atmospheric model
and its application in computing the seasonal wintertime snow mass budget**

Jing Yang¹, M.K.Yau¹, X. Fang² and J. W. Pomeroy²

[1] McGill University, Montréal, Canada

[2] Centre for Hydrology, University of Saskatchewan, Saskatoon, Canada

Correspondence to: Jing Yang (yangj@zephyr.meteo.mcgill.ca)

Abstract

Many field studies have shown that surface sublimation and blowing snow transport and sublimation have significant influences on the snow mass budget in many high latitude regions. We developed a coupled triple-moment blowing snow-atmospheric modeling system to study the influence of these processes on a seasonal time scale over the Northern Hemisphere. Two simulations were performed. The first is a 5 month simulation for comparison with snow survey measurements over a Saskatchewan site to validate the modeling system. The second simulation covers the 2006/2007 winter period to study the snow mass budget over the Northern Hemisphere. The results show that surface sublimation is significant in Eurasian Continent and the eastern region of North America, reaching a maximum value of 200 mm SWE (Snow Water Equivalent). Over the Arctic Ocean and Northern Canada, surface deposition with an average value of 30

mm SWE was simulated. Blowing snow sublimation was found to return up to 50 mm SWE back to the atmosphere over the Arctic Ocean, while the divergence of blowing snow transport contributes only a few mm SWE to the change in snow mass budget. The results were further stratified in 10 degree latitudinal bands. The results show that surface sublimation decreases with an increase in latitude while blowing snow sublimation increases with latitude. Taken together, the surface sublimation and blowing snow processes was found to distribute 23% to 52% of winter precipitation over the three month winter season.

Keywords: blowing snow; surface sublimation; transport; coupled model.

1. Introduction

Snow, the main form of precipitation throughout high latitudes and alpine regions, can accumulate on the land surface for the entire winter season. In fact, the duration of snow cover usually exceeds 180 days in continental areas north of 60°N, where winter storms are common (see, e.g., the weekly NOAA satellite data set, <http://www.ccin.ca/cms/en/socc/snow/snowAtlas.aspx>). Field studies (Pomeroy and Gray, 1990; Pomeroy and Male, 1992; Liston and Sturm, 1998; Bintanja, 1998; Pomeroy and Li, 2000; Box et al., 2004) have shown that the movement of air above a snowpack can impact significantly the surface mass budget. Winds may transport and redistribute snow at the surface leading to heterogeneities in the snow cover. Winds may cause the suspension of blowing snow particles which undergo sublimation when the air is subsaturated with respect to ice. Even when wind speeds do not exceed the threshold for

transport of snow, surface sublimation transfers water vapor directly between the snowpack and the atmospheric boundary layer. Thus surface sublimation, blowing snow transport, and blowing snow sublimation are the three essential processes affecting the spatial and temporal variations of the surface water mass budget at high latitudes and alpine regions.

Over snowpacks, very few direct measurements of turbulent fluxes exist for validation of snow sublimation estimates. There are indirect estimates of turbulent fluxes and parameterization using bulk transfer and flux-gradient techniques, especially over snow-covered sea ice in winter (Andrea, 2002; Andrea et al., 2005; 2008; 2010). Those factors contributing to the difficulties and problems in estimating turbulent exchange from bulk transfer and flux-gradient techniques include stability and small, uncertain exchange coefficients. Typically, snowcovers have low thermal conductivities and high albedos and emissivities, and a snow surface can be very cold, especially at night. This results in increased stability and hence a reduction of turbulent mixing (Male, 1980).

The Monin-Obukhov similarity theory is generally used in stably stratified conditions. The roughness lengths for wind speed, temperature, humidity, and the stability function are thus important factors in estimating the turbulent fluxes. Several stability functions have been proposed (Webb, 1970; Lettau, 1979; Holtslag and de Bruin, 1988; Launianien, 1995; Vihma, 1995; King et al., 1996; Jordan et al., 1999; Andreas et al., 2005; Grachev et al., 2007) and Andreas (2002) found that the one developed by Holtslag and de Bruin (1988) yields the best results in terms of the calculation of the Richardson, Deacon, and turbulent Prandtl numbers in the limit of extreme stable stratification. Nevertheless, radiative flux divergence in the atmospheric surface layer

may cause problem in the application of the Monin-Obukhov similarity theory and limit the universal application of the Holtslag and de Bruin (1988) stability function. More field measurements and further study on turbulent fluxes are therefore warranted.

The uncertainty in the exchange coefficients is further complicated by the fact that the eddy diffusivities for temperature and water vapor are the same but are different from that for momentum, and by low turbulence due to the extreme aerodynamic smoothness of snow surfaces (Male and Granger, 1979). Grachev et al. (2007) give a comprehensive review of the diffusivities in stable stratification based on a very large data set.

Surface sublimation may contribute either positively or negatively to the mass budget, which depends on the humidity gradient between surface and the air above. Male and Granger (1979) showed with lysimeter and profile observations over continuous open snowfields in the Canadian Prairies that surface sublimation was smaller than 0.2 mm day^{-1} . Such small values resulted because sublimation during the day was compensated by condensation at night. Some studies showed that surface sublimation can return a significant amount of the snow mass to the air over high altitude regions. For example, Hood et al. (1999) reported that 15% of the precipitation at an alpine site in the Colorado Rocky Mountains was lost to surface sublimation over the winter season. Over the Greenland ice sheet, the total annual sublimation was estimated to be about $1.85 \times 10^{14} \text{ kg yr}^{-1}$, corresponding to 23% of the annual precipitation (Box and Steffen, 2001). Note, however, that this is due to a combination of surface and blowing snow sublimation. On the other hand, studies over high latitude regions revealed that surface sublimation has small values, and negative sublimation (hereafter deposition) is observed to occur. For example, over Arctic pack ice, the annual surface sublimation was showed to have small

values around 0.03 mm SWE from various studies (Ebert and Curry, 1993; Lindsay, 1998; Persson et al., 2002). Deposition was found to occur in winter and early spring, whereas sublimation was showed to occur in the summer season (Persson et al., 2002). Over the Antarctic, Kameda et al. (1997) reported a downward water vapor flux onto the surface of 5.5 kg m^{-2} at the Dome Fuji observation site. Similarly, King et al. (2001) observed small amounts of deposition during the winter at Halley, Antarctica; whereas surface sublimation can remove around 10% of the precipitation at the same location in summer. Andreas et al. (2004) also demonstrated that deposition dominated most of the time during days 56-150 in 1992 at Ice Station Weddell in Antarctica, with the latent heat flux of $1\text{-}3 \text{ Wm}^{-2}$, equivalent to a daily sublimation of 0.03-0.09 mm SWE.

When surface wind speeds surpass a certain threshold, blowing snow may occur. Blowing snow particles undergo a phase change from ice to water vapor if the air is sub-saturated with respect to ice. Some of the snow mass on the ground can be returned back to the air through blowing snow sublimation, which has been studied at various sites over the Canadian Prairies, and various high altitude and high latitude regions. In the Canadian Prairies, blowing snow sublimation can amount to 29% of the solid precipitation and the measured sublimation rate can be as high as $1.2\text{-}1.8 \text{ mm day}^{-1}$ during blowing snow events (Pomeroy and Essery, 1999). At a high terrain region in southeastern Wyoming, Schmidt (1982) estimated that 39% of transported snow will sublimate. Over an Arctic site, Pomeroy and Li (2000) reported that, on average, 22% of the solid precipitation will be eroded by blowing snow sublimation. In Antarctic coastal regions, observations indicated that the annual blowing snow sublimation can be as much as 170 mm SWE (Snow Water Equivalent) (Bintanja, 1998). All these studies indicated

that blowing snow sublimation is a non-negligible process in the winter water mass budget.

In blowing snow transport, surface inhomogeneity and wind speed accelerations can redistribute snow on different spatiotemporal scales. The surface snow mass change due to blowing snow transport thus has different contributions to the hydrology and climatology, depending on the scales considered. Over the Canadian Prairies, redistributed snow has been shown to be important for fresh water management (Pomeroy and Essery, 1999). In alpine regions, small scale snow redistribution plays an important role in snow packing and the formation of avalanches. At high latitude regions, the mass balance from snow transport over the Greenland and the Antarctic ice sheets can be vital in the study of global sea level changes (Cuffey and Marshall, 2000; Alley et al., 2005).

Field studies are invaluable in research on the surface mass budget. However, they are expensive to carry out. At high latitudes and remote regions, such as over northern Canada, field observations are available only infrequently over a very limited number of sites. The interpretation of the measurements is also subject to a great deal of uncertainty because of the extreme cold temperatures and strong wind conditions encountered (Groisman et al., 1991; Pomeroy and Goodison 1997; Goodison et al., 1998; Déry and Stieglitz, 2002). As a result, numerical modeling has become a useful tool to complement field measurements in the study of the surface water mass budget, and a number of blowing snow models have appeared in the literature (e.g. Pomeroy et al., 1993; Liston et al., 1993; Mobbs and Dover, 1993; Déry et al, 1998; Mann et al., 2000; Bintanja, 2000; Déry and Yau, 2001b). These models range from the computationally

demanding spectral bin model (Déry et al, 1998) to the computationally efficient bulk single moment (Déry and Yau, 1999), double moment (Déry and Yau, 2001b), and triple-moment (Yang and Yau, 2008) models.

Typically the blowing snow models are used in a stand-alone mode to compute the blowing snow sublimation in an air column over a fixed site or fetch. Consequently, mass budget calculations on large spatial and temporal scales are scarce; with a few exceptions that include the work of Déry and Yau (2002), Sugiura and Ohata (2008), and Box et al (2004). In these studies, a blowing snow model is employed to develop a parameterization for blowing snow sublimation. The parameterization is then used in conjunction with a global or a regional meteorological dataset, like the ECMWF reanalysis or the output from a regional climate model, to compute the blowing snow fluxes like sublimation. This strategy however may suffer from a number of shortcomings. In particular, a parameterization is usually developed using the model runs and observations from one site and therefore may yield large errors over other sites. In addition, the meteorological or regional climate model datasets usually have coarse spatial and temporal resolutions and may not adequately resolve the mesoscale structures influencing blowing snow (Stewart et al., 1995). Moreover, a stand-alone blowing snow model acts like an isolated air column and it is difficult to account for processes like horizontal advection, lateral entrainment and the interaction between blowing snow and the atmospheric boundary layer.

To alleviate these problems, Déry and Yau (2001a) coupled a double moment blowing snow model to a mesoscale atmospheric model MC2 (version 3.2, see Benoit et al. 1997), and applied the modeling system to simulate a blizzard event over the Arctic.

Because version 3.2 of MC2 is not a parallel code, they were able to perform a simulation of only 48 hours duration over a region of the Arctic. With the advent of powerful computer clusters and the availability of a parallel MC2 code (Benoit et al., 1997; Thomas et al., 1998) (version 4.9.8), it is possible to develop a new coupled blowing snow-atmospheric model to perform seasonal simulations over the entire hemisphere.

The goal of this study is to develop a new parallel blowing snow-atmospheric modeling system by coupling the triple-moment blowing snow model of Yang and Yau (2008) to version 4.9.8 of MC2. The new modeling system will be applied to study the influence of surface sublimation, and blowing snow sublimation and transport on the snow mass budget over the Northern Hemisphere on a seasonal time scale. The paper is organized as follows. Section 2 describes the coupled modeling system and the experimental design. Section 3 contains results of Simulation 1 to validate the modeling system against measured snow depths at the St. Denis National Wildlife Area (SDNWA) in south-central Saskatchewan. The results of the computed seasonal snow mass budget over the Northern Hemisphere are presented in Sect. 4. A comparison with computations using some empirical formulas forms the subject of Sect. 5. A discussion and conclusions are given in Sect. 6 and 7, respectively.

2. Modeling system

In this section, we briefly describe the mesoscale MC2 model and the triple-moment blowing snow model (PIEKTUK-T), followed by the coupling strategy and experimental design.

2.1 MC2 model

The Canadian Mesoscale Compressible Community Model (MC2) is a nonhydrostatic, limited area model with a comprehensive physics package. The governing equations are solved using a semi-implicit semi-Lagrangian algorithm. Topographic effects are included through the use of the terrain-following Gal-Chen coordinates. The model has been applied in various applications, including the simulation of tropical convection (Nagarajan et al. 2001), hail storms (Milbrandt and Yau, 2006), mid-latitude cyclones (Misra et al. 2000) and Arctic ground blizzard (Déry and Yau 2001a). Interested readers are referred to Benoit et al. (1997) and Mailhot et al. (1998) for detailed description of the dynamical core and physics package in the model.

In our simulations, MC2 is configured to include surface fluxes aggregated over land, water, glacier and sea ice based on the force–restore concept of Deardorff (1978), within which snow is considered as the first layer. The treatment of atmospheric boundary layer (ABL) processes is based on a turbulent kinetic energy scheme developed by Mailhot and Benoit (1982) and Benoit et al. (1989). Although not expected to be a significant factor in winter situation, large-scale convection is parameterized by following a Kuo-type scheme implemented by Mailhot and Chouinard (1989). The Kong and Yau (1997) explicit microphysics package determines the grid scale cloud and precipitation through microphysical processes involving water vapor, cloud water, rainwater, ice/snow and graupel.

2.2 Blowing snow model

The triple-moment blowing snow model PIEKTUK-T (Yang and Yau, 2008) is a physically based one-dimensional column model including the processes of vertical turbulent diffusion, sedimentation and sublimation of blowing snow. It represents an extension of the double-moment model PIEKTUK-D (D ery and Yau, 2001b) by assuming that the size distribution of blowing snow is governed by a three parameter gamma function. By predicting three moments of the size distribution, namely the zeroth moment or the total number concentration N (m^{-3}), the third moment which is related to the blowing snow mass mixing ratio q_b (kgkg^{-1}), and the sixth moment the radar reflectivity Z (m^6m^{-3}) which has monotonic relationship to the extinction coefficient of blowing snow particles and visibility, the evolution of the size distribution and the sublimation of blowing snow can be completely determined. PIEKTUK-T also includes predictive equations for air temperature T_a (K) and water vapor q_v (kgkg^{-1}) to allow for thermodynamic feedback from blowing snow sublimation which acts as a source of water vapor and a sink of heat. Following D ery and Yau (1999), blowing snow is activated when the surface is snow covered, the temperature is colder than 0°C , and the wind speed surpasses a certain threshold given by Li and Pomeroy (1997)

$$U_t = 6.98 + 0.0033(T_a + 27.3)^2 \quad (1)$$

Here, T_a is the 2-m air temperature and U_t is a threshold for the wind speed at 10 m height. This empirical equation was developed from six years of hourly meteorological data from 16 Canadian prairies stations. It demonstrates that the threshold wind speed has a close relationship with the surface air temperature. If the temperature is relatively warm, say greater than -10°C , cohesive forces increase dramatically with increasing temperature due to the increase of liquid water surrounding the snow crystals. If the

temperature is very cold, elasticity and kinetic friction increase with the decreasing temperature, resulting in increased shear stress to initiate snow transport. Therefore, the intermediate temperature range $-30^{\circ}\text{C} < T_a < -10^{\circ}\text{C}$ would provide favorable conditions for snow transport. We emphasize that, computationally, PIEKTUK-T is much more efficient than the spectral PIEKTUK model (Déry et al., 1998) and is therefore the preferred choice for coupling to the atmospheric model MC2.

2.3 Coupling strategy

Our coupling strategy followed closely Déry and Yau (2001b). Since blowing snow reaches altitudes of only tens to a few hundred metres (King and Turner 1997), 24 levels are used in PIEKTUK-T at heights of 0.10, 0.15, 0.22, 0.33, 0.50, 0.74, 1.11, 1.66, 2.48, 3.70, 5.51, 8.23, 12.3, 18.3, 27.3, 40.8, 60.8, 90.7, 135.3, 201.9, 301.2, 449.3, 670.3, and 1000 m. For MC2, 46 levels are used with the lowest 12 levels (starting at 12.3 m) matching those of PIEKTUK-T. The remaining 34 levels above 1 km in MC2 are uniformly spaced with a vertical grid size of 500m. The top of the MC2 domain is set at 18.5 km. The time steps for PIEKTUK-T and MC2 are 5 s and 60 s, respectively.

The sequence of computation during a typical MC2 time step in a coupled simulation of the two models is as follows. First, the MC2 model computes the 3-D semi-Lagrangian advection of predictive quantities including the winds, q_v , and T_a . The 3-D semi-Lagrangian advectations of q_b , N , and Z are also performed by the MC2 for matching levels (i.e., $12.3 \text{ m} \leq z \leq 1 \text{ km}$). For levels exclusive to PIEKTUK-T ($z < 12.3 \text{ m}$), it was assumed that vertical advection is small such that MC2 performs only the horizontal advection of q_b , N , and Z there. In addition, the horizontal wind components are

prescribed using a typical logarithmic profile below $z = 12.3$ m. Next, MC2 calculates the thermodynamic tendencies that arise from microphysical activities before calling the PIEKTUK-T subroutine.

Vertical profiles of q_v , T_a , U , V , q_b , N , and Z are thus transferred to the blowing snow model. Upon receiving this information, PIEKTUK-T first checks whether the blowing snow criteria are met at each grid point. If the criteria are satisfied, PIEKTUK-T then initializes its dynamic and thermodynamic profiles using those of MC2 for their coincident levels (i.e., $12.3 \text{ m} \leq z \leq 1 \text{ km}$). At other PIEKTUK-T levels ($z < 12.3 \text{ m}$), the initialization of the dynamic and thermodynamic profiles is conducted following Déry and Yau's (2001b) methodology. In brief, they assume that the relative humidity with respect to ice RH_i follows a logarithmic profile from the measurement height of 2 m down to the snow surface, at which saturation with respect to ice is assumed. In the coupled simulation, we follow the same methodology to initialize RH_i with the exception that the "measurement height" is at $z = 12.3 \text{ m}$, the first matching vertical grid point of the two models.

Using the diagnosed surface ($z = 0$) and prognosed air ($z = 12.3 \text{ m}$) temperatures of the MC2 model, we similarly prescribe an initial T_a that is also based on similarity theory for $z < 12.3 \text{ m}$. PIEKTUK-T then numerically integrates its five prognostic equations using a time step of 5 s. In PIEKTUK-T, blowing snow particles are susceptible to sublimation, diffusion, and sedimentation. The sedimentation velocities for q_b , N and Z are bulk values weighted by the respective moments of the size distribution. q_v and T_a are affected only by diffusion and blowing snow sublimation. Because q_v and T_a have already undergone vertical diffusion within MC2, we have opted to diffuse only the

thermodynamic perturbations due to blowing snow sublimation within PIEKTUK-T. Having integrated to a full MC2 time step (i.e., 12 PIEKTUK-T time steps), PIEKTUK-T then outputs the column-integrated sublimation and transport rates of blowing snow. The associated thermodynamic tendencies for q_v and T_a from PIEKTUK-T are applied to the matching levels of MC2. The MC2 model finally adjusts the T_a and q_v fields before repeating this sequence of events until the end of the integration.

2.4 Experimental design

Two distinct experiments are conducted. The purpose of Simulation 1 is to verify that the coupled model can produce reasonable results against snow measurements over the St. Denis National Wildlife Area (SDNWA, 52.03°N, 106.1°W) in south-central Saskatchewan (Fang and Pomeroy 2009). The model domain consists of 180x180 grid points centered over SDNWA. A five month simulation, from 31 October 2005 to 27 March 2006, was conducted. The purpose of the second experiment, Simulation 2, is to obtain quantitative estimates of the surface mass and blowing snow budget over the Northern Hemisphere during the winter season of 2006-2007. In this case, the model domain has 640x640 grid points centered over the North Pole. The integration covers the period from 1 December 2006 to 28 February 2007. Both simulations are conducted at a horizontal spacing of 18 km and are initialized at 0000 UTC, and the lateral boundary conditions are updated every 6 h using the CMC (Canadian Meteorological Centre) global analysis.

To minimize errors arising from a regional model integrated over long time duration, we adopted the strategy of Guichard et al. (2003) by conducting the simulations as a

sequence of 54-h integrations. Every two days, a 54-h mesoscale numerical simulation was performed with initial and lateral boundary conditions interpolated from CMC analysis data. A time series is then constructed by discarding the first 6 h of each 54-h run to avoid the problem of spin-up, and then combining the remaining 48-h simulation periods to construct the long time integration.

3. Results of Simulation 1

Before applying the coupled MC2-PIEKTUK-T model to the computation of the seasonal snow and blowing snow budgets over the Northern Hemisphere, it is desirable to establish its validity by comparing with field measurements. To this end, we will compare model results with snow survey observations from a field experiment over SDNWA in south-central Saskatchewan (Fang and Pomeroy 2009). The SDNWA is a small basin with an area of 3.85 km². Snow surveys were carried out from January to April 2006 along four transects within the basin, and snow depth and snow density measurements are available every 5 m and 20 m interval along the transects. The total number of sampling points is 138.

Hourly meteorological observations, such as air temperature, relative humidity, 10-m wind speed and snowfall rate, were also recorded at the automatic weather station within SDNWA (Fig. 1). Snowfall rate was measured by Alter-shielded Geonor precipitation gauge, and corrected for wind-undercatch using the algorithm of MacDonald and Pomeroy (2008). The air temperature falls below 0°C starting in November and snowfall is observed from November to April. There were 9 snow survey days during the period from 3 January to 27 March 2006 before snowmelt. Table 1

displays the snow density, snow depth and Snow Water Equivalent (SWE) averaged over the 138 samples in the 4 transects over the basin for the 9 days. The increase in SWE with time before 8 March and the decrease thereafter is consistent with the heavier snowfall before 8 March and much lighter snowfall thereafter depicted in Fig. 1. The decrease in SWE may be an indication that surface sublimation and blowing snow processes have contributed to changes in the surface mass balance.

Figure 2 shows the blowing snow sublimation over SDNWA from Simulation 1. The data points represent the sublimation over a 48-h period in each segment of the simulation discussed in Sect. 2.4. Episodes of blowing snow were simulated and the peak sublimation was around 0.35 mm SWE. For comparison, the stand-alone PIEKTUK-T, driven by the hourly observed meteorological fields in Fig. 1 as input, was also run. The calculated sublimation rates, also plotted in Fig. 2, indicate very good agreement with the coupled model results. Additionally, we calculated the total blowing snow sublimation over SDNWA from Simulation 1. Its value of 2.13 mm SWE is of the same order of magnitude as the 3.7 mm SWE computed using the fully distributed Prairie Blowing Snow Model at 6-m grid cell resolution (Fang and Pomeroy, 2009).

To calculate the snow mass from Simulation 1 to compare with the observed snow depth, we make use of the expression for the time rate of change of snow mass, B , given by Pomeroy and Essery (1999) as

$$B = P - E - Q_s - \nabla \cdot \vec{Q}_t \quad (2)$$

where P is the snowfall flux, E is the sublimation flux from the surface snow cover, Q_s is the blowing snow sublimation, and the last term is the divergence of blowing snow transport. The snowfall flux is predicted by the microphysics scheme in MC2. The details

of the calculation of the remaining three terms on the right of Eq. (2) are given in Equations (5)-(7) in Sect. 4. Snow melt and runoff are neglected because of subfreezing conditions.

The snow mass as a function of time in Simulation 1 is obtained by integrating Eq. (2) with respect to time from 0000 UTC 31 October 2005, with the initial snow depth given by the CMC analysis. Figure 3 depicts the measured snow accumulation (mm SWE) averaged over the basin for the 9 days (last row in Table 1) as well as the computed values from Simulation 1. Except for 8 March, the simulated snow depth is somewhat larger than the observed depth. However, the slopes of the curves are quite similar. This indicates that the coupled model captures well the time rate of change of snow depth. The magnitude of the difference between the simulated and the observed snow depths is also consistent with that found in Fang and Pomeroy (2009) using a different stand-alone blowing snow model. The reasonable agreement of the results lends support to the validity of applying the coupled model system to the study of seasonal snow mass budget over large areas.

4 Results of Simulation 2

4.1 Comparison with surface measurements

Air temperature, relative humidity, and wind speed are the three important factors determining the onset of blowing snow, blowing snow sublimation, and blowing snow transport. To gauge the performance of the coupled model to simulate these variables, comparison will be made with observations at two automatic weather stations which recorded the highest frequency of blowing snow events over Canada. Baker Lake (64.3°N,

96.08°W) had a total of 384 h of blowing snow during the winter season of 2006/2007. Rankin Inlet (62.82°N, 92.12°W), another observation site located in the Nunavut Territories, had an average temperature of -25°C and 462 h of blowing snow over the same period.

Figures 4 and 5 depict the simulated and hourly observed values of surface temperature, wind speed, relative humidity with respect to ice, and surface pressure at Baker Lake and Rankin Inlet respectively. The simulated values were obtained from three hourly model output interpolated to the location of the stations. The observed relative humidity with respect to water RH was converted to the relative humidity with respect to ice RH_i using

$$RH_i = \frac{q_v}{q_{si}} = \frac{q_v}{q_s} * \frac{q_s}{q_{si}} = RH * \exp\left((T_a - T_0) * \left(\frac{17.27}{T_a - 35.86} - \frac{21.87}{T_a - 7.66}\right)\right) \quad (3)$$

where q_s and q_{si} are the saturation mixing ratio with respect to water and ice respectively, and $T_0 = 273.16$ K. The minimum, maximum and mean values of these variables, together with the correlation coefficients between the simulation and observation over the whole winter season, are also tabulated in Table 2.

As indicated, the simulated surface pressure follows closely the observed at Baker Lake (Fig. 4) and the correlation coefficient has a high value of 0.97 (Table 2). The seasonally averaged pressure is around 1011 mb with minimum and maximum values at 979.1 and 1034.6 mb respectively. The simulated and observed screen level temperatures also agree well, with a correlation coefficient around 0.85. The range of temperature spans from -37.5°C to -11.6°C and the seasonal mean value is -25.5°C. This mean value is close to the optimal temperature of -27°C which corresponds to the smallest wind

threshold for the initiation of blowing snow according to the empirical relation proposed by Li and Pomeroy (1997). They noted that if the surface temperature is too cold, cohesion associated with strengthening elastic and frictional forces reduces the wind capacity to displace snow from the surface and a higher wind threshold is required. On the other hand, if the temperature is too warm, some of the melted snow water will increase the cohesion among the particles, and a high wind threshold is needed to eject snow particles.

The measured wind speed generally exhibits high temporal and spatial variability and it is a challenge to compare the instantaneous winds from a 18-km resolution model with the hourly averaged point observations. Nevertheless, Fig. 4 shows that the model wind follows the evolution of the observed 10-m wind quite well although the correlation coefficient is only 0.71. The mean wind speed of about 6 ms^{-1} is not particularly strong. It is therefore the intermittent peak wind values that cause frequent blowing snow events at Baker Lake. In comparison, the correlation coefficient is the lowest for the relative humidity with respect to ice. Nevertheless, the agreement of the mean value and the range is still reasonable.

In general, a similar picture emerges for Rankin Inlet (Fig. 5 and Table 2), with the evolution of the surface fields reasonably well captured by the coupled model. Since these surface fields are the key parameters in determining the heat and moisture exchanges between blowing snow particles and the atmosphere, the reasonable performance of the coupled model in the simulation of surface variables is gratifying and lends support to the validity of the computed surface mass budgets.

4.2 Results of water mass budget

We present in this section some details of the calculation and the results of the Northern Hemisphere seasonal distribution of the three terms on the right of Eq. (2) – the blowing snow transport, blowing snow sublimation and surface sublimation.

4.2.1 Blowing snow transport

The zonal and meridional components of blowing snow transport \dot{Q}_i are given by

$$Q_{tx} = r \int_{z_{lb}}^{z_{ub}} q_b(z) U(z) dz \quad , \quad Q_{ty} = r \int_{z_{lb}}^{z_{ub}} q_b(z) V(z) dz \quad (4)$$

where r is the air density, q_b is the blowing snow mixing ratio, and U and V are the zonal and meridional wind speed at height z respectively. z_{lb} and z_{ub} are the lower and upper level of the blowing snow model, with values of 0.12 m and 1000 m respectively. The seasonal transport is the accumulation of the whole column-integrated mass transport over the three winter months.

Figure 6 displays the magnitude of the seasonal blowing snow transport (in color) and the transport vectors (indicated by arrows) over DJF 2006/2007. Transport events occur mostly over the Pan Arctic areas, the Bering Sea between Alaska and Russian, the Sea of Okhotsk, Greenland, the Davis Strait, and Hudson Bay. At the coastal edge of Greenland, strong katabatic winds transport large quantities (up to 2000 Mg m⁻¹) of snow mass from the ice sheet to the ocean. The winds result from radiative cooling over the very high topography of Greenland, creating bitterly cold air temperatures and air with high density. There is thus a semi-permanent high pressure center over the interior of the Greenland Ice Sheet. Additionally, our simulation also indicates a series of synoptic scale

cyclones moving northward to the east side of Greenland (not shown) resulting in the establishment of a prominent climatological low pressure center between southeastern Greenland and Iceland. The outward pressure gradient force between this low and the semi-permanent high over the continent then results in strong surface wind sweeping down to the coast. The down-slope katabatic wind at the coastal edge of Greenland is often very strong and results in the frequent occurrence of blowing snow and large transports of snow to the ocean.

Over the Arctic Ocean, the seasonal mass transport is circumpolar around the North Pole, with the largest values on the Alaskan side and the northeast of Greenland. These areas of large transport correspond to regions of strong winds located at the edge of semi-permanent Aleutian low and the Icelandic low. Over the continent, local maxima are also found in Kazakhstan, Mongolia, the northern Canadian Arctic, the subarctic tundra-forests, as well as the Great Plains east of the Rocky Mountains. The transports over continent are less than 100 Mg m^{-1} , almost one order of magnitude smaller than those over the frozen Ocean.

The horizontal divergence of the transport is the net contribution to the surface mass budget, and is written as:

$$D = \nabla \cdot \mathbf{Q}_t = \left(\frac{\partial Q_{tx}}{\partial x} + \frac{\partial Q_{ty}}{\partial y} \right) \quad (5)$$

with x and y being the horizontal distance in the zonal and meridional directions, respectively. The divergence at a given grid point is calculated from the four neighbouring grid points. The horizontal divergence of the snow will lead to a net mass erosion over windswept open areas and accumulation at other deposition areas where

surface friction increases or wind decelerates. Figure 7 depicts the spatial pattern of the divergence of blowing snow transport over DJF 2006/2007. Most areas in the frozen Arctic Ocean experience snow mass loss by wind redistribution with typical magnitudes of about 1 mm SWE. The divergence rates are typically no more than a few mm SWE, except in some localized areas and coastal regions where values can reach 30 mm SWE. Prominent areas of convergence are mainly located at the marginal sea ice zones, where the sea ice cover gradually disappears.

Over the continents, the divergence and convergence areas are in close proximity, indicating that blowing snow redistribution may be important in the surface water budget at small scales. However, when averaged over large scales, the contribution of transport would not be very significant since positive and negative divergences largely cancel one another. Pomeroy and Li (2000) also pointed out that using different fetch length can affect the calculation of the divergence of snow transport on snow erosion.

4.2.2 Blowing snow sublimation

During the transport of blowing snow, the suspended particles will experience sublimation if the air is subsaturated with respect to ice. The bulk sublimation rate Q_s (mm SWE) for the whole air column over a unit horizontal area is

$$Q_s = -r' \int_{z_{lb}}^{z_{ub}} S_b dz \quad (6)$$

where S_b ($\text{kgkg}^{-1}\text{s}^{-1}$) denotes the blowing snow sublimation rate which is a function of the temperature and water vapor deficit. The symbol r' is a unit conversion factor that gives the sublimation in units of SWE. The negative sign in Eq. (6) denotes that

positive/negative values correspond to sublimation/deposition. Integrating the bulk sublimation rate with time produces the accumulated column sublimation.

Figure 8 shows the simulated seasonal blowing snow sublimation over DJF 2006/2007. There are several areas of maxima similar in location to those of blowing snow transport. Although blowing snow events occur frequently there, the sublimation is constrained by the very cold temperature and high relative humidity. It is clear that sublimation is more active along the high latitude coasts such as Greenland, Bering Strait, the Sea of Okhotsk, Baffin Basin and Davis Strait. Over the frozen Arctic Ocean, values are smaller but can nonetheless reach values up to 50 mm SWE. Sublimation is more moderate over the continent, and local maxima can be found in the Inner Mongolia Autonomous Region in China, the northwest of Mongolia, central Kazakhstan, Scandinavia, Northern Siberia and the US Great Plains. In comparison, for most parts of Siberia and open sites in the Canadian boreal forest region, blowing snow sublimation is much less than the Canadian prairies.

Vegetation data from the US Geological Survey (USGS 2002), which are used in our simulation, indicate largely evergreen needle-leaf trees and mixed wood forests over the Canadian boreal forests, and deciduous needle-leaf trees over Siberia (Fig. 9a-c). These tall trees result in larger roughness lengths over forested area above the trees than over the tundra and prairies (Fig. 9d). Within the forest canopy, winds are greatly reduced and do not reach the wind threshold for blowing snow for surface snow within the forest canopy. Indeed, if a fully operational land surface scheme such as CLASS (Verseghy, 2000) is used, the presence of vegetation would cause sub-canopy wind

speeds to be extremely low resulting in almost no blowing snow transport or sublimation where there are forests (Pomeroy et al., 1999).

4.2.3 Surface sublimation

Surface sublimation is the turbulent water vapor flux between the surface and the lowest layer of the atmospheric boundary layer. The turbulent flux in the thin turbulent region in the coupled model is calculated using Monin-Obukhov similarity theory but with a non-constant transfer coefficient when the stratification is stable (Delage, 1997). This surface sublimation over snow cover is calculated as:

$$E = \overline{rw'q_s'} = rC_D U^* (q_{surf} - q_a) \quad (7)$$

where q_{surf} and q_a are the specific humidity at the surface and lowest atmospheric level respectively and U^* is the friction velocity. The humidity q_{surf} is assumed saturated with respect to ice at the surface temperature. C_D is an integrated bulk transfer coefficient over the surface layer, determined by the surface roughness and a stability function

$$C_D = \frac{1}{k} \int_{z_0}^{z_a+z_0} (1 - z/h_e) j(z/L) \frac{dz}{z} \quad (8)$$

where k is Von Kármán constant and L is the Obukhov length, and z_0 , z_a and h_e indicate the roughness lengths for moisture, surface height and boundary layer height for the stable case, respectively. In the coupled model, the stability function is calculated using a linear relationship with the local Richardson number for statically stable conditions. The term $(1-z/h_e)$ is introduced to include the variation of fluxes with height within the surface layer, i.e., because the surface layer in atmospheric model often exceeds the lowest one

tenth of the boundary layer (i.e., the constant flux layer). Note that positive/negative values of E indicate sublimation/deposition.

The spatial pattern of the seasonal accumulated surface sublimation over DJF 2006/2007 (as distinct from blowing snow sublimation) is depicted in Fig. 10. Over the Arctic Ocean, Siberia and the Canadian Arctic, the humidity gradient is directed from the atmosphere to the surface, and deposition occurs with maximum values reaching 30 mm SWE. The indicated deposition over Arctic Ocean is in agreement with the previous studies. Based on 45 years of surface meteorological observations from the drifting ice stations in the Beaufort and Chukchi Seas from 73 to 90°N, the calculated latent heat flux indicated deposition for winter months, with the monthly averaged values around 1.1 Wm^{-2} (Lindsay, 1998). According to this latent heat flux, the accumulated surface deposition would be around 3 mm SWE for the three months DJF. Our simulated seasonal deposition over the Arctic Ocean has a similar value. Other studies also showed deposition over Arctic ice in the winter months (Maykut, 1982; Ebert and Curry, 1993; Persson et al., 2002; Andreas et al., 2010) with smaller values but similar order of magnitude. On the other hand, surface sublimation is prominent over continental regions such as the eastern part of North America and Northern Europe. The maximum values of surface sublimation can exceed 180 mm SWE. In the Canadian Prairies, large surface sublimation on the western side of Alberta is simulated, which is due to the relatively warm air from the Chinooks. The surface sublimation is relatively small in south-central Saskatchewan, with values of several mm SWE over the winter season and some localized deposition regions are displayed as well. The small sublimation is consistent with the reported daily mean value of net evaporation rates 0.1 mm SWE day^{-1} over

continuous snow in central Saskatchewan by Male and Granger (1979) and is mainly due to the cold surface of the Prairies.

4.2.4 Distribution over latitude bands

To determine quantitatively the relative importance of sublimation and transport at different latitudes, we calculated the averages of surface sublimation, blowing snow sublimation, and divergence of transport for four 10° latitudinal bands over the three winter months. The time evolution of the cumulative surface and blowing snow sublimations are depicted in Fig. 11. In general, surface sublimation decreases with an increase in latitude. In fact, surface deposition is indicated north of 70°N. In contrast, blowing snow sublimation increases with latitude, except during the first part of December. The reason for the different behaviour of surface and blowing snow sublimation is that at very high latitudes, the near surface air is usually saturated with respect to ice though the moisture content is very low. Andreas et al. (2002) demonstrated that over sea ice, even a small fraction of leads and polynyas can provide enough water vapor to saturate the atmospheric boundary layer, resulting in the surface air near ice saturation or supersaturation for temperatures between -40°C and 0°C. The relative humidity with respect to ice was usually around 100% in winter, with much less variability than in summer. As a result, over the entire Arctic Ocean, the water vapor flux is downward leading to surface deposition. On the other hand, the air aloft may be dry because of advection and entrainment, so that the blowing snow sublimation will still have significant contribution in high latitude regions.

Table 3 gives a summary of surface sublimation, blowing snow sublimation, and divergence of transport for the four bands. At lower latitudes (50° - 60°), surface sublimation (13 mm SWE) predominates over other terms (3.7 mm SWE for blowing snow and only 0.04 mm SWE for divergence). Blowing snow sublimation increases to 13.3 mm SWE for the 80° - 90° band. The divergence term is rather small and its magnitude is about two orders of magnitude smaller than the other two terms. Taking together, the three terms remove 23% to 52% of the total solid precipitation and are therefore important contributors to the snow mass budget. It should be bear in mind that the smallness of the divergence term is affected by the grid spacing of 18 km, which is still too coarse to resolve the fine scale features in the divergence field. Inside the grid size of 18 km, the snow surface is assumed to be homogeneous and subgrid scale phenomena are not considered in our coupled system. For example, snow interception by high vegetation is neglected in our model. The vegetation type, density and height are factors that can affect blowing snow transport and in-transit sublimation. The lead fraction in the sea ice cover is another factor that can affect our results. In our coupled system, the fraction of leads is assumed to be 3% but surface heat and moisture fluxes are very sensitive to the assumed lead fraction. The leads also provide a sink for blowing snow and therefore decrease the blowing snow transport and in-transit sublimation fluxes.

5 Comparison with empirical formula

In the literature, there are several empirical formula for inferring blowing snow sublimation and surface sublimation. Based on observations in a Wyoming field experiment, Schmidt (1982) proposed a linear relation between the blowing snow

sublimation rate and transport, which in turn was found to vary strongly with the wind speed. Thus his empirical expression is mainly dependent on surface winds. Water vapor deficit, a key factor in determining the sublimation rate, is not considered. Other formulas have been proposed based on the application of a blowing snow model. These include Déry and Yau (2001b), Bintanja (2000), and Gordon et al. (2006).

We will compare our model results of blowing snow sublimation with the empirical formula of Déry and Yau (2001b), which is based on curve fitting of 30 minute simulations of their double-moment blowing snow model (PIEKTUK-D) over a range of initial conditions with varying temperatures, humidity, and wind speeds. Their proposed relation has the form

$$Q_s = (a_0 + a_1x + a_2x^2 + a_3x^3 + a_4U_{10} + a_5xU_{10} + a_6x^2U_{10} + a_7U_{10}^2 + a_8xU_{10}^2 + a_9U_{10}^3)/U' \quad (9)$$

In Eq. (9), U' is a normalization factor to remove the dependence on the saltation mixing ratio. The thermodynamic parameter, ξ is defined as a function of the temperature and water vapor deficit; U_{10} is the wind speed at 10 m height, and a_0 - a_9 are empirical coefficients. Interested readers are referred to Déry and Yau (2001b) for the details of Eq. (9) and the values of the coefficients a_0 - a_9 .

Using 6-h CMC analysis and Eq. (9), we obtained the empirical seasonal blowing snow sublimation over DJF 2006/2007 (Fig. 12). When compared to the results from Simulation 2 (Fig. 8), it is evident that there is qualitative agreement in the spatial patterns. There are, however, differences. For example, the model yields somewhat larger values than the empirical formula, and captures some localized regions with maximum blowing snow sublimation (such as the north-western side of the United States near the

Rocky Mountains, and the northern and western part of Mongolia) that are absent in Fig.

12. A possible reason for this difference is that surface winds at these high topography regions are usually weak with infrequent large values so that the occurrence of blowing snow in these areas is sporadic. The relatively coarse temporal and spatial resolutions in the CMC analysis may not capture the sporadic blowing snow events.

Another reason for the difference may be due to the fact that the Déry and Yau (2001b) empirical formula was developed with meteorological data collected at a site in the Canadian Arctic and may yield less accurate results for other sites. To investigate this possibility, we apply the empirical formula and PIEKTUK-T for the blowing snow cases observed by Schmidt (1982) at a Wyoming observation site (elevation 2360 m) at different times. Ten sets of observation were made but three sets or runs had problems with humidity measurements. The seven good runs provide observations of humidity, temperature, wind speed, friction velocity and particle size distribution at several levels. Using the observed size distribution and the other measurements, Schmidt computed directly the blowing snow sublimation at given levels and obtained the integrated sublimation by summing all levels in the vertical. A comparison of calculated sublimation values from Déry and Yau's empirical relation and from PIEKTUK-T (initialized using the observed conditions and particle size distribution) with Schmidt's results (Fig. 13), shows that the simulated sublimation rates from PIEKTUK-T are very close to the measured values from Schmidt. In contrast, the empirical formula yields larger errors.

The larger errors of the empirical formula are attributable to two main factors. First the recorded surface pressure at the Wyoming site was 765 mb, much lower than the

typical pressure at the Arctic site where measurements from near sea level were used to derive the empirical formula. Second, blowing snow sublimation is very sensitive to the initial particle radius and shape parameter of the size distribution. This type of information is not accounted for in the empirical formula. Thus the empirical relation can yield realistic patterns of blowing snow sublimation but could be less accurate compared to a coupled model when applied over a large area because the variability of surface conditions and initial conditions are not fully taken into account.

For comparison of surface sublimation, we followed Déry and Yau (2002) and used the empirical formula of van den Broeke (1997) with the form

$$Q_{surf} = r' u^* q^* \quad (10)$$

where u^* and q^* are friction velocity and the scale for turbulent moisture fluctuation from Garratt (1992) as given in Déry and Yau (2002). Using Eq. (10) and the 6-h CMC analysis, the surface sublimation is calculated for the winter season of 2006/2007 and the results are displayed in Fig. 14. Comparison with the results from Simulation 2 in Fig. 10 indicates that the patterns are similar. However, the magnitude of surface sublimation is larger in the coupled model than the empirical formula.

It is interesting to remark that our results show regions of deposition at high latitudes, while in the snow mass budget of Déry and Yau (2002), the Arctic Ocean is dominated by surface sublimation. The reason is that their results are for annual averages. Indeed, when we applied Eq. (10) to compute surface sublimation for the seasons of spring, summer and autumn, we found large amount of surface sublimation over the Arctic regions especially during the summer season when surface air is relatively warm and

moist. Therefore when summed over the whole year, a net annual surface sublimation is observed over the Arctic Ocean.

6 Discussion

Our three-month simulation provides spatial distribution of surface sublimation and blowing snow related processes and their contributions to the surface mass budget over the Northern Hemisphere. Because there are few blowing snow measurements for validation, we mention here some limitation and uncertainties in our results.

(1) The wind speed threshold to initiate blowing snow is calculated from a relatively simple expression. This formula is derived from the data over the Canadian Prairies, and is found to be a function of the temperature. However, there are other factors which affect blowing snow initiation and termination. For example, the character of the snow, such as snow age and snow compactness can also play a role, and the general applicability of the threshold expression to other sites still needs to be validated.

(2) The negative thermodynamic feedbacks in our model limit further blowing snow sublimation, resulting in relatively low sublimation rates of blowing snow compared to other snowdrift models.

(3) The horizontal grid resolution of the current simulation is 18 km, within which homogeneity is assumed. As such, fine scale variation in topography and surface characteristics are not resolved, as well as the micro-relief over sea ice associated with snowdrifts and pressure ridges. The relatively coarse resolution may also reduce the wind speed, and modify the snow transport and concurrent sublimation.

(4) In our current model, we neglected forest canopy effects and vegetation interception in snow transport. If these two factors were taken into account, the snow on the ground will be sheltered from transport and the transported snow will be partly intercepted by the forest. These factors will probably reduce the surface and blowing snow sublimation.

(5) Although lead fraction is crudely taken account into in the coupled model by its effect on the surface turbulent fluxes via a weighting factor, the role of sea ice leads as a direct sink of blowing snow transport is neglected in the model. Consideration of this subgrid scale process will decrease blowing snow transport.

(6) A stability function was used in the boundary layer scheme of MC2 to deal with stratification effects. However, in the blowing snow module, neutral stability is assumed in extrapolation of the wind profiles below first MC2 level. Additionally, the vertical turbulent transport of blowing snow follows the relatively simple representation appropriate for neutral conditions.

These uncertainties may change the magnitude of the simulated surface sublimation and blowing snow related processes, and modify their contributions to the snow mass budget. However, it is our belief that the overall characteristics of the spatial patterns would not be overly sensitive to these uncertainties. Since this experiment is the first to explicitly simulate blowing snow processes covering the entire Northern Hemisphere, it provides a useful reference for comparison with future studies of the snow mass distribution over large spatial and temporal scales.

7 Conclusions

This paper describes the development of a triple-moment blowing snow-atmospheric modeling system and its application to compute the winter season snow mass budget over the Northern Hemisphere. The following main conclusions were obtained.

1. The modeling system is able to simulate well the evolution of the fields of surface winds, temperature, pressure, and relative humidity at high latitude stations.
2. A seasonal mass budget for the 2006/2007 winter months was computed and compared with empirical results. The simulations indicate that surface sublimation and blowing snow sublimation have significant contributions to the mass budget.
3. Over the Arctic Ocean, deposition is more common in winter months. Surface sublimation is more evident over mid-latitude continental and alpine areas.
4. Large amounts of blowing snow particles are transported over the Arctic Ocean, coastal edge of Greenland, Bering Sea and Sea of Okhotsk. However, the divergence of the transport has smaller effect in the snow mass budget on a large scale, being two orders of magnitude smaller than the surface and blowing snow sublimation terms.
5. The importance of surface and blowing snow sublimation varies in different latitudinal bands. Band averaged surface sublimation decreased with the latitude whereas blowing snow sublimation increased with latitude. The combined effects could remove 23%~52% of the solid precipitation.

Acknowledgements. We would like to thank Dr. Badrinath Nagarajan for his help in running the coupled model on a Linux clusters and for helpful suggestions. Dr. Lei Wen also offered helpful suggestions in editing the manuscript. We are also grateful to Dr.

Edgar L. Andreas and the other reviewer for their comments, which helped to improve this article. This research is supported by the Natural Science and Engineering Research Council of Canada and the Drought Research Initiative network (DRI) funded by the Canadian Foundation for Climate and Atmospheric Sciences.

Date	03/01	19/01	08/02	03/03	08/03	15/03	21/03	23/03	27/03
Density (kgm^{-3})	91.4	141.5	181.7	173.8	211.2	198.2	201.6	206.5	207.8
Depth (cm)	11.09	18.97	20.77	36.89	38.37	40.57	37.13	36.79	36.08
SWE (mm)	9.996	27.46	37.10	63.40	80.61	80.32	75.02	75.99	74.87

Table 1: Observed snow density, snow depth and Snow Water Equivalent (SWE) averaged over four transects within SNDWA, Saskatchewan, Canada (52.03°N, 106.1°W)

	Model			Observation			R^2
	Mean	Min	Max	Mean	Min	Max	
Baker Lake (64.3°N, 96.08°W)							
Wind speed (ms^{-1})	5.84	0.47	14.95	6.05	0.	21.67	0.7078
Air temperature ($^{\circ}\text{C}$)	-25.46	-37.49	-11.59	-26.07	-39.9	-5.5	0.8485
Surface pressure (mb)	1011.1	979.11	1034.6	1012.2	981.0	1036.5	0.9662
Relative humidity(%)	82.3	54.57	106.65	83.9	70.39	109.16	0.5061
Rankin Inlet (62.82°N, 92.12°W)							
Wind speed (ms^{-1})	5.56	0.2	13.72	6.77	0.	18.61	0.8055
Air temperature ($^{\circ}\text{C}$)	-24.24	-34.86	-10.55	-24.76	-39.9	-6.6	0.8744
Surface pressure (mb)	1012.9	985.88	1039.6	1008.8	982.40	1035.9	0.9689
Relative humidity (%)	90.74	60.75	118	91.27	62.13	110	0.6747

Table 2: Comparison of observed and simulated surface variables at Baker Lake and Rankin Inlet, Nunavut, Canada. The relative humidity is with respect to ice. R is the correlation coefficient.

Band	Q_{surf}	Q_s	Div.	Sum	Precip.	Percentage
50°-60°	13.0	3.7	0.044	16.8	66.5	25%
60°-70°	6.5	7.4	-0.057	13.8	59.5	23%
70°-80°	-0.15	9.7	0.0012	9.5	36.1	26%
80°-90°	-6.0	13.3	-0.12	7.2	13.9	52%

Table 3: Seasonal average surface sublimation (Q_{surf}), blowing snow sublimation (Q_s), divergence of blowing snow transport (Div), and precipitation amount over latitudinal bands in units of mm SWE. Sum denotes the sum of surface sublimation, blowing snow sublimation and divergence of transport, and Percentage is defined as the ratio of Sum to the total solid precipitation (Precip.).

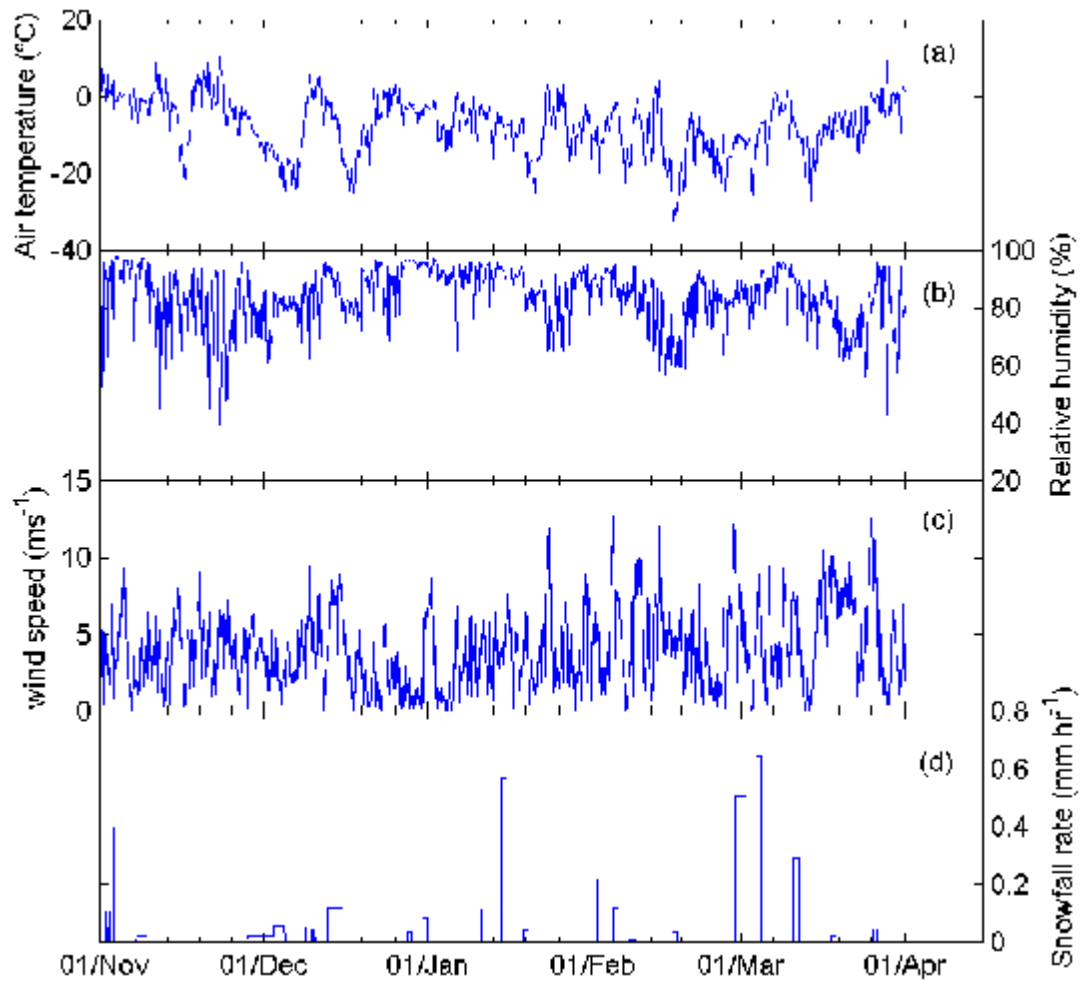


Figure 1: Hourly observations of air temperature (a), relative humidity with respect to ice (b), wind speed (c), and snowfall rate (d) from 31 October 2005 to 30 April 2006 over SDNWA, Saskatchewan, Canada.

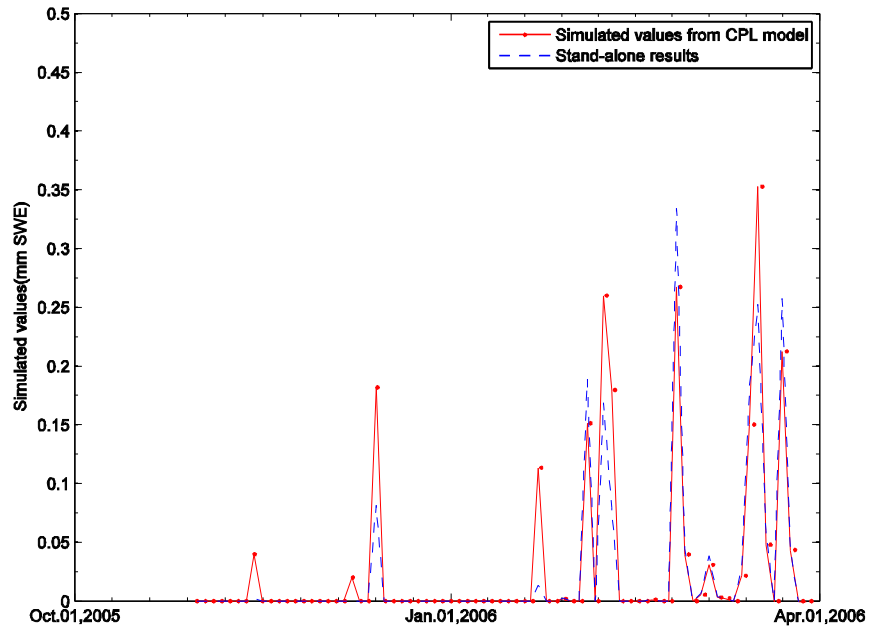


Figure 2: Comparison of blowing snow sublimation from stand-alone blowing snow model (PIEKTUK-T) and coupled model (CPL) from 31 October 2005 to 30 April 2006 over SDNWA. Units in mm SWE.

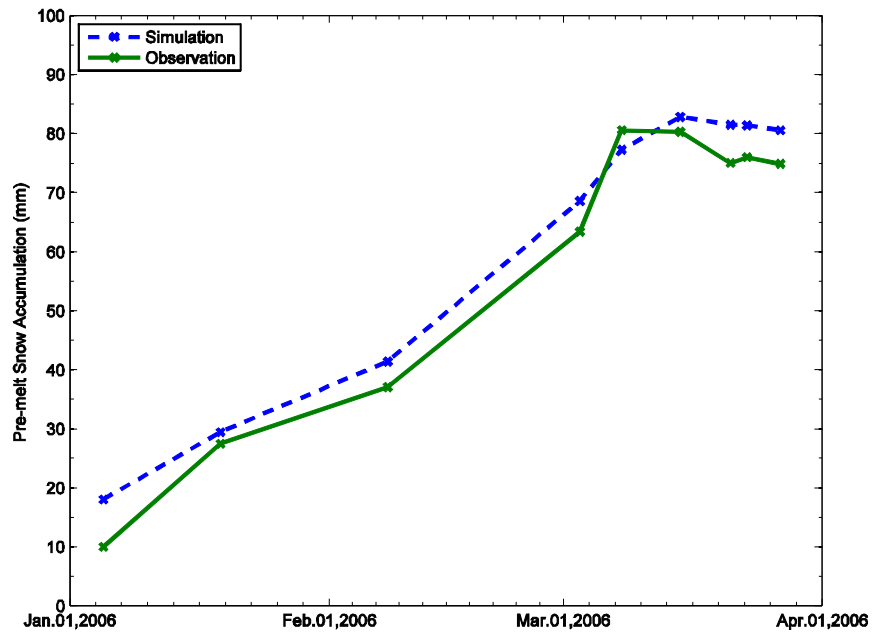


Figure 3: Comparison of the evolution of observed and simulated pre-melt snow accumulation from January 2005 to April 2006 over SDNWA. The solid line represents the observation. The simulated pre-melt SWE is obtained by interpolating the grid point values to the station site.

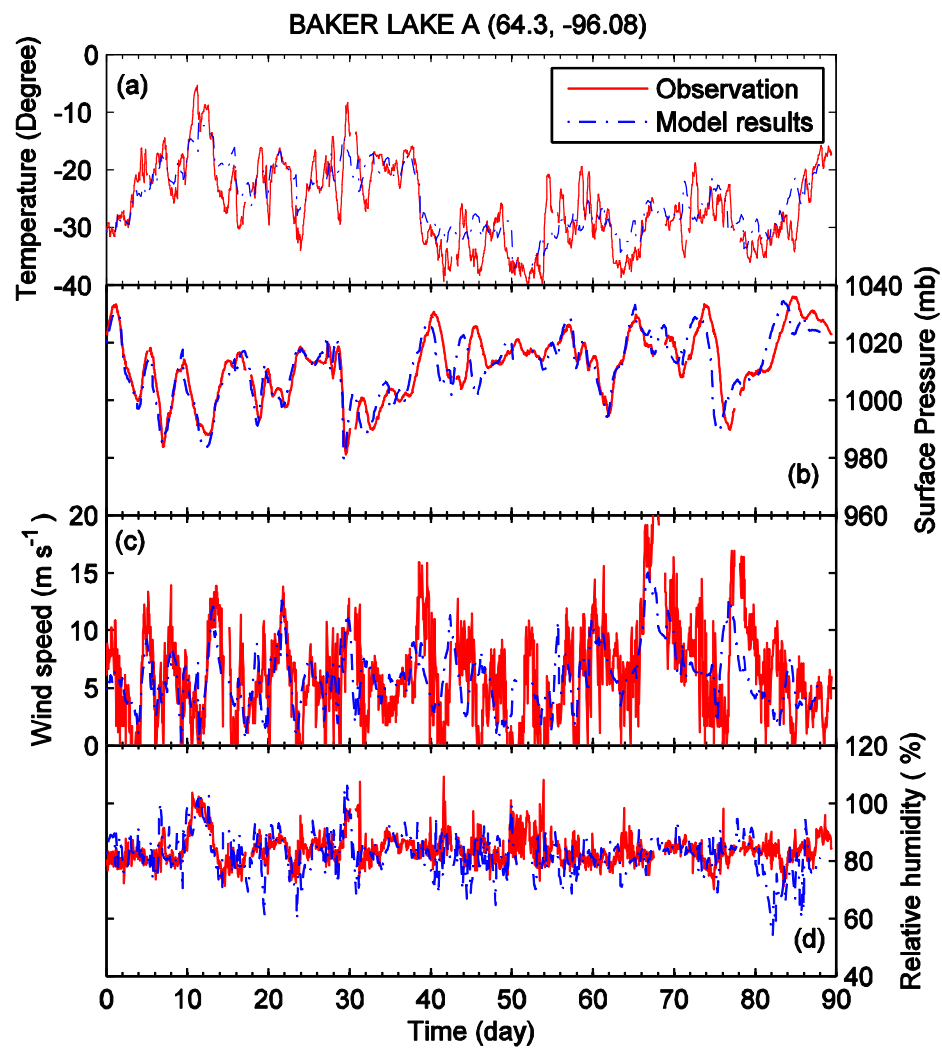


Figure 4: Comparison of observed and simulated air temperature (a), surface pressure (b), wind speed (c) and relative humidity with respect to ice (d) at Baker Lake (64.3 °N, 96.08 °W) from December 2006 to February 2007.

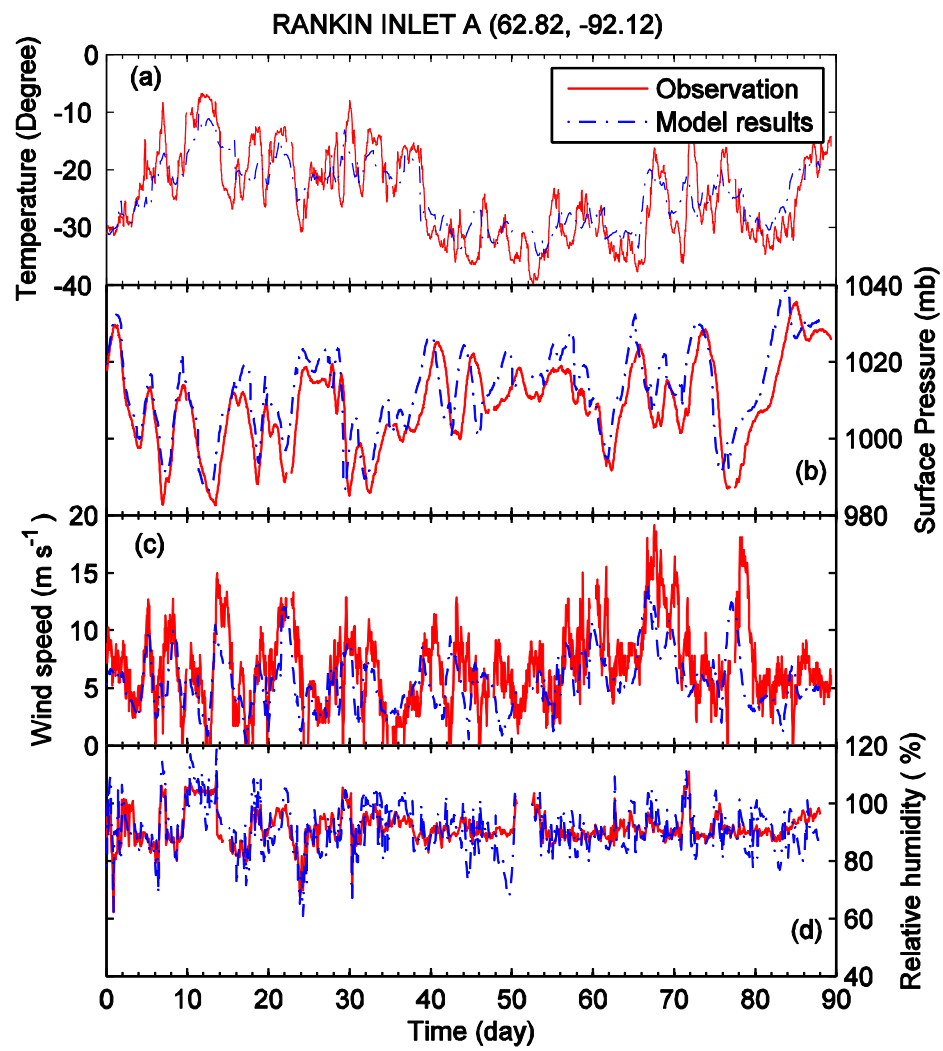


Figure 5: Same as Fig. 4, but for Rankin Inlet (62.82°N, 92.12°W).

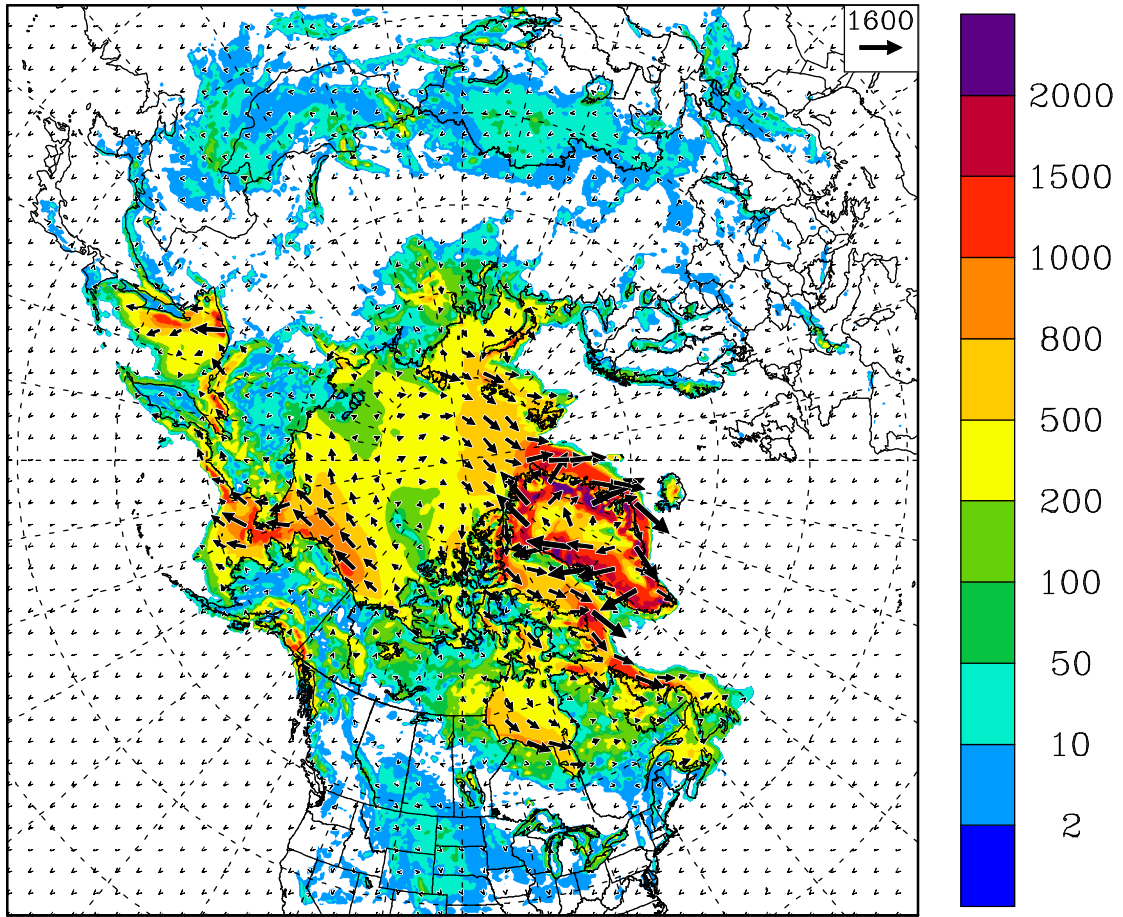


Figure 6: Winter season blowing snow transport from coupled model over DJF 2006/2007. The arrows denote the transport vectors. Units in Mg m^{-1} .

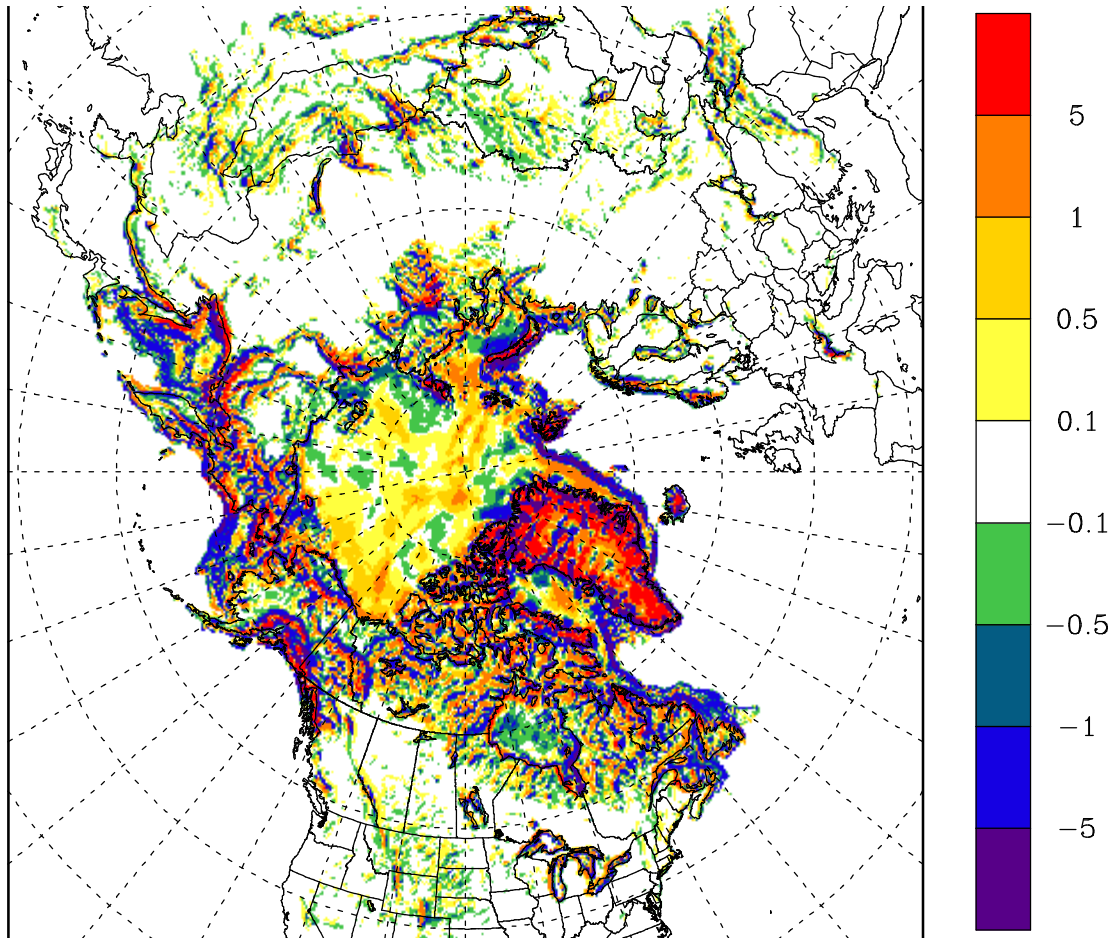


Figure 7: Winter season divergence of blowing snow transport from the coupled model over DJF 2006/2007. Units in mm SWE.

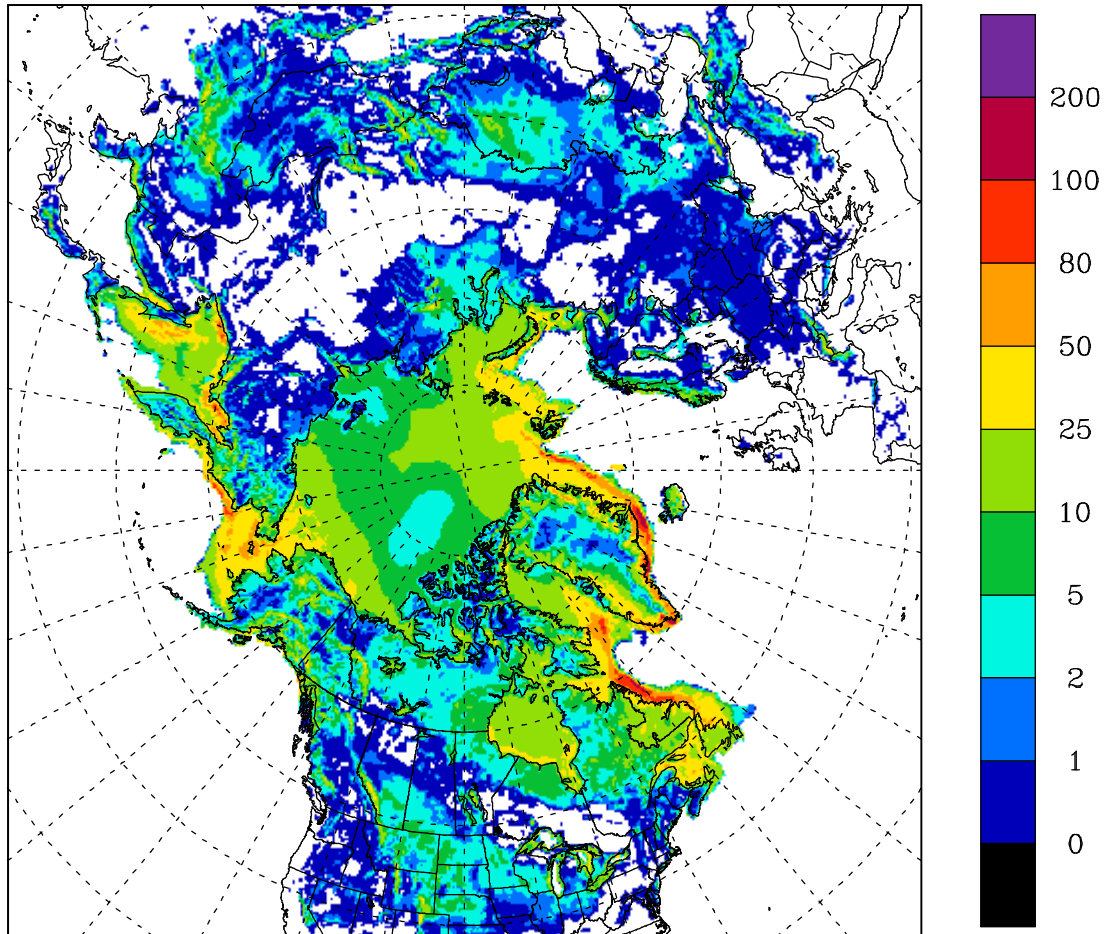


Figure 8: Winter season blowing snow sublimation from the coupled model over DJF 2006/2007. Units in mm SWE.

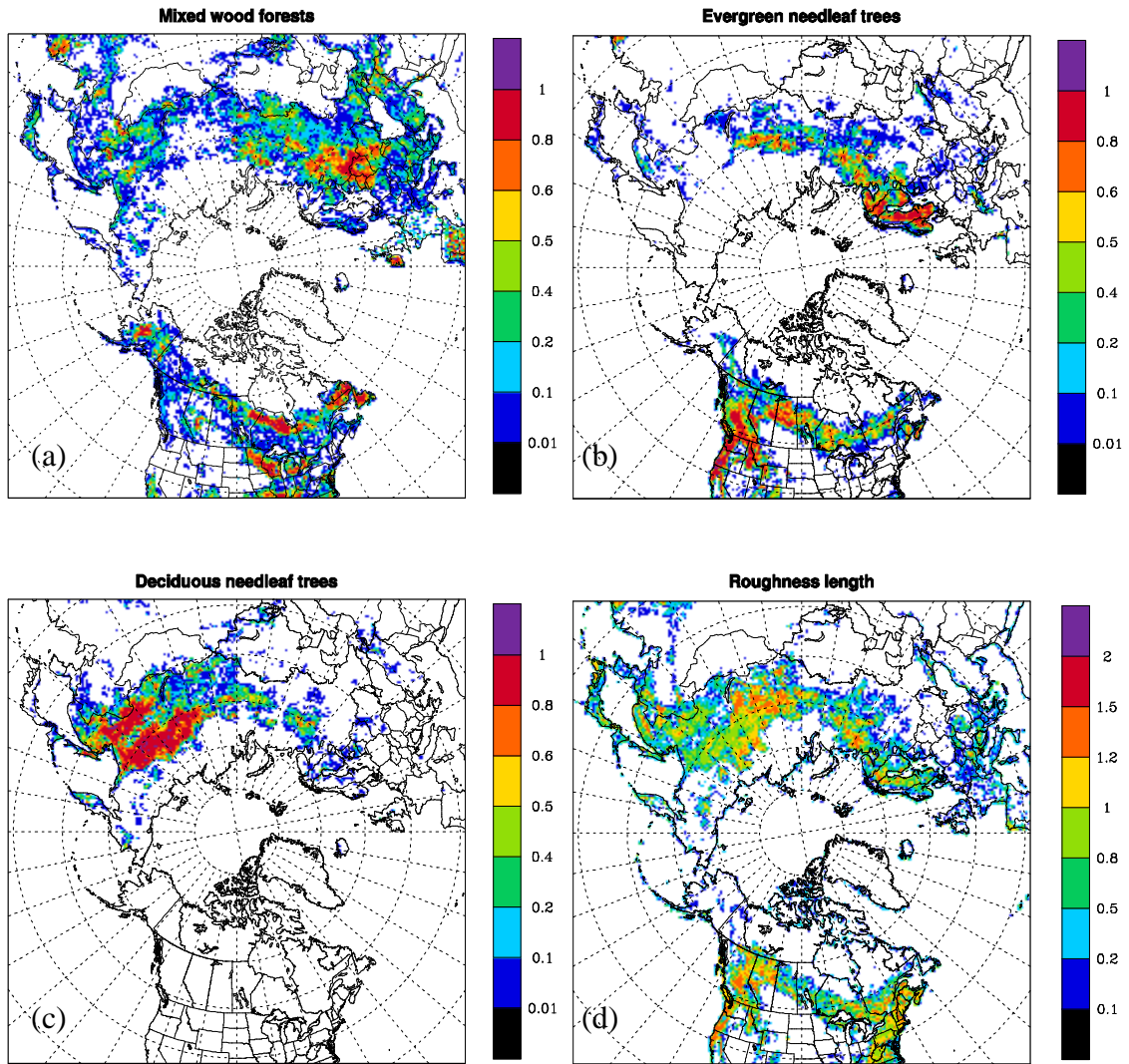


Figure 9: Spatial distributions of different vegetation types: (a) mixed wood forests, (b) evergreen needle-leaf trees, (c) deciduous needle-leaf trees (units in fraction), and (d) roughness length (units in m).

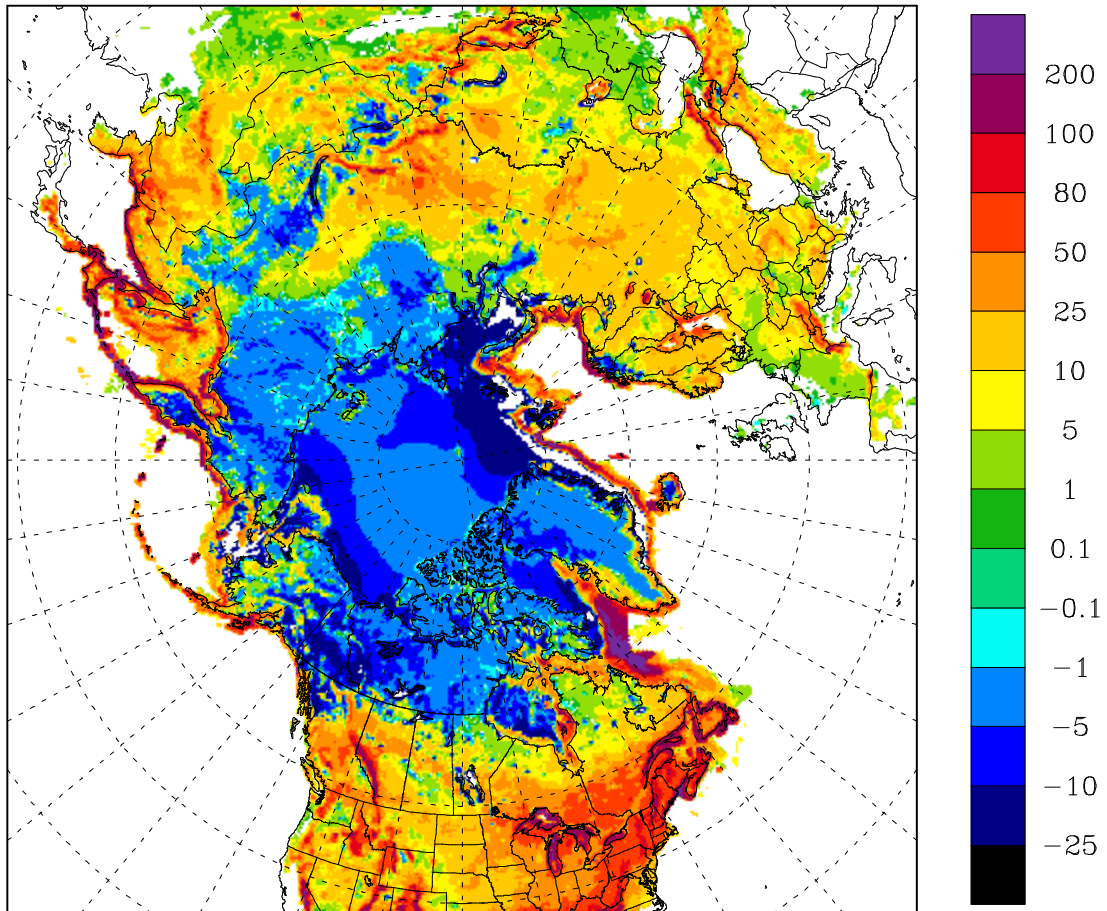


Figure 10: Winter season surface sublimation from the coupled model over DJF 2006/2007. Units in mm SWE.

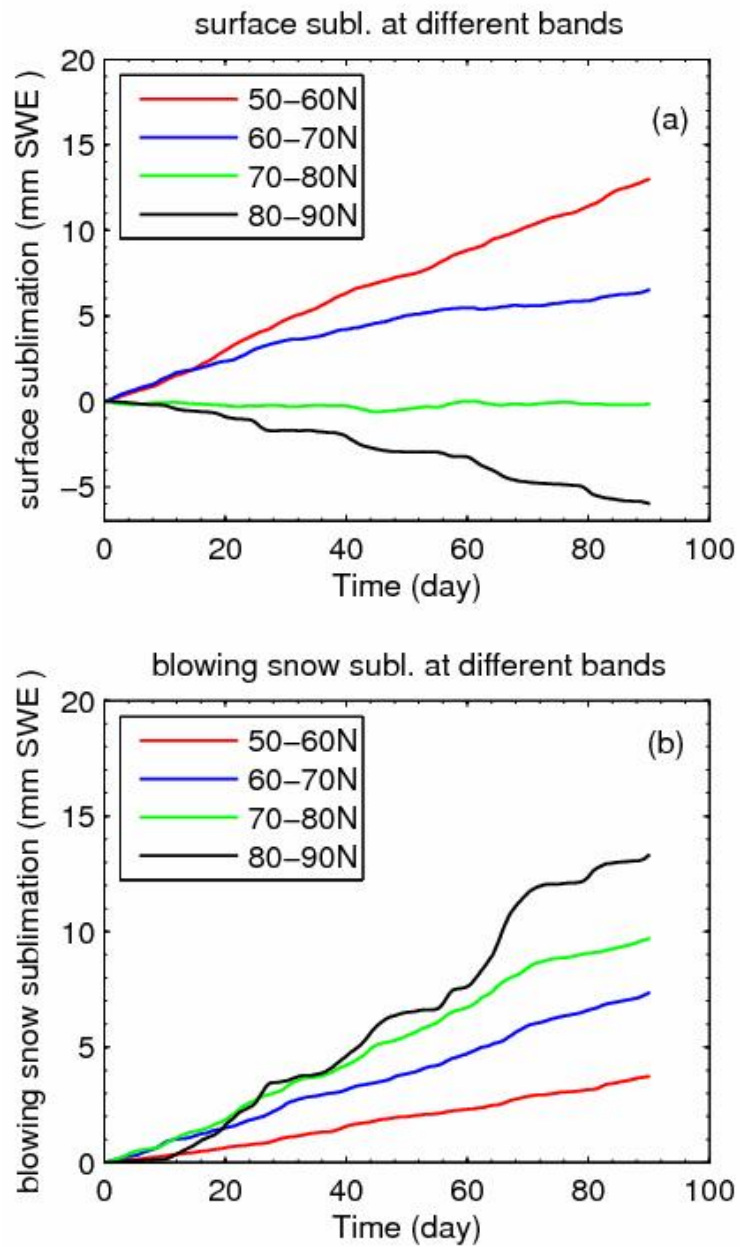


Figure 11: Time evolution of surface sublimation (a) and blowing snow sublimation (b) averaged over latitudinal bands. Units in mm SWE.

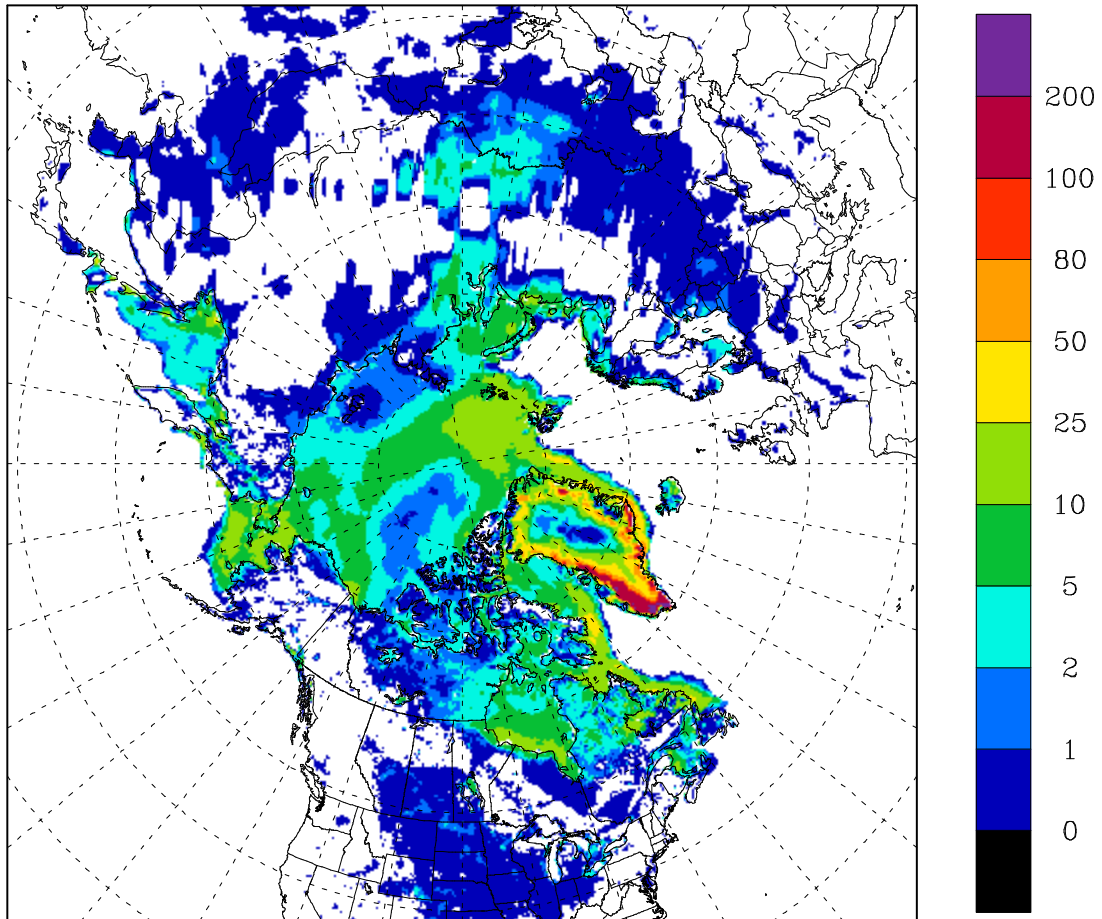


Figure 12: Winter season blowing snow sublimation from empirical formula over DJF 2006/2007. Units in mm SWE.

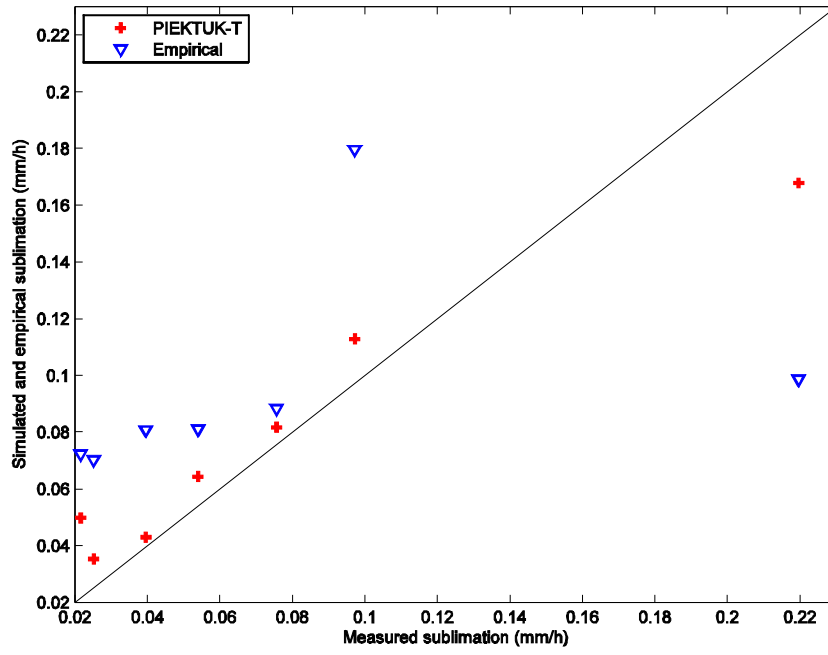


Figure 13: Comparison of blowing snow sublimation from PIEKTUK-T, the empirical formula, and observation over the Wyoming site. Units in mm h^{-1} .

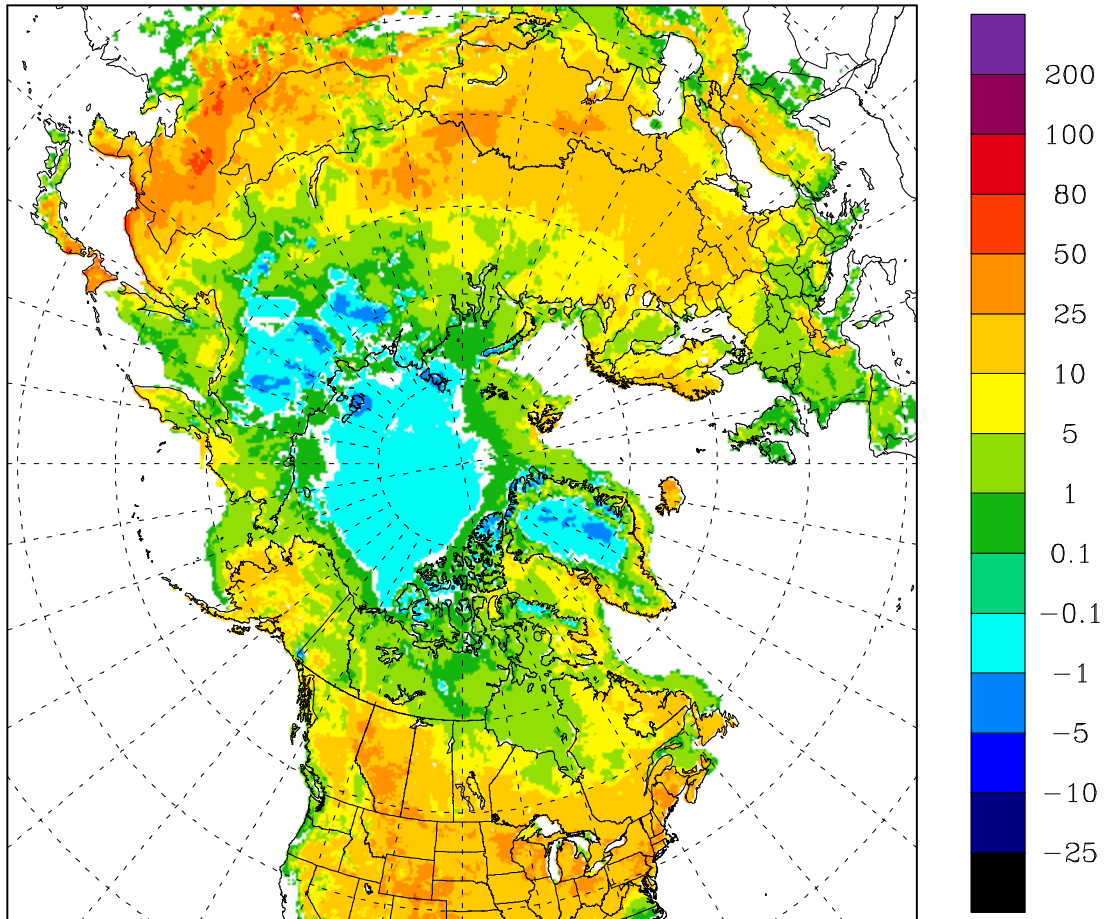


Figure 14: Winter season surface sublimation from empirical formula over DJF 2006/2007. Units in mm SWE.

Chapter 4

Blowing snow cooling effects on anticyclogenesis

In the previous chapter, we have investigated the blowing snow contribution to the hydrological cycle over the winter season on the hemispheric scale. Blowing snow is not only an important contributor in the hydrological process due to its ability in snow redistribution, but also has close relationship with the synoptic systems. It usually occurs between regions of cyclones and anticyclones, where strong surface wind is associated with steep pressure gradients. During blowing snow events, the sublimation of blowing snow particles can be a source of water vapor and a sink of sensible heat. The cooling of the boundary layer can play a role in the dynamics of anticyclogenesis. In this chapter, we will examine blowing snow cooling effects in the lower boundary layer to anticyclogenesis on the synoptic scale.

This chapter forms a paper submitted for publication in the *Journal of Geophysical Research* as ‘Jing Yang and M.K. Yau, Blowing snow cooling effects on anticyclogenesis’. The co-author Dr. M.K. Yau played a role as a supervisor and contributed to the editing of the manuscript.

Blowing snow cooling effects on anticyclogenesis

Jing Yang and M.K. Yau

McGill University, Montréal, Canada

Corresponding author: Jing Yang (yangj@zephyr.meteo.mcgill.ca)

Abstract: This paper focuses on blowing snow and its effect, through thermodynamic forcing, on anticyclogenesis. A triple-moment blowing snow model (PIEKTUK-T) is coupled to an atmospheric model (MC2) and this system is used to simulate an anticyclogenesis event. For comparison, an uncoupled version of MC2 is also used to model the same event. The coupled model showed colder low level temperatures in regions where blowing snow occurred. This cooling extended throughout the boundary layer and contributes to a rise in sea level pressure relative to the uncoupled simulation.

A potential vorticity (PV) diagnostic is then applied to quantify how this microphysical cooling affects the geopotential height and balanced wind fields. Surface potential temperature differences between the coupled and uncoupled runs were used as lower boundary conditions for the inversion. The results showed that the cooling induces positive geopotential height and anticyclonic flow perturbations extending up to 500 mb over the cooling regions. The averaged inverted geopotential height anomaly at 1000 mb level over the anticyclone region is up to 4.5 dam in 72 hours. The corresponding anticyclonic flow is significant with the maximum value of 27 knots, situating south of

the anticyclone center in 72 hours. These results demonstrate that surface cooling can play a role in the anticyclogenesis. However, our results are sensitive to the amount of supersaturated water vapor in the low levels. In a sensitivity experiment where the relative humidity with respect to ice in the blowing snow module is allowed, the effect of blowing snow sublimation cooling was found to be much reduced.

Keywords: blowing snow; coupled model; anticyclogenesis; PV inversion

1. Introduction

Anticyclones, with their central barometric pressure higher than the surrounding environment, are characterized by low-level divergent flow and descending air motion, resulting in relatively fair weather. As a result, anticyclones and anticyclogenesis are considerably less well studied than cyclones and cyclogenesis. However, understanding the development and movement of anticyclones is nonetheless important. For example, transient waves, associated with cyclones and anticyclones, are largely responsible for weather changes. Additionally, anticyclones are closely related to wintertime cold air outbreak and blowing snow. The accompanied blizzard conditions can affect safety in transportation and may cause the loss of lives.

Theoretical studies have suggested various mechanisms which can trigger the formation of anticyclones. They include upper-level velocity convergence associated with differential vorticity advection (Fleagle 1947; Bodurtha 1952; Bowling et al. 1968; Dallavalle and Bosart 1975; Boyle and Bosart 1983; Ramage 1971; Tan and Curry 1993);

the warming below an upper-level ridge associated with warm air advection or diabatic processes (Bodurtha 1952); orographic forcing (Charney and Devore 1979; Dole 1986a, 1986b; Sperenza 1986; Ioannidou and Yau 2008), and low level diabatic cooling (Wexler 1951; Dallavalle 1975; Boyle and Bosart 1983; Curry 1983, 1987). Depending on the forcing mechanisms and their thermal characters, anticyclones have been classified as cold, warm, or mixed by Wexler (1951). Warm anticyclones move slowly and are deep systems associated with a warm, deep troposphere but a cold, high stratosphere. They are believed to be related to cold air advection in the upper levels, resulting in upper level convergence and descent. In contrast, cold anticyclones are associated with cold, dense air near the surface and a warm, low stratosphere. They are generally shallow features characterized by rapid movement following the passage of an intense cyclone. Cold anticyclones typically form in the source regions for Continental Polar Air and are usually the dominant feature of the high latitude circulation during the winter (Curry 1987; Dole 1986b; Ioannidou and Yau 2008). The nocturnal radiative cooling of snow-covered surfaces decreases the surface temperature and the layer of air near the surface is cooled by heat loss from conduction to form polar anticyclones. Additionally, radiative cooling from condensate in the atmosphere, mainly low level ice crystals that form in the cooling air, also drives anticyclogenesis. Curry (1987) demonstrated this process using an idealized cylindrical model.

Past studies of diabatic cooling effects on anticyclogenesis have focused mainly on radiative cooling. However, there is another cooling effect related to blowing snow which occurs frequently in high latitude snow-covered regions (Déry and Yau 2002). Strong surface winds over loose snow will result in blowing snow saltation and the

saltated particles will be further transported from the lower atmospheric boundary layer to higher levels by turbulence. The suspended snow particles will sublime if the air is subsaturated with respect to ice. The sublimation process cools and moistens the air during the phase change. With a one-dimensional triple moment blowing snow model PIEKTUK-T, Yang and Yau (2008) simulated observed blowing snow events and showed that the sublimation from blowing snow, in terms of snow water equivalent (SWE), can amount to 0.25-1.4 mm day⁻¹. If the sublimation of 1.4 mm SWE is assumed to cool a 3-km column of air (e.g. from the surface to about 700 mb), the cooling rate will be around 1.1 K day⁻¹. This value amounts to the same order of magnitude of 2.6 K day⁻¹ from net radiative cooling averaged over a 5-day simulation (Curry 1983). Blowing snow sublimation therefore would exert a contribution similar to radiative cooling and diabatic forcing to anticyclogenesis. The neglect of blowing snow may explain some of the systematic errors in the forecasts of near-surface meteorological fields at high latitudes (Colucci and Bosart 1979; Grumm and Gyakum 1986).

Déry and Yau (2001) coupled a double-moment blowing snow model to the atmospheric model MC2 and showed that blowing snow can increase the sea level pressure in an Arctic blizzard event. Although they demonstrated that sea level pressure increased by 2 mb in 2 days in an experiment including the cooling effect from blowing snow sublimation, they did not perform a detailed diagnostic study of the cause. In this paper, we will examine specifically the effect of blowing snow cooling on anticyclogenesis using potential vorticity inversion techniques.

The paper is organized as the follows. A synoptic analysis of a polar anticyclogenesis event is described in Section 2. Section 3 presents the model and the set up of the experiments. The simulation results for two simulations are given in Section 4 while Section 5 contains diagnostic results using the inversion of potential vorticity (PV). The results for a sensitivity experiment and concluding remarks are in Section 6.

2. Case description

The anticyclone under consideration (indicated by **H** in Fig. 1a) was situated over the East Siberian Sea and the western Arctic Ocean. A climatological analysis (Ioannidou and Yau 2008) showed that anticyclogenesis is active over this region and the typical lifetime of the anticyclones is about 5 days. The surface anticyclone formed over the western Arctic Ocean; with a central pressure of 1024 mb at 1200 UTC on 25 November 2005. To the west of the anticyclone, a cyclone with two sub-centers (indicated by **L1a** and **L1b** in Fig.1a) was situated over the western and southeastern sides of the Kamchatka Peninsula with the central pressures of 992 mb. Strong winds on the southeast side of the cyclone advected warm air through the Bering Sea to the northeastern flank of Siberia (Fig.1b). In response to the low level warm advection, an upper-level ridge formed between **L3** and **L4** at 250 mb (thick dash line in Fig. 1c) extending from the central Siberian Plateau to the northern coastline of east Siberia. The 850-500 mb thickness field (Fig. 1d) also indicated warm air over the eastern side of the Kamchatka peninsula, where cold air with small thickness values less than 388 dam resided over a large region covering Siberia, the Arctic Ocean, and Alaska.

Figure 2 presents an overlay of sea level pressure (SLP) and temperature at 850 mb every 12 h for the period of anticyclogenesis from 0000 UTC 26 November to 1200 UTC 28 November 2005. Warm air initially over the Bering Sea moves northeast toward the anticyclogenesis region (indicated by **H** in Fig. 2a), and it spread and penetrated to the western Arctic Ocean. This warm advection to the west of the surface anticyclone contributes to the development of the anticyclone. At 0000 UTC on 26 November, the 1022 mb close contour extends over a large region and the central pressure is around 1026 mb (Fig. 2a). In the subsequent times, the central SLP kept intensifying, attaining values of 1032 mb, 1040 mb and 1048 mb at 1200 UTC on 26, 27, and 28 November, respectively (Figs. 2b,d,f). The total increase of the central pressure of the anticyclone was around 22 mb in 60 h, corresponding to a rate of about 9 mb day^{-1} , and falls into the anticyclogenesis category defined by Colucci and Davenport (1987).

This intensifying anticyclone moves very slowly and persists over the Arctic Ocean for about a week, as is characteristic of the blocking type. The anticyclone blocked the eastward movement of the cyclone (indicated with **L1** in Fig. 2. Note that **L1a** and **L1b** were used in Figs. 2a-c to indicate the two sub-centers of **L1**) over the Bering Sea. This cyclone weakened and dissipated gradually, with the central pressure increasing from 980 mb (Fig. 2a) to 1000 mb (Fig. 2f). To the southeast of the anticyclone, another strong cyclone was situated over northwestern Canada with a central SLP of 980mb (indicated by **L2** in Fig. 1a). As the anticyclone intensifies, **L2** also weakened with time and subsequently split into two centers (**L2a** and **L2b** in Fig. 2a) at 1200 UTC 26 November. The sub-center **L2b** then moved northward and stayed over the Beaufort Sea for several days. As the center of the cyclonic circulation shifted closer to the strengthening

anticyclone, a strong SLP gradient formed between the anticyclone and cyclone. The associated strong surface winds exceeded 36 knots (figures not shown) and blowing snow occurred around the edge of anticyclone.

3. Model description and setup of experiment

The coupled blowing snow-atmospheric model is a two-way interactive modeling system which includes the atmospheric component MC2 (Canadian Compressible Community Model) (Tanguay et al. 1990; Benoit et al. 1997) and a one-dimensional triple-moment blowing snow model PIEKTUK-T (Yang and Yau 2008). MC2 is a three-dimensional fully elastic non-hydrostatic model which has been successfully applied in a variety of studies such as Arctic ground blizzard (Déry and Yau 2001), mid-latitude cyclones (Misra and Yau 2001), mesoscale convective system (Nagarajan et al. 2004), hail storms (Milbrandt and Yau 2006), and real-time forecast of severe floods (Lin et al. 2010).

MC2 consists of a dynamical core and various physics packages. The governing equations for perturbation pressure, temperature, specific humidity, horizontal winds, vertical velocity, as well as mixing ratios of cloud water, rain water, and ice substances are integrated using a semi-Lagrangian and semi-implicit numerical scheme. The terrain following Gal-Chen coordinate system is used in the vertical. The physics package (Benoit et al. 1997; Mailhot et al. 1998) includes solar and infrared radiation treated interactively with clouds (Fouquart and Bonnel 1980; Garand 1983), a planetary boundary layer (PBL) parameterization based on a time dependent turbulent kinetic energy with fully implicit vertical diffusion, and a stratified surface layer based on

similarity theory (Mailhot and Benoit 1982; Benoit and Mailhot 1989). The surface variables are aggregated from predicted values of four surface types: land, glacier, ice, and water. Although not expected to be important for our winter event, a convective parameterization is included. For explicit cloud and precipitation, there are predictive equations for water vapor, cloud water, rainwater, ice, snow, and graupel following Kong and Yau (1997). The triple moment model PIEKTUKT-T was coupled to MC2 to treat blowing snow.

PIEKTUK-T is a one-dimensional blowing snow model which yields blowing snow number concentration, mixing ratio, and radar reflectivity with high efficiency. Temperature and humidity profiles are also predicted. The model has been validated against observations (Yang and Yau 2008). There are 24 vertical levels spaced logarithmically from the surface to a height of 1 km with high resolution near the ground. The coupling of PIEKTUK-T and MC2 allows for the feedback of blowing snow sublimation on the thermodynamics, which acts to decrease the air temperature and increase the humidity. The winds and thermodynamic fields from MC2 determine the occurrence of blowing snow. The time step for PIEKTUK-T is 5 s and that for MC2 60 s. The details of the coupling procedure are described in Yang et al. (2010). As blowing snow particles also affect the visible light flux reaching the ground, the contribution of blowing snow particles to the cloud fraction at lower levels is also taken into account in the radiation scheme.

We performed three simulations for the anticyclogenesis case described in Section 2. One simulation was run without blowing snow and is referred to as the STD run. The other two simulations, CPL and CPL2, are run using the coupled MC2 - PIEKTUK-T

modeling system. In experiment CPL2, the water vapor distribution in PIEKTUK-T is allowed to be supersaturated with respect to ice. However, in experiment CPL, when the water vapor becomes supersaturated with respect to ice in PIEKTUK-T, it is reset to the saturation value. Experiment CPL is motivated by the year long observation of Andreas et al. (2002) during the Surface Heat Budget of the Arctic Ocean experiment (SHEBA) that fog, rains of “diamond dust” are frequently observed near the surface, as well as episodes of severe hoarfrost and rime that accumulated on structures. They suggested that the near-surface relative humidity is often near ice saturation over Arctic sea ice. The results of Andreas et al. (2002) are consistent with other observations that diamond dust is a common phenomenon occurring over cold areas such as the Arctic Ocean and the Antarctic. For example, Intrieri and Shupe (2004) indicated that diamond dust occurred 13% of the time during November 1997 to May 1998 over the south-central Arctic Ocean region. Maxwell (1981) reported high frequency of diamond dust at Canadian Arctic islands and adjacent water, ranging from 20% to 50% of the time. As fog and diamond dust removes water vapor from the atmosphere and these processes are not treated in PIEKTUK-T, the water vapor content in PIEKTUK-T may be too high to affect the subsequent blowing snow sublimation. In addition, there are few accurate water vapor measurements in the Arctic and the distribution of water vapor is subject to great uncertainty. Thus the two experiments CPL and CPL2 can be viewed as two sensitivity tests on the bounds of the effect of blowing snow sublimation, with run CPL yielding the upper bound and run CPL2 the lower bound.

Apart from the blowing snow module, and the adjustment for supersaturated water vapor in experiment CPL, all other physical processes were identical in the three

simulations. The solar and IR radiation schemes were invoked every 30 minutes. The simulation domain of MC2 contains 380x380 horizontal grid points, including the 10-point sponge zone. Horizontal resolution is 18 km, which is true at 60° N in polar stereographic projection. The domain has an area of 6840x6840 km², covering the entire Arctic Ocean and contiguous Canada. 46 vertical Gal-Chen levels were used, with the model lid at 18 km and the lowest level at 12 m. Between 12 m and 1 km, there are 12 matching levels for MC2 and PIEKTUK-T. Above 1 km, there are 34 regularly spaced levels with a grid size of 500 m.

4. Simulation results

We first present results from experiment CPL, including the time series of surface variables, and the evolution of sea level pressure and blowing snow mixing ratio. A comparison between the CPL and STD runs will then be presented, to be followed by the results from run CPL2.

4.1 Simulation CPL

The coupled model was initialized using the Canadian Meteorological Centre (CMC) analysis and the lateral boundary conditions were updated every 6 h. A 96 h simulation was performed covering the period from 1200 UTC 25 November to 1200 UTC 29 November 2005. The beginning of the simulation is designated as $t=0$ h and the end of the simulation as $t=96$ h.

Surface variables are important in determining the occurrence of blowing snow as well as the amounts of blowing snow sublimation and transport. It is therefore important to validate these variables against observations. Hourly measurements from the Coral Harbour station (64.19°N, 83.36°W), located on the Southampton Island at an elevation of 64 m, were used for this purpose. At this station, blowing snow was observed between 25 to 27 November. Figure 3 compares the hourly observed surface temperature, surface relative humidity with respect to ice, and surface winds against the model output at 3 h intervals. The observed relative humidity with respect to water is converted to relative humidity with respect to ice using Teten's formula (Murray 1967). As indicated, the model captures qualitatively the temporal evolution of the surface variables. The surface temperatures show excellent agreement. The wind speeds are somewhat smaller in the model. The simulated relative humidity is generally smaller before 45 h but agrees well thereafter.

The simulated sea level pressure maps every 12 h between $t=12$ h and $t=72$ h are given in Fig. 4, with the symbol **H** indicating the anticyclone of interest. These six times cover the incipient, intensifying, and mature stages of the anticyclone. The simulated SLPs are very similar to the patterns from the analysis (Fig. 2), indicating that the evolution of anticyclone is properly simulated with regard to its location, intensity and structure.

From Fig. 4, it can be seen that with the intensification of anticyclone situated over the Arctic Ocean, both the SLP gradients and horizontal wind speeds increase considerably. For example, horizontal wind speeds over the Beaufort Sea increase from 20 knots at $t=12$ h to 30 knots at $t=72$ h over the strengthening SLP gradient regions, and the region

with intensified wind speed shifted north with time in association with the northward movement of the cyclone (indicated by **L** in Fig. 4).

Blowing snow is found at the edge of the anticyclone. The evolution of the blowing snow mixing ratio at 12 m (the first level of MC2) is depicted in 24 h intervals in the left panels of Fig. 5. As can be seen, blowing snow mainly occurred over northern and northeastern Siberia, the western Arctic Ocean and the Canadian Arctic Archipelago. These regions were also characterized by strong surface winds (Fig. 4). Over the anticyclonogenesis region (indicated with **H** in Fig. 4d), blowing snow mixing ratios attained values up to 0.02 g kg^{-1} at $t=48 \text{ h}$ (Fig. 5c) and the maximum values remain relatively constant thereafter. In contrast, the region covered by blowing snow becomes elongated in the east-west direction in association with the developing anticyclone. The blowing snow mixing ratio decreases rapidly with height as a result of particle sedimentation so blowing snow is mainly trapped in the lower boundary layer.

The right panels of Fig. 5 show 3-hourly column-integrated (from the ground up to 1 km) blowing snow sublimation ending at 24, 48, and 72 h respectively. The sublimation is determined by the mass of blowing snow, the particle size distribution, atmospheric water vapor deficit, and the ventilation effects (due to the settling of suspended particles). The 3-hourly blowing snow sublimation is relatively small over the anticyclonogenesis region, with values of only 0.05 mm snow water equivalent (SWE), much less than the sublimation rates over the Baffin Island regions. The reason is that the temperature over the Arctic Ocean is very cold, and the corresponding saturated water vapor pressure rather small. This results in a high relative humidity and a low water vapor deficit, thus limiting the sublimation rates. Although other factors affect the amount of sublimation,

the sublimation regions are nonetheless collocated with high blowing snow mixing ratio areas.

4.2 Comparison between the CPL and STD simulations

Figure 6 presents 12 hourly temperature differences between the two simulations at 12 m (Gal-Chen level). The CPL run depicts several areas of enhanced cooling against the STD run over the Bering Strait, Mackenzie Bay, southern Yukon Territory, Hudson Bay, Quebec and Greenland at $t=12$ h. The areas where blowing snow occurred (Figs. 5a, 5c and 5e) over the western Arctic Ocean were consistent with the cooling regions (Figs. 6b, 6d and 6f), and the cooling effects are seen to intensify with time (Fig. 6). At $t=12$ h, the maximum temperature difference between the two simulations over the Beaufort Sea area is about -5°C (Fig. 6a), but is limited to a relatively small area. At $t=24$ h, the cooling area extended to the western Arctic Ocean, and the temperature difference became -10°C (Fig. 6b). The cooling in this region continued to strengthen until $t=72$ h when the difference was as large as -14°C (Fig. 6f).

Figure 7a depicts a vertical section of the temperature difference at 72 h along a line from A to B illustrated in Fig. 6f. The cooling is confined to the boundary layer and becomes negligible above 1 km. It is interesting to note that significant cooling extends to heights above the region of blowing snow. Most blowing snow particles reside within a few tens of meters from the surface and the blowing snow mixing ratio decreases with height rapidly thereafter. Since few particles are found at levels higher than 100m, blowing snow sublimation would not contribute significantly to the temperature

decreases at these levels. Moreover, blowing snow sublimation is a self-limiting process as sublimation increases the air humidity and decreases the temperature. The air soon reached saturation with respect to ice and sublimation would cease unless advection and mixing can bring in drier environmental air. As a result, the accumulated blowing snow sublimation in 72 hours over the western Arctic Ocean was not large, amounting to less than 1 mm SWE (Fig. 7b). Other processes must be in operation to bring about the large temperature differences between the CPL and STD runs.

We examine other factors which may influence cooling. These include explicit microphysics, solar radiation, infrared radiation and vertical diffusion from the boundary layer processes. A comparison of these terms indicated that vertical diffusion is the leading factor. In MC2, eddy vertical diffusion (Benoit and Mailhot 1989) is used to treat the ABL transport. In experiment CPL, blowing snow sublimation cooling and the removal of the supersaturated water vapor with respect to ice change the vertical profile of virtual potential temperature, especially near the first level of MC2. The colder virtual potential temperature at $z=12$ m greatly decreased the local gradient Richardson number and stability in the surface layer, thus enhancing the downward heat flux. The increased downward heat flux then accounts for much of the temperature decrease at higher levels.

Figure 8 shows sea level pressure differences between the CPL and STD runs. Note that there are several regions where sea level pressure in the CPL run was higher. These regions were consistent with areas of cooling. Over the region of anticyclogenesis, the simulated SLP in CPL was 5 mb higher than in STD at the end of simulation. This signifies that the cooling effect may have a non-negligible contribution to the dynamics of anticyclones.

5. PV inversion

Potential vorticity (PV) is a conserved dynamic variable in adiabatic and inviscid flow. The invertibility of PV makes it possible to recover the mass and wind fields given a PV distribution. Based on these two characteristics (conservation and invertibility), Davis and Emanuel (1991) developed a piecewise PV inversion technique to quantify the effects of local PV anomalies on the flow field. This approach has been applied to examine the dynamical effects of PV anomalies on surface cyclogenesis, mesoscale vorticies, and frontal precipitation (Davis and Emanuel 1991; Black and Dole 1993; Davis 1993; Hakim et al. 1996). We will apply this tool to investigate the cooling effects from blowing snow on the dynamics of high latitude wintertime anticyclongenesis. A summary of the relevant equations for PV inversion are given in Appendix 1.

5.1 Basis for PV diagnostics of the effects of blowing snow sublimation

It is known that surface potential temperature (θ) perturbations can be thought of as equivalent to a PV anomaly at the surface (Hoskins et al. 1985; Davis and Emanuel 1991; Davis 1992). This ‘surface PV anomaly’ can contribute substantially to the low level pressure and circulation fields of cyclones (Thorpe 1986; Robinson 1989). Warm surface temperature anomalies correspond to cyclonic vorticity and cold anomalies correspond to anticyclonic vorticity. We anticipate that surface cooling anomalies can play a role in anticyclongenesis. With the appropriate boundary conditions (Dirichlet condition in the horizontal and Neumann condition in the vertical), one can obtain by iteration the

nonlinear balanced flow associated with a given PV anomaly. The individual balanced flow from the piecewise PV inversion can then be summed to obtain the complete perturbation flow. We use data from 12 pressure levels (1000, 950, 850, 700, 600, 500, 400, 300, 250, 200, 150 and 100 mb) for the inversion. Specifically, the horizontal winds, the temperatures, and the geopotential heights at these levels were used to calculate θ and PV. For points below the ground level, we followed Davis et al. (1993) and Davis (1997) by setting the surface θ anomalies to the values at the lowest level above the ground and the PV to the Coriolis parameter f .

PV anomalies are usually calculated as departures from values averaged over one synoptic scale wave period (Davis and Emanuel 1991; Hakim et al. 1996; Chen et al. 2006). In the present case, however, we follow another approach proposed by Davis (1992). In our study, we are interested not in the PV perturbations relative to a time average, but rather in PV anomalies calculated as the difference in PV (and surface temperature) between the CPL and STD runs. Inversion of the surface θ and PV anomalies defined in this way allows one to obtain the net effect of diabatic cooling on the overall anticyclogenesis at any level within the atmosphere.

It is known that PV inversion is a smoothing operator and does not work efficiently with high resolution datasets (Davis et al. 1993). In the study of Davis et al. (1993), the data were coarsened by a factor of three (from 45 km to 135 km) before the PV inversion was performed. Their results demonstrated that coarsening of the resolution does not affect the solution significantly on scales greater than 200 km. In our calculation, we

followed the same procedure by coarsening the model data from 18 km to 54 km in the horizontal while keeping the volume integral of the data unchanged.

5.2 Diagnostic results

Figure 9 depicts the evolution of the surface θ anomaly and the associated 850 mb geopotential height perturbation obtained by inverting this anomaly at 12 hour intervals. θ anomalies over the western Arctic Ocean were seen south of the surface anticyclone where there is a steep surface pressure gradient. The anomalies are associated with diabatic cooling and their inversion yields an appreciable surface anticyclonic circulation. The inverted geopotential height peaks at the surface and is in phase with the cooling region. At $t=24$ h, the center of the cooling over the Arctic anticyclone under consideration is about -7°C (Fig. 9b), and the associated geopotential height perturbation amounts to 2.8 dam at 850 mb. With time the lower level diabatic cooling intensified and the inverted geopotential height values strengthened and extended to a large domain over the Arctic Ocean north of Alaska. For example, the central value of the cooling region is about -9.5°C , and the resulting geopotential height is relatively large with a value up to 9.6 dam at 850 mb at $t=48$ h (Fig. 9d). By $t=72$ h, further cooling resulted in a maximum geopotential height perturbation of 14.9 dam at 850 mb. At 1000 mb, the value is as high as 19 dam and the inverted geopotential height perturbation extends vertically to 200 mb (not shown). Thus the effect of lower level cooling can extend to the entire atmosphere.

Notice that the cooling areas and the associated geopotential height anomalies are along the regions of steep pressure gradient around the edge of the anticyclone. To gauge

how these anomalies alter the overall strength of the anticyclone, we computed the distribution of the horizontally averaged inverted geopotential height over the areal extent of the anticyclone (within the closed SLP contour of 1028 mb). The results (Fig. 10) indicate the largest effect near the surface. The averaged 1000 mb inverted geopotential height anomaly is 0.77 dam at $t=24$ h, and increases to 2.9 dam at $t=48$ h and 4.5 dam at $t=72$ h. However, the perturbation height associated with blowing snow cooling extends much higher than the vertical extent of the direct cooling which is confined to the boundary layer.

The dominance of the anticyclonic flow at low levels is easily seen from Fig. 11 which presents the inverted horizontal wind and the potential temperature field at 850 mb. At $t=24$ h, anticyclonic flow over the Arctic Ocean becomes evident with maximum wind speed of 5 knots. With the intensification of the cooling, this anticyclonic flow increased to 12 knots at $t=48$ h and 17 knots at 72 h south of the center of the anticyclone. By superposing the inverted wind field and the surface thermal field, it can be seen that warm air is being advected from the Bering Sea to the northwest of the anticyclone. This low level warm advection contributes to the amplification of the upper level ridge important for anticyclogenesis.

6. Discussion and concluding remarks

An additional experiment (CPL2) which allows for supersaturated water vapor with respect to ice to remain in the air was also performed. This corresponds to a lower bound for blowing snow sublimation. Fig. 12 depicts the 12 m temperature differences between

the CPL2 run and the STD run every 12 h. By comparing Fig. 12 with Fig. 6, it is clear that the sublimation cooling is much smaller in experiment CPL2 than in experiment CPL. The cooling in CPL2 is short-lived. At the start of the blowing snow event, the air is subsaturated with respect to ice and blowing snow sublimation acts to decrease the air temperature and to increase the water vapor content. As the temperatures over the anticyclone of interest are colder than -20°C , only a small increase in water vapor is sufficient to saturate the air with respect to ice and blowing snow sublimation ceases, even though blowing snow particles remain suspended in the boundary layer. Horizontal advection and entrainment of dry air can allow for subsaturated conditions to be reestablished. However, the surface θ anomalies in CPL2 were much weaker than in the CPL run. As a result, the warm advection associated with the inverted wind and temperature was much weaker in CPL2.

In summary, a coupled blowing snow-atmospheric model was used to simulate a case of Arctic anticyclonogenesis event to examine the effects of blowing snow on the anticyclone. The anticyclone belongs to the blocking type, and this deep system stayed over the Arctic Ocean for about one week. Comparing the results between the CPL and STD runs indicated significant cooling effects and the cooling regions were consistent with areas with blowing snow. Part of the cooling arises from blowing snow sublimation and the accompanying phase change and part of the cooling results from an enhanced downward heat flux. The cooling effects gave rise to a sea level pressure increase. Although the increased SLP is located on the edge of the anticyclone, it has a relatively large magnitude (up to 5 mb) and therefore a non-negligible effect on anticyclonogenesis.

The conservation and invertibility of PV allow for an inversion to obtain the balanced flow fields associated with the PV anomaly field. Specifically, the balanced geopotential height and wind fields corresponding to the surface θ anomaly were recovered and the related contribution to the lower level anticyclone development was examined and quantified. The results showed that the cooling effects correspond to a balanced geopotential height perturbation of 19 dam at 1000 mb and 14.9 dam at 850 mb. The anomalies have large horizontal scales and are centered near the edge of the anticyclone. Horizontal averages over the areal extent of the anticyclone show that blowing snow cooling can result in a 4.5 dam increase in the overall anticyclone strength at 1000 mb. The inverted geopotential height anomalies extend to the upper levels, although the magnitude decreases significantly with height. It thus appears that blowing snow cooling can play a significant role on the dynamics of anticyclogenesis. We caution, however, that these results represent an upper bound. By allowing the supersaturated vapor with respect to ice to remain in the atmosphere in experiment CPL2, a much smaller blowing snow sublimation cooling and dynamic response resulted.

Acknowledgements. The authors are grateful to Dr. Badrinath Nagarajan for his help in running the coupled model on a Linux clusters, and helpful suggestions in editing the manuscript as well. This research is supported by the Natural Science and Engineering Research Council of Canada.

Appendix 1 Potential vorticity inversion diagnostic equations

For a fully baroclinic and compressible flow, Ertel's potential vorticity (EPV) (Ertel 1942; Rossby 1940) is defined as

$$q = \frac{1}{r} \vec{h} \cdot \nabla q \quad (1)$$

where r is density, \vec{h} is the three dimensional absolute vorticity vector, q is potential temperature and ∇ is the three dimensional gradient operator. In the absence of diabatic and frictional effects, q is a conserved dynamical field. q is measured in pvu, with 1 pvu = $10^{-6} \text{ kg}^{-1} \text{ K m}^2 \text{ s}^{-1}$.

Making the traditional approximation, the absolute vorticity \vec{h} is given by $\vec{h} = f\vec{k} + \nabla \times \vec{V}$, where \vec{V} is the three-dimensional velocity vector. In Cartesian coordinates, q becomes

$$q = \frac{1}{r} \left[\left(\frac{\partial v}{\partial x} - \frac{\partial u}{\partial y} + f \right) \frac{\partial q}{\partial z} + \left(\frac{\partial w}{\partial y} - \frac{\partial v}{\partial z} \right) \frac{\partial q}{\partial x} + \left(\frac{\partial u}{\partial z} - \frac{\partial w}{\partial x} \right) \frac{\partial q}{\partial y} \right] \quad (2)$$

By further assuming that the irrotational component of the wind is small compared to the non-divergent component yields Charney's nonlinear balance equation (Charney 1955), which can be written as

$$\nabla^2 f = \nabla \cdot f \nabla y + 2m^2 \left[\frac{\partial^2 y}{\partial x^2} \frac{\partial^2 y}{\partial y^2} - \left(\frac{\partial^2 y}{\partial x \partial y} \right)^2 \right] \quad (3)$$

where ∇^2 is the two-dimensional Laplacian operator, f denotes the geopotential height, y is the streamfunction, f is the Coriolis parameter, and m is the map scale factor.

Finally, by making the hydrostatic approximation, neglecting the vertical velocity contribution to PV, and replacing the horizontal winds in Equation 2 by the non-divergent winds, the EPV can be expressed as a nonlinear function of f and y as:

$$q = \frac{gkp}{p} \left[(m^2 \nabla^2 y + f) \frac{\partial^2 f}{\partial p^2} - m^2 \frac{\partial^2 y}{\partial x \partial p} \frac{\partial^2 f}{\partial x \partial p} - m^2 \frac{\partial^2 y}{\partial y \partial p} \frac{\partial^2 f}{\partial y \partial p} \right] \quad (4)$$

Here p is pressure, $k=R_d/C_p$ is the ratio of dry gas constant and specific heat capacity at constant pressure, and the Exner function p is the vertical coordinate which is defined as

$$p = C_p \left(\frac{p}{p_0} \right)^k, \text{ with } p_0 \text{ set to 1000 mb.}$$

Once the PV distribution and lateral boundary conditions are given, Equations 3 and 4 can be solved by a standard successive over-relaxation iterative numerical method. Here, Dirichlet conditions are used for y and f at the lateral boundaries and Neumann conditions, i.e.

$$\frac{\partial f}{\partial p} = f \frac{\partial y}{\partial p} = -q \quad (5)$$

are specified at both lower and upper boundaries.

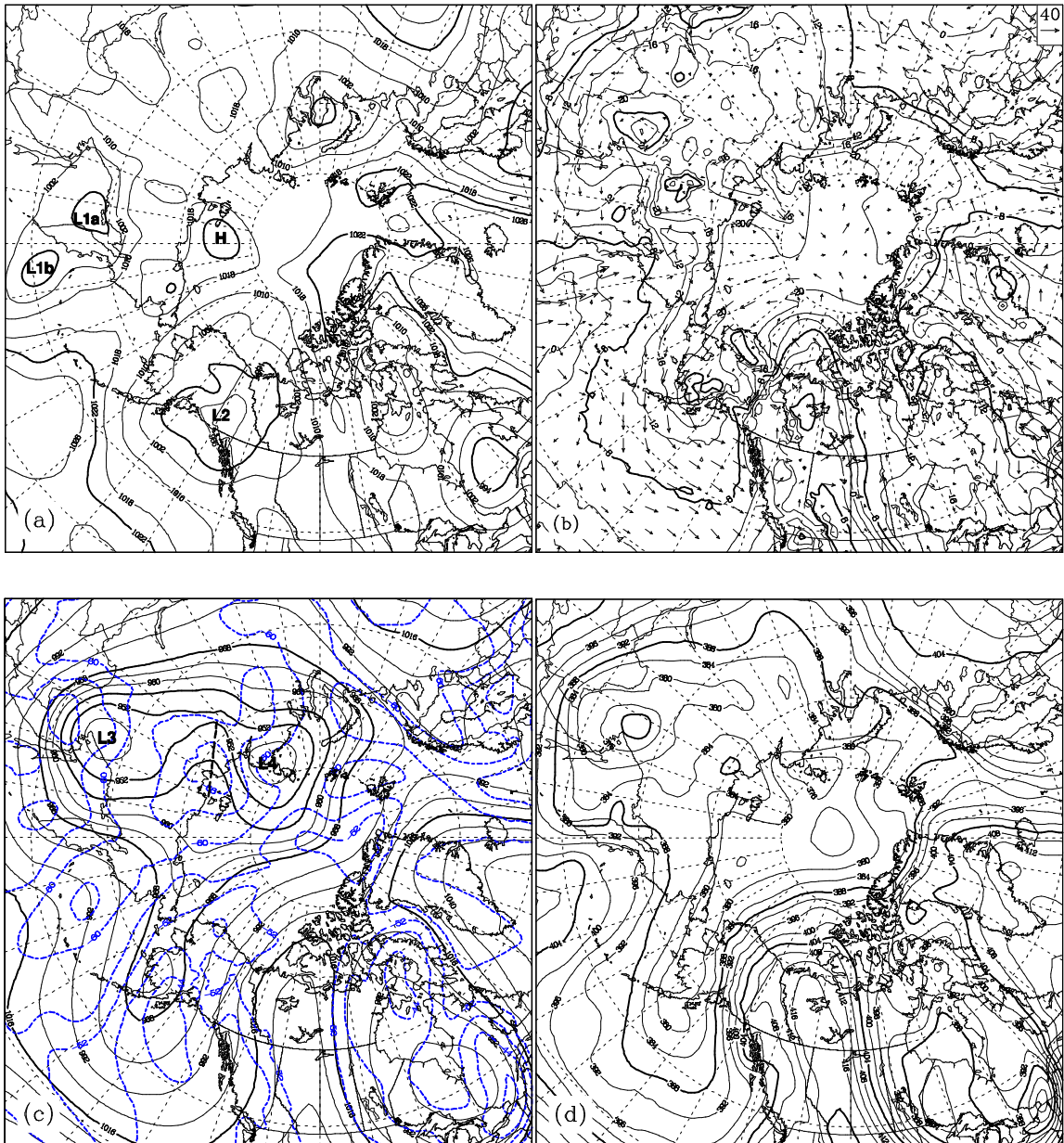


Figure 1: (a) Sea level pressure (solid contours every 8 mb below 1018 mb and every 4 mb above 1018 mb), (b) 850-mb temperature (solid contours every 4 °C) and wind speed (unit: knots), (c) 250-mb geopotential height (solid contours every 4 dam) and temperature (blue dashed contours every 4 °C), and (d) 850-500 mb thickness (solid contours every 4 dam) at 1200 UTC Nov 25 2005 from CMC analysis data.

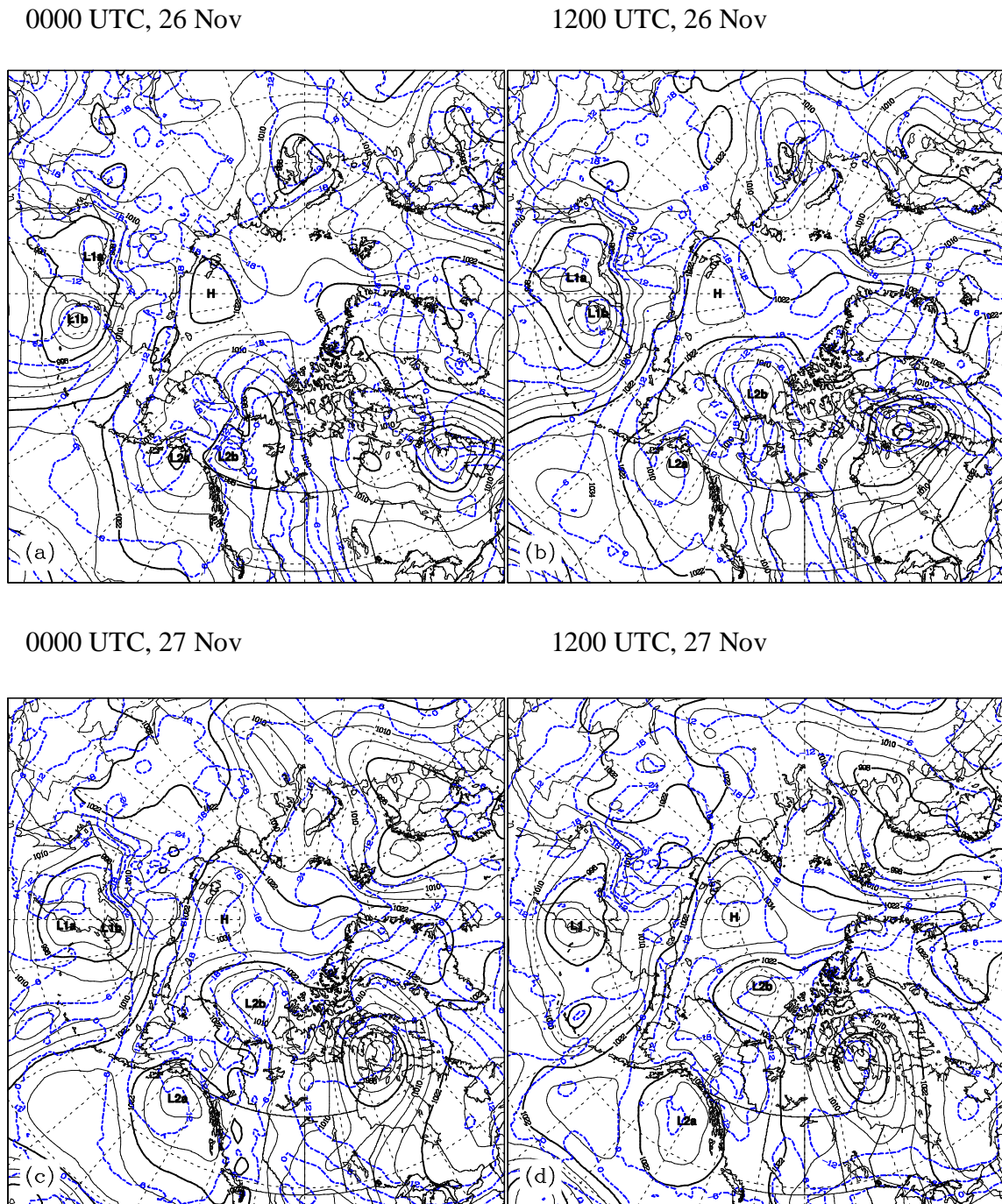


Figure 2: Sea level pressure (black solid contours every 6 mb) and 850-mb temperature (blue dashed contours every 6 °C) from 0000 UTC 26 Nov 2005 to 1200 UTC 28 Nov at 12 h intervals (a-f) from CMC data.

0000 UTC, 28 Nov

1200 UTC, 28 Nov

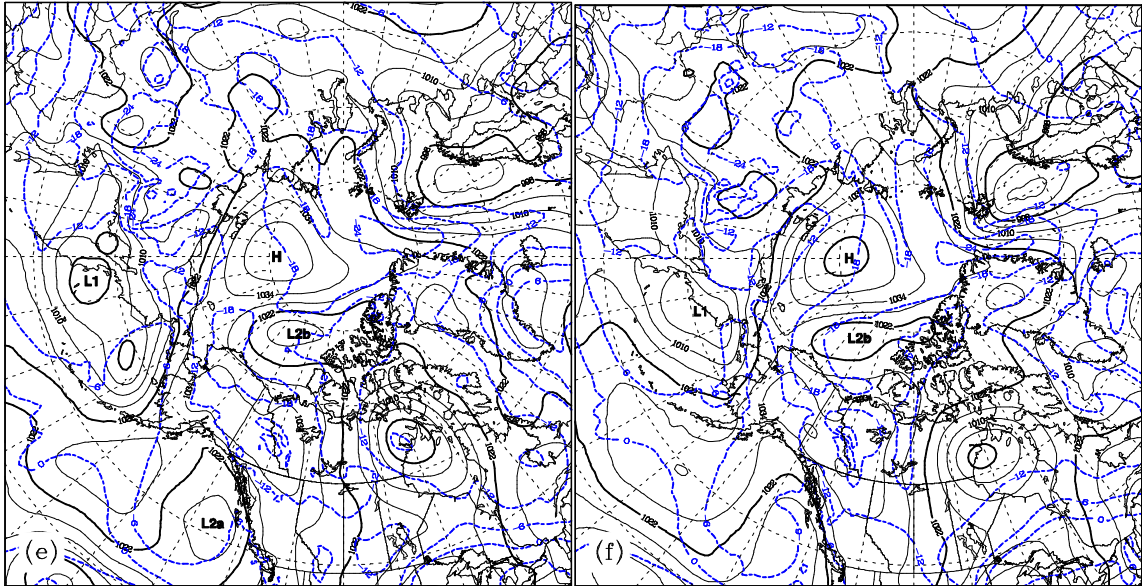


Figure 2: (Continued)

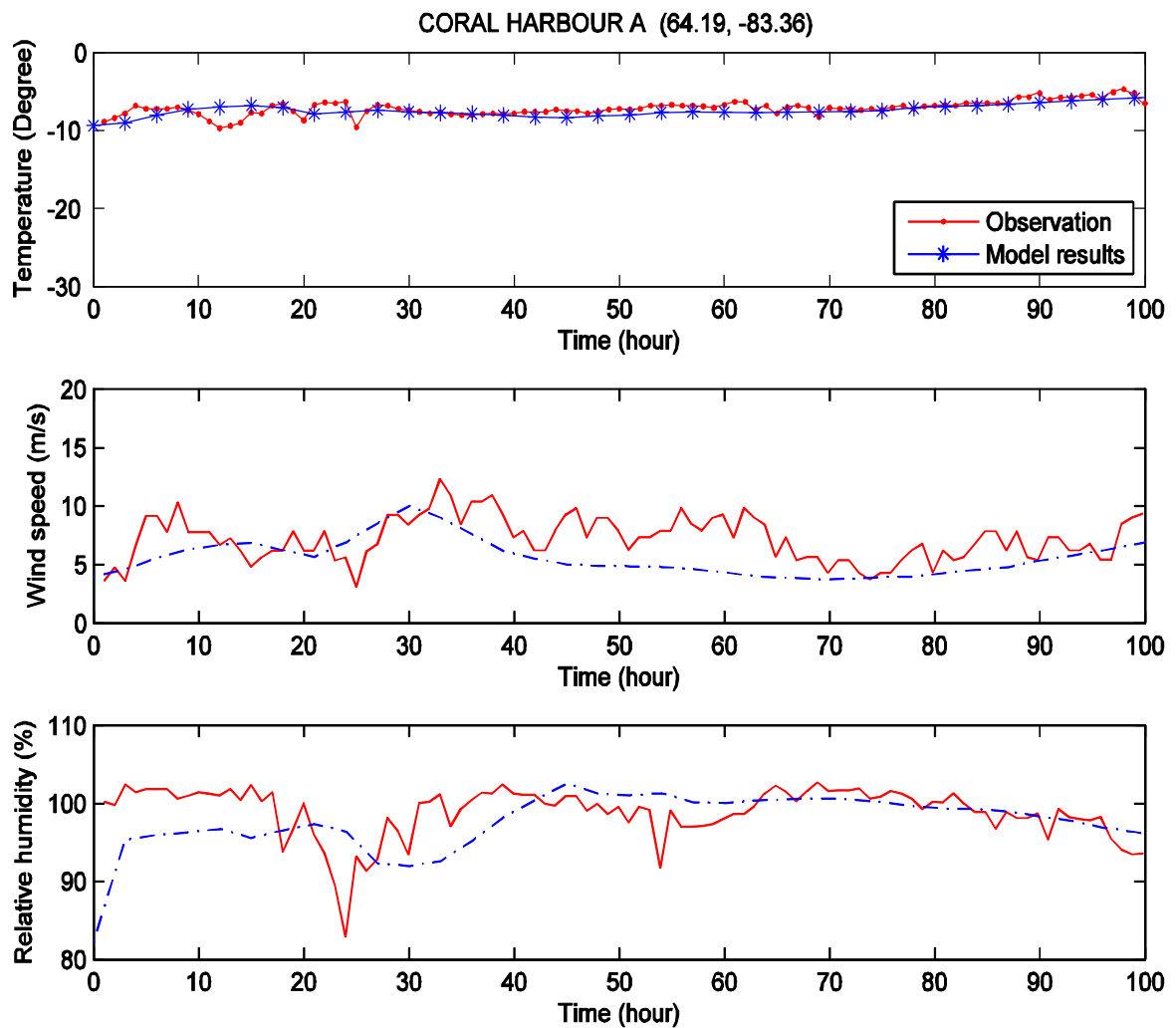


Figure 3: Comparison of observed and simulated (a) air temperature (unit: °C), (b) wind speed (unit: ms^{-1}) and (c) relative humidity with respect to ice at Coral Harbour station (64.19 °N, -83.36 °W) from 1200 UTC 25 November to 29 November.

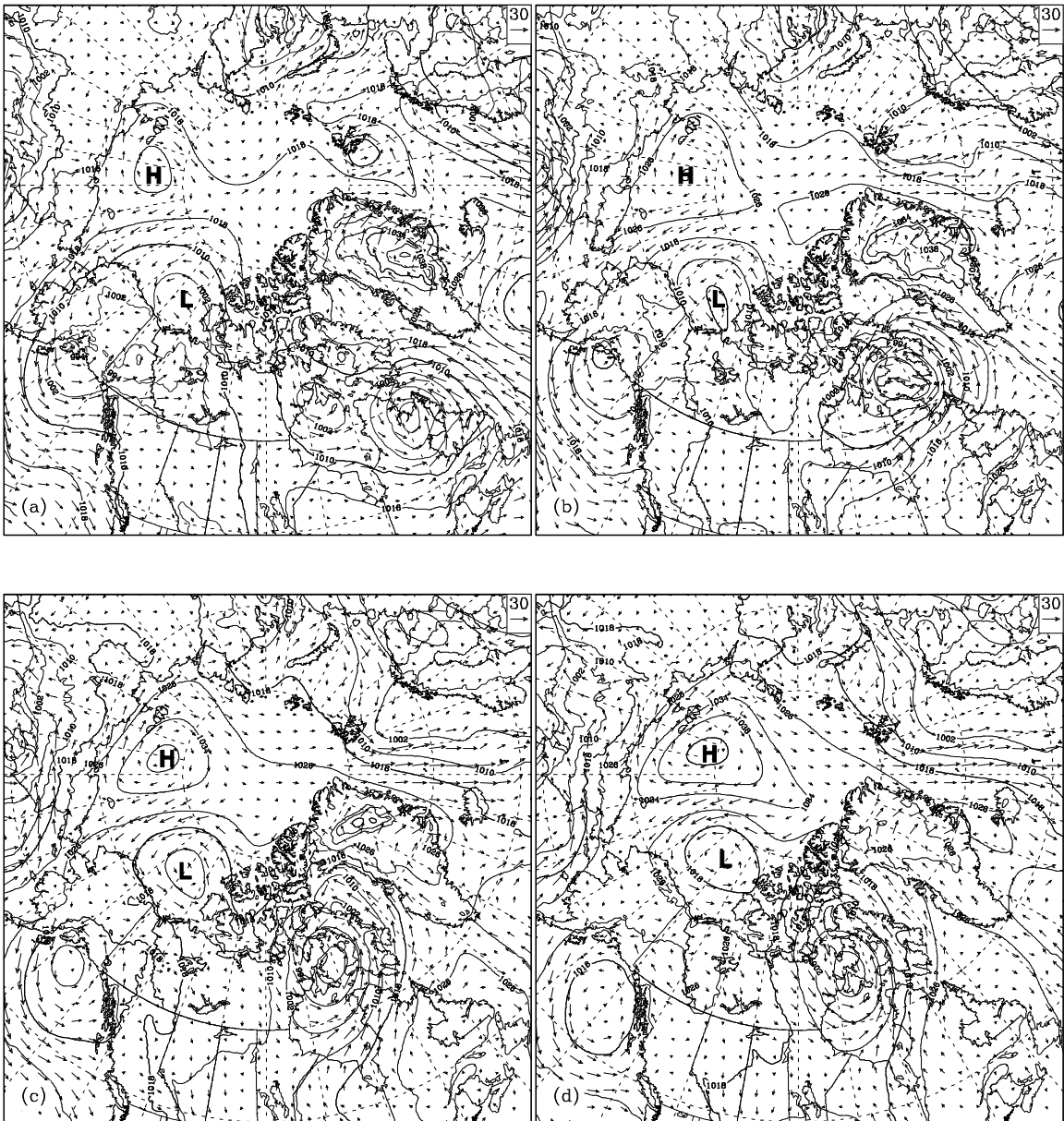


Figure 4: Sea level pressure (solid contours every 8 mb) and surface wind vectors (unit: knots) at $t=12, 24, 36, 48, 60$ and 72 h (a-f) from the CPL run.

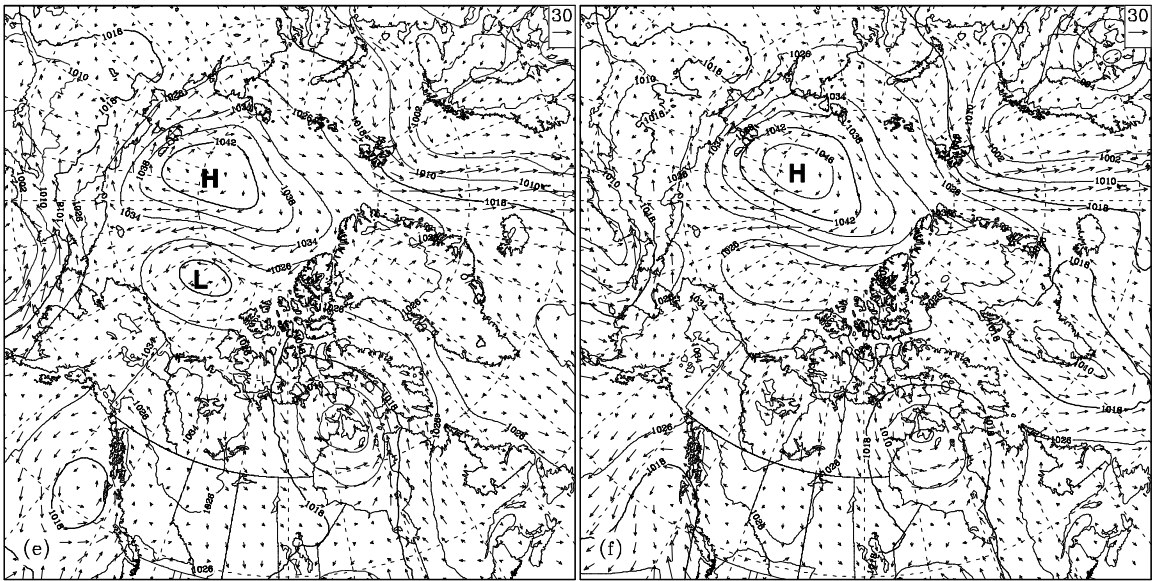


Figure 4: (Continued)

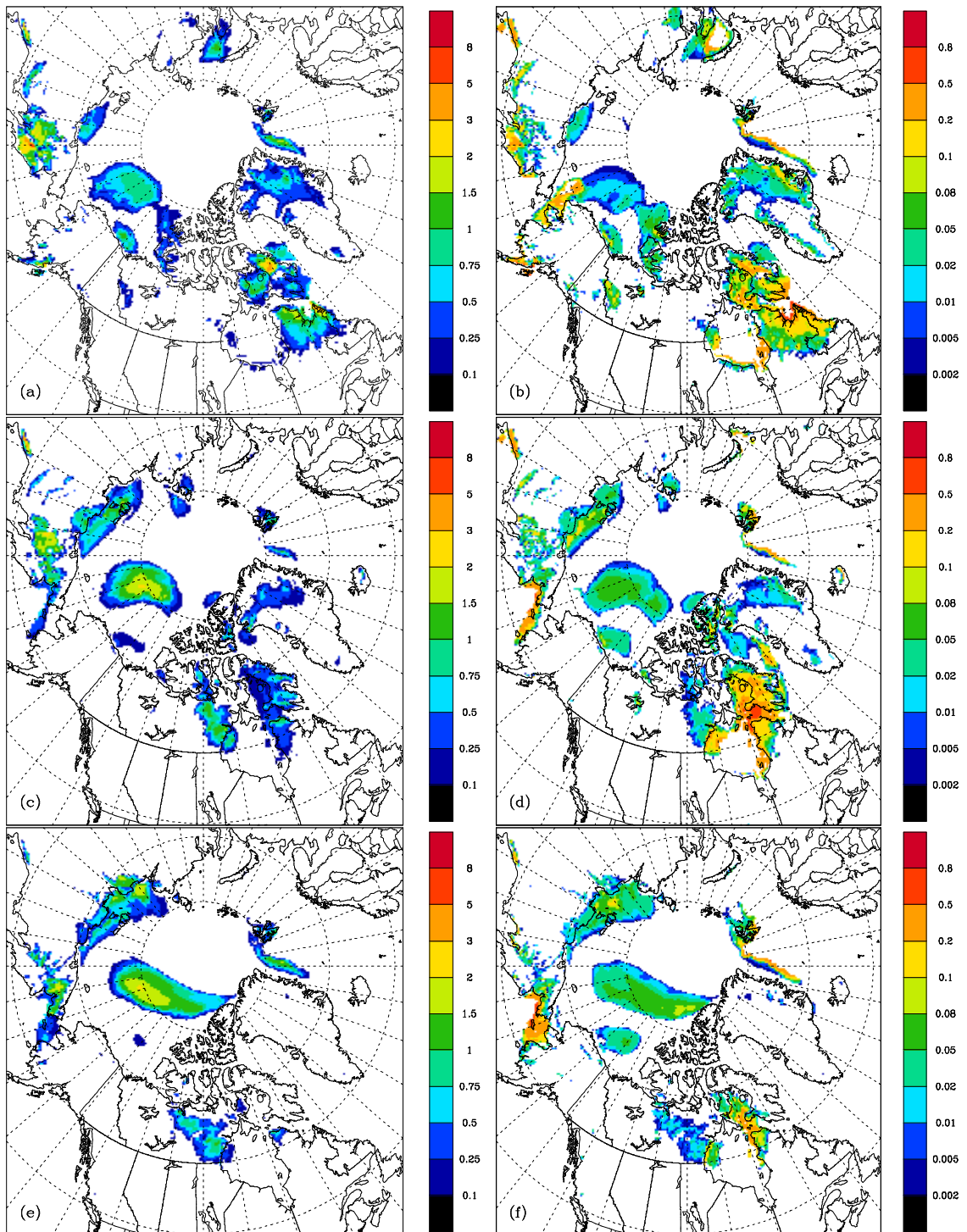


Figure 5: Blowing snow mixing ratio q_b at 12 m (a, c and e in the left panel, unit: 10^{-5} kgkg^{-1}), and 3-hour accumulated blowing snow sublimation (b, d and f in the right panel, unit: mm SWE) at $t=24$, 48 and 72 h from the CPL run.

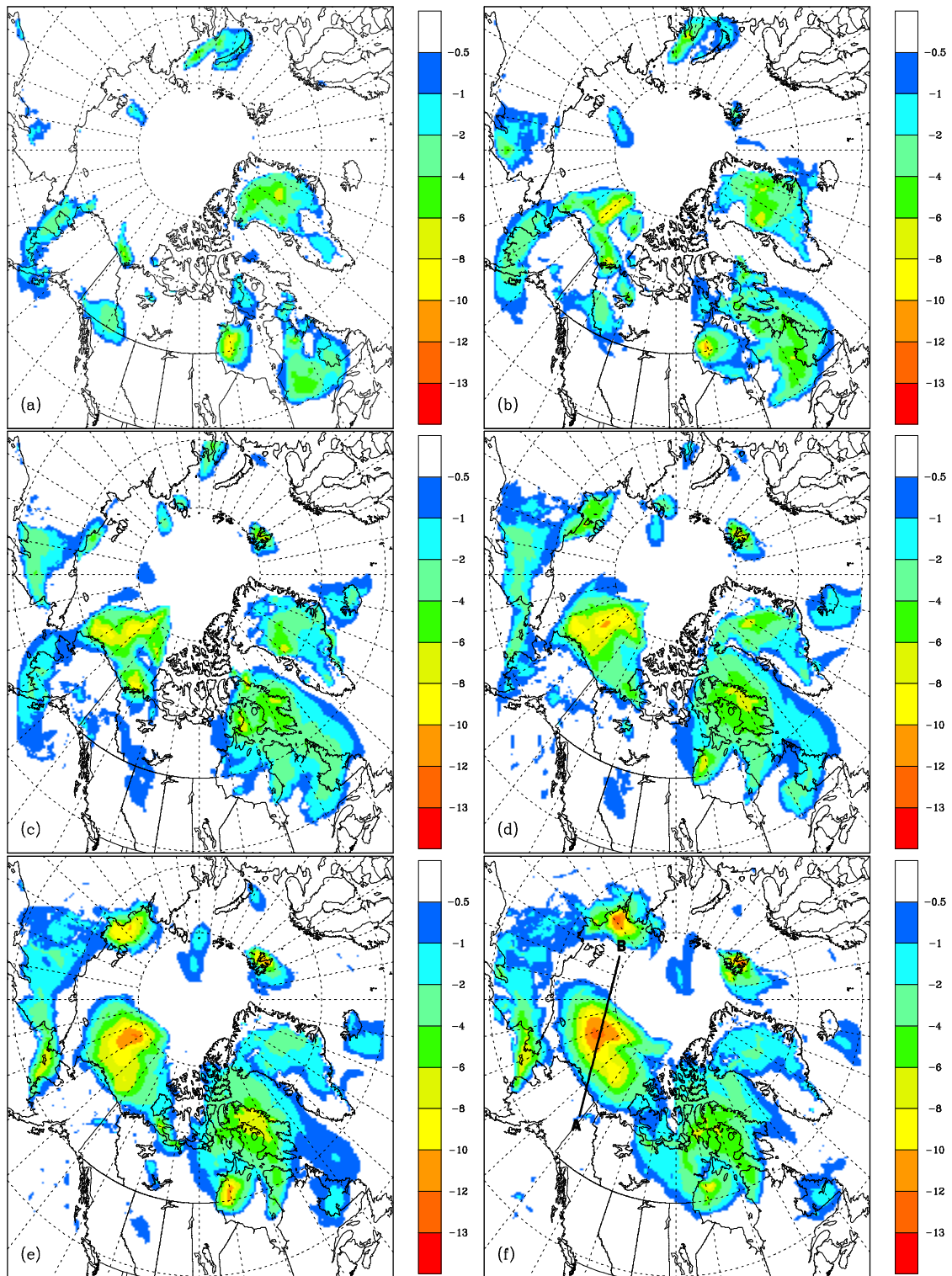


Figure 6: Temperature differences (unit: $^{\circ}\text{C}$) at 12 m between the CPL and STD runs at $t=12, 24, 36, 48, 60$ and 72 h (a-f).

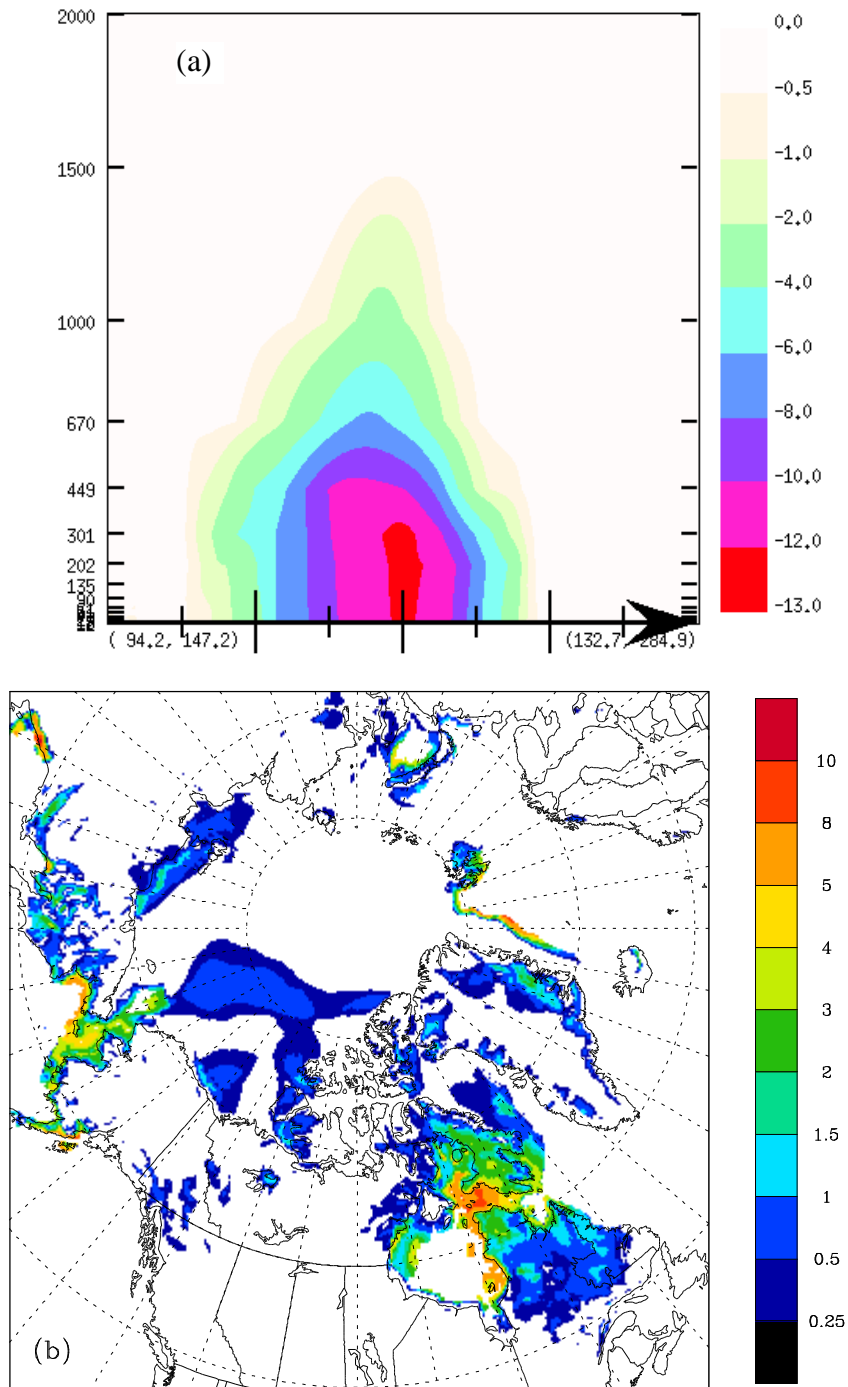


Figure 7: (a) Vertical cross section of temperature differences (unit: $^{\circ}\text{C}$), and (b) 72-hr accumulated blowing snow sublimation (unit: mm SWE).

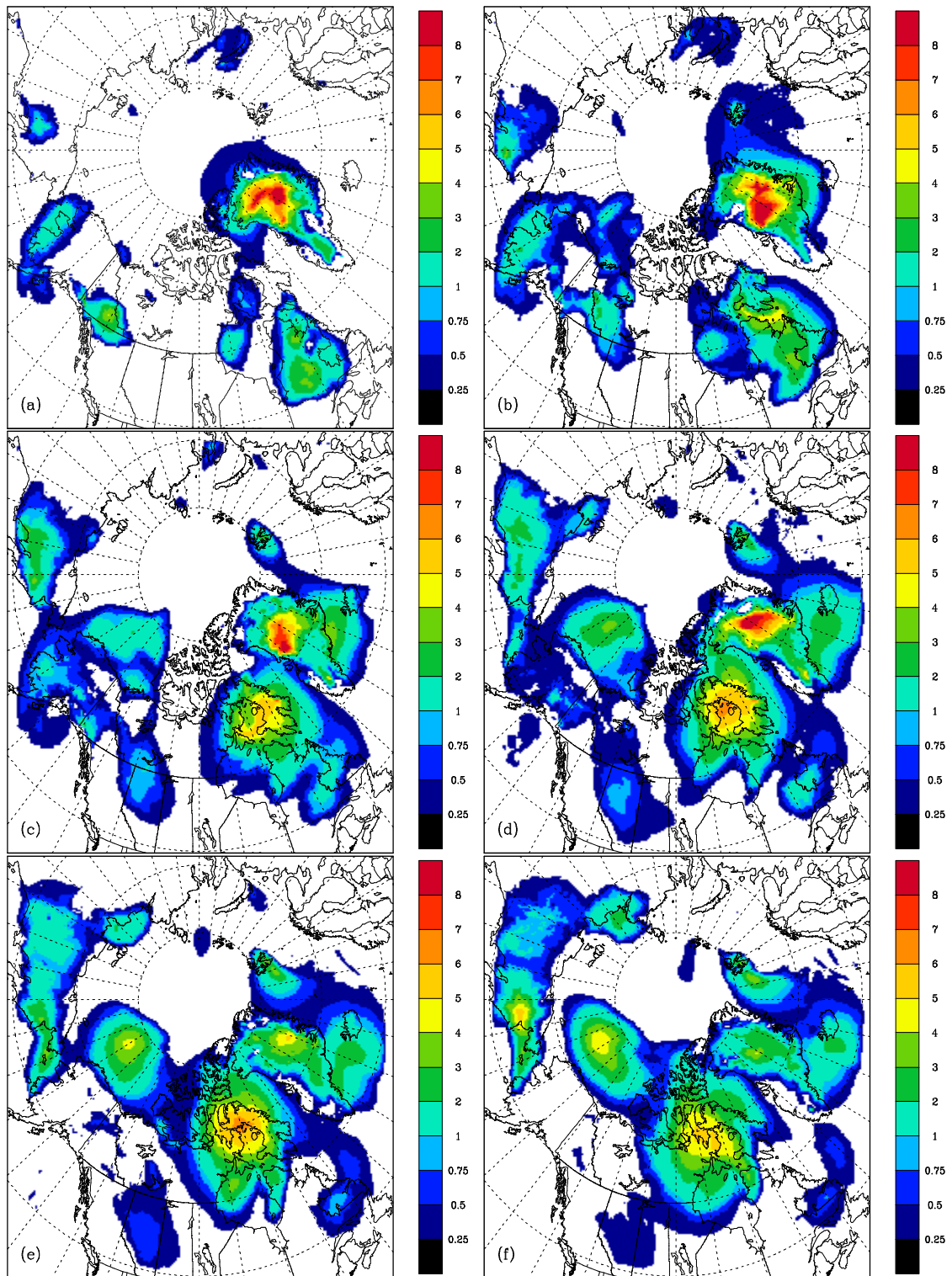


Figure 8: Sea level pressure differences (unit: mb) between the CPL and STD runs at $t=12, 24, 36, 48, 60$ and 72 h (a-f).

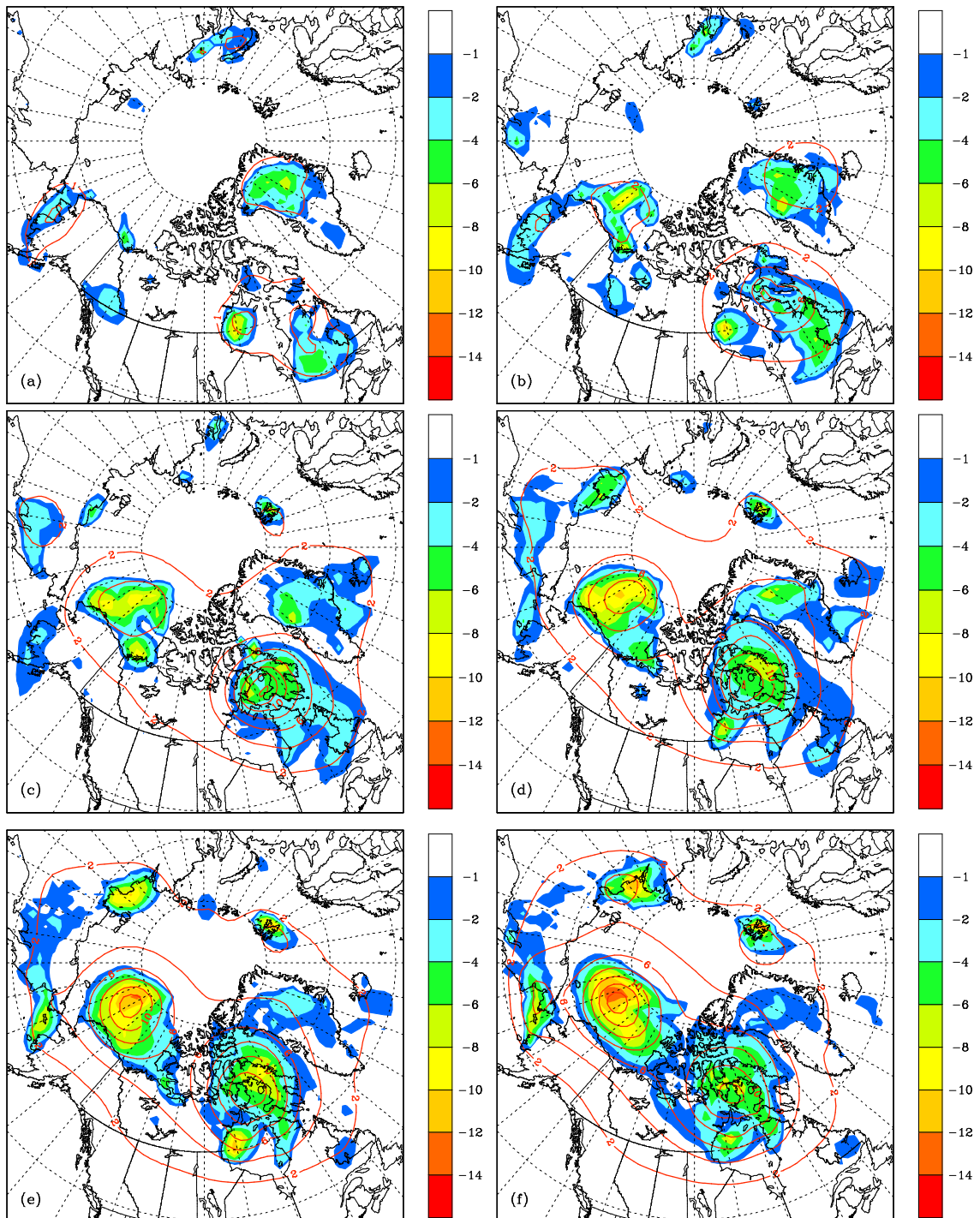


Figure 9: Potential temperature θ differences (color shading, unit: K) between the CPL and STD runs and the inverted 850-mb geopotential height (red solid contours every 2 dam) at $t=12, 24, 36, 48, 60$ and 72 h (a-f).

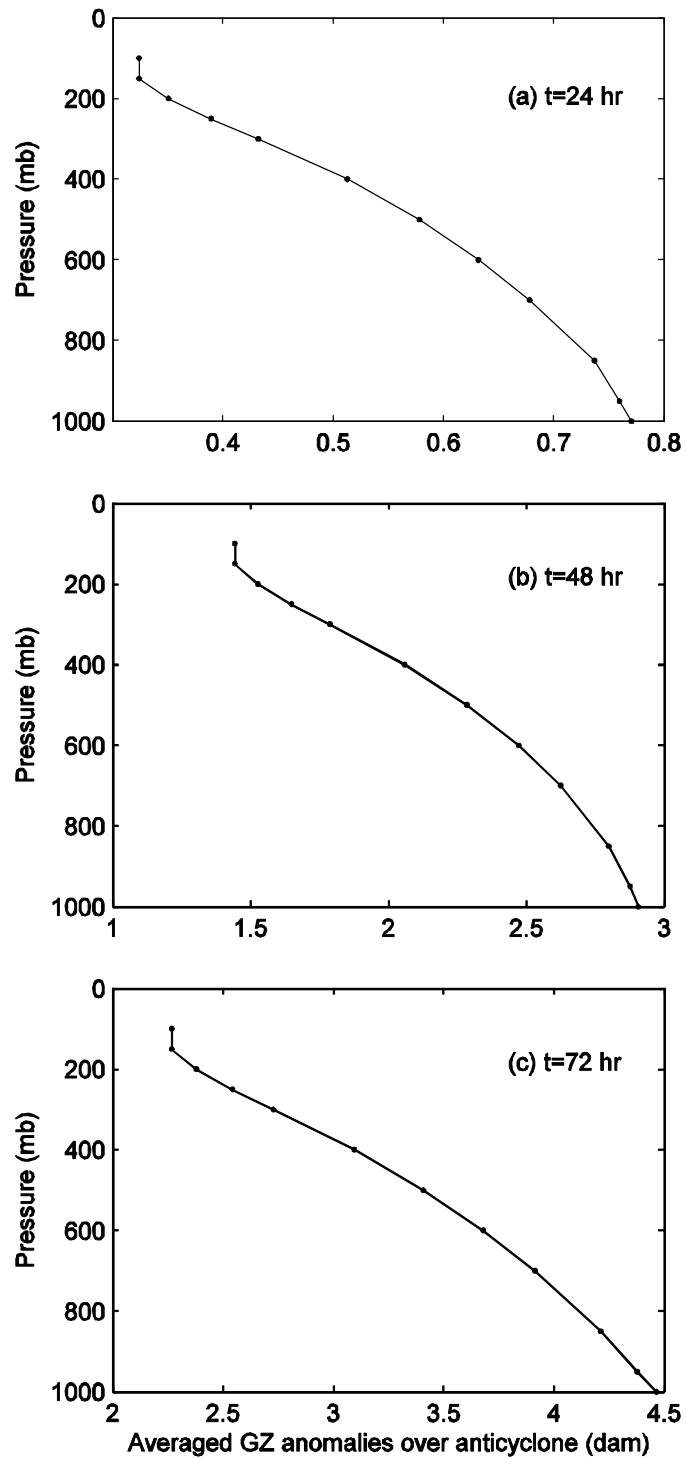


Figure 10: Vertical profiles of inverted geopotential height (unit: dam) averaged over the areal extent of the anticyclone at $t=24$, 48 and 72 h (a-c).

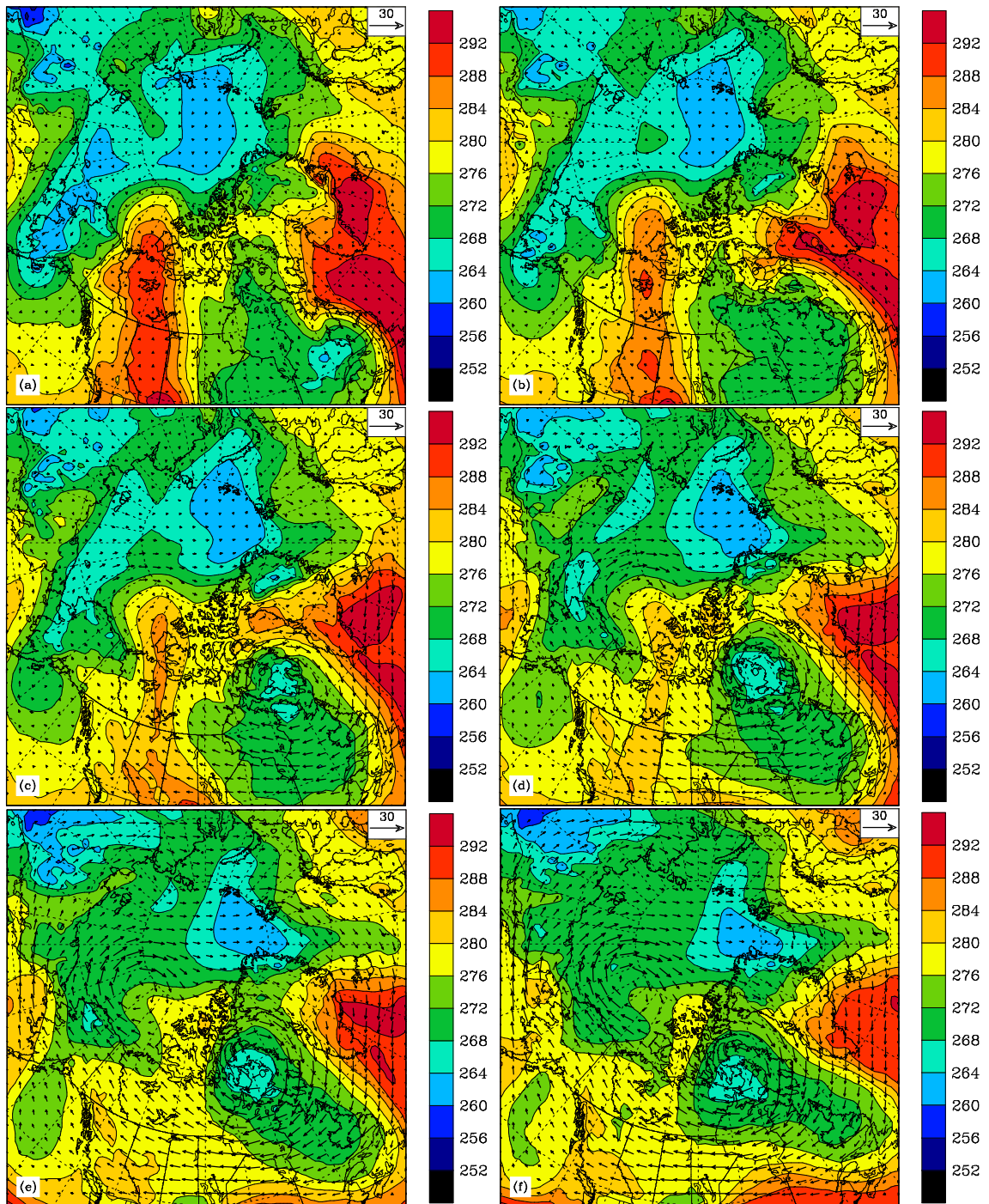


Figure 11: 850-mb potential temperature θ (color shading, unit: K) and balanced velocity (vector, unit: knots) at $t=12, 24, 36, 48, 60$ and 72 h (a-f).

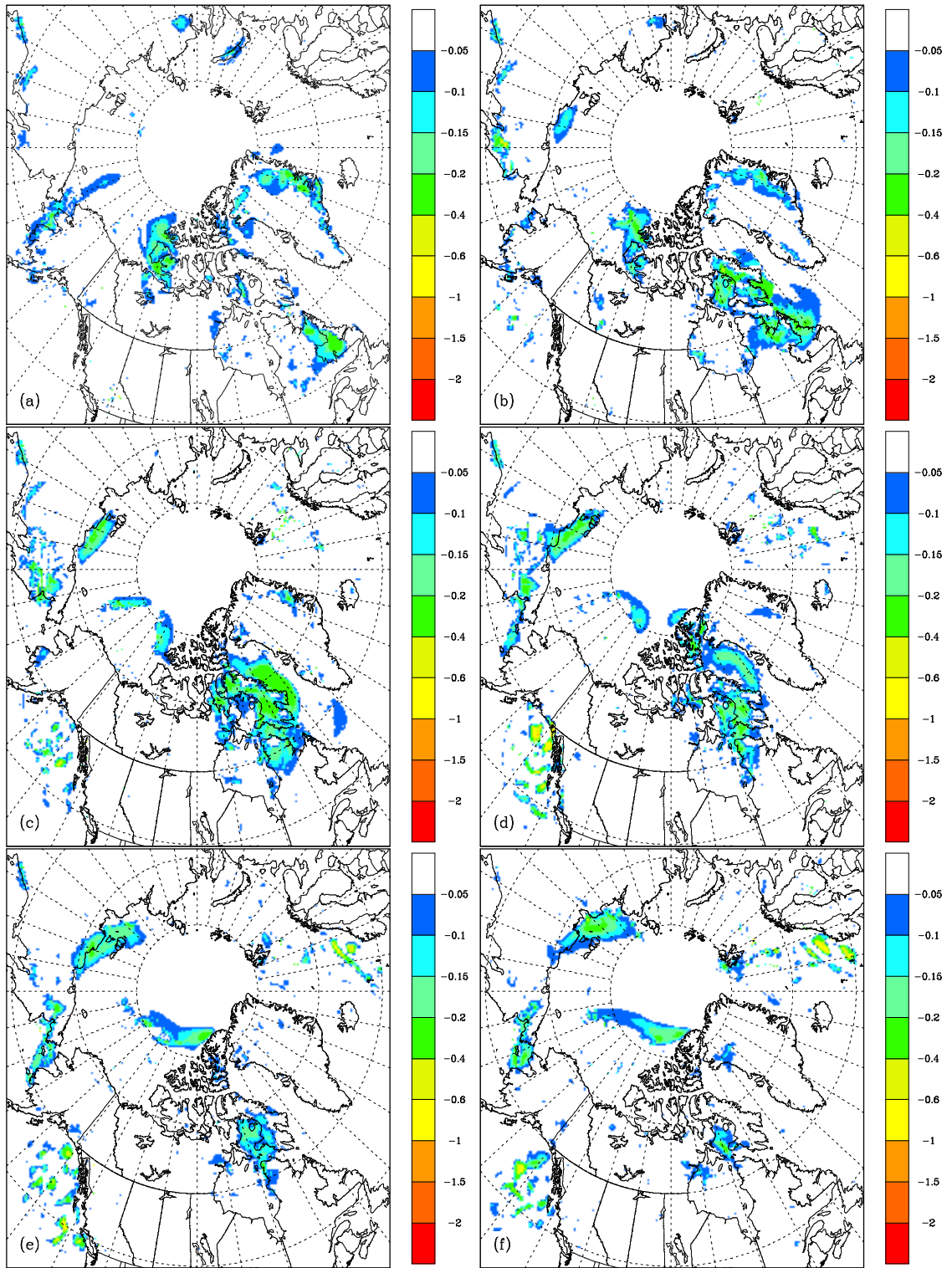


Figure 12: Temperature differences (unit: K) at $z=12$ m between the CPL2 and STD runs at $t=12, 24, 36, 48, 60$ and 72 h (a-f).

Chapter 5

Summary and conclusions

1 Summary

Strong winds over snow covered surfaces lead to blowing snow, which occurs frequently in high latitude and high altitude regions. The averaged annual blowing snow days can be more than 90 days in northern Canada and over the Arctic Ocean. When wind lifts up snow particles from loose snow surface, snow particles will be suspended in the air due to the balance of upward turbulent diffusion and downward gravitational settling. Smaller particles are easier to be diffused to higher level than larger particles, and the mean particle radius thus decreases with height. The number concentration of suspended particles mainly depends on surface wind speed, air temperature and surface characters, and can have an order of magnitude of 10^6 m^{-3} . Blowing snow significantly reduces visibility as well as redistributes the snow cover through transport and in-transit sublimation. To fully examine these processes, a triple-moment blowing snow model PIEKTUK-T was developed and then coupled to the Canadian Mesoscale Compressible Community Model (MC2, V4.9.8). We used this coupled system to model blowing snow and analyze its effect on the hydrological cycle and on the development of an anticyclone.

Field experiments indicate that blowing snow particles follow a three parameter (N , α , and β) Gamma particle size distribution. Therefore, the evolution of the size spectrum

can be obtained by predicting the time evolution of these three parameters. This suggests an alternative to spectral models, which divide the particle size spectrum into a large number of size bins and solve equations for the evolution of each bin. Instead, we developed a bulk model solving the evolution equations for three moments of the size distribution, and recover the three parameters N , α , and β using diagnostic relations. .

Our starting point is an existing double-moment bulk blowing snow model (Déry and Yau, 2001), which includes blowing snow diffusion, sedimentation, and sublimation processes. By assuming a constant shape parameter, α , the zeroth and third moments of the Gamma size distribution, i.e., number concentration, N , and mixing ratio, q_b , are predicted to close the system. Comparing with spectral model results, this model yields similar evolutions of blowing snow sublimation and transport rates, as well as temperature and specific humidity.

However, both field observations and spectral model results have demonstrated that the particle size spectrum becomes narrower with height, implying that the shape parameter α increases with height. To avoid the restriction of assuming a constant shape parameter in the size distribution, an added moment equation is required. In principle, any added moment will suffice. Here, we formulate the tendency equation for the radar reflectivity factor, the sixth moment of the size distribution, in addition to the other two predictable tendency equations for N and q_b . The advantage of introducing radar reflectivity, Z , is that this variable can be obtained from the radar measurements in field experiments.

With the added equation for Z , the double-moment blowing snow model is extended to a triple-moment version, PIEKTUK-T. The fall velocities for N , q_b and Z are weighted by the order of the respective moments to consider the size sorting effects due to gravitational forces. By comparing with observations, it was shown that PIEKTUK-T performed better than the double-moment model. Specifically, it yields the profiles of blowing snow number concentration and mixing ratio, sublimation rate and particle size distribution closer to those from field measurements. It is also noteworthy that our simulations showed a power law relationship between the radar reflectivity factor and the extinction coefficient. (A similar relationship has been observed in snowstorms, although the exponents differ.) Since meteorological visibility is inversely proportional to the extinction coefficient, it is then feasible to base visibility forecasts on the radar reflectivity, which is therefore a valuable predicted variable.

PIEKTUK-T performed as well as the spectral model in simulating the blowing snow particle size distribution evolution, but with much less computation load. The highly efficient PIEKTUK-T allows coupling to an atmospheric mesoscale model for studies of blowing snow effects in water mass budget and weather systems. The coupling process involved implementing a fully parallel scheme to handle horizontal advection of the blowing snow. The coupled model was then applied to study the influence of surface and blowing snow sublimation and blowing snow transport on the snow mass budget over the Northern Hemisphere on a seasonal time scale.

The performance of the coupled model in the surface fields (i.e., air temperature,

relative humidity, and wind speed) is first verified against station data. The coupled system is further validated by comparing the simulated water mass budget with field observation data at one site in Saskatchewan. Following the model verification, the simulation domain was enlarged to cover the entire Northern Hemisphere and a simulation spanning three winter months was performed.

The simulation yields spatial patterns of the seasonal accumulated blowing snow sublimation and transport, as well as surface sublimation over the Northern Hemisphere. Blowing snow sublimation is found to return up to 50 mm SWE back to the atmosphere over the Arctic Ocean. Although large amounts of blowing snow were transported over the Arctic Ocean, the divergence of blowing snow transport contributes only a few mm SWE to the change in snow mass budget. This demonstrated that when averaged over large scales, the contribution of transport would not be very significant since positive and negative divergences largely cancel each other. However, blowing snow redistribution may be important in the surface water budget at small scales, such as basin scale and the Canadian Arctic Archipelago. Surface sublimation was found to be significant in the Eurasian Continent and the eastern region of North America, reaching a maximum value of 200 mm SWE. Deposition is more significant in high latitude regions such as the Arctic Ocean and Northern Canada, where averaged values were about 30 mm SWE. This is probably because the air near surface is always close to saturation with respect to ice over polar sea ice (Andreas et al., 2002), so that a downward water vapor flux results in deposition. We further stratified the blowing snow sublimation and surface sublimation in 10 degree latitudinal bands. The results indicated that band averaged

blowing snow sublimation increased with latitude, whereas surface sublimation decreased with latitude. The combined blowing snow and surface sublimation effects could return 23%~52% of the solid precipitation back to the atmosphere over the winter season. Additionally, the coupled model captures sporadic blowing snow events that are poorly represented by the alternative method of applying empirical formulae to reanalysis data.

It is known that blowing snow occurs frequently over the Arctic Ocean in association with anticyclogenesis and cyclogenesis events. The steep pressure gradient in these events results in strong winds to initiate blowing snow. In Chapter 4, we simulated an Arctic anticyclogenesis event with the coupled model and compared it with a reference simulation without blowing snow. The cooling effect is obtained by calculating the temperature differences between the two runs (experiments CPL and STD). When supersaturation with respect to ice was removed in the blowing snow module, it was found that the cooling extended throughout the boundary layer. Part of the cooling arises from blowing snow sublimation in the lowest tens of meters of the atmosphere, and the other part is contributed from an enhanced downward heat flux. However, when supersaturation with respect to ice is allowed in the blowing snow module in experiment CPL2, the cooling effects become much less significant.

A potential vorticity (PV) diagnostic system was then applied to examine and quantify how the cooling effects in the CPL run affect the dynamics of the anticyclone. The balanced geopotential height and wind fields corresponding to surface θ anomalies were obtained by a piecewise PV inversion method. It was shown that the positive geopotential

height and anticyclonic flow extend up to the 500 mb level over the cooling regions. The averaged inverted geopotential height perturbation at the 1000 mb level over the anticyclone region can be 4.5 dam 72 h after the simulation. This demonstrated that surface cooling can play a role in anticyclonogenesis.

This study represents a first attempt to explicitly simulate the blowing snow processes over the entire Northern Hemisphere for a whole winter season. The spatial patterns of the blowing snow sublimation and transport, and surface sublimation are informative and important to hydrological and climatological studies. Our results for the Arctic anticyclonogenesis event suggested that water vapor in the air plays key role in the mechanism of blowing snow effects on anticyclonogenesis. More measurements of water vapor profiles in high latitude regions would be highly desirable.

2 Suggestions for future work

Despite the advancement in our understanding of the blowing snow phenomenon through the research conducted in this thesis, much research remains. For example, snow mass budgets over sea ice can be improved by including more explicitly sub-grid scale features such as leads. In our coupled system, we assumed a constant lead fraction of 3% over sea ice. This fraction affects the calculation of the near surface air temperature and humidity and in turn impacts the blowing snow transport and sublimation characteristics. However, lead can be a sink for snow transport and may be more important than the loss of snow through wind divergence or blowing snow sublimation. With high resolution observed sea ice mask and lead fraction (such as from the lead data from the National Snow and

Ice Data Center), it would be extremely useful to introduce a parameterization for lead distribution into the model to refine the calculation of the surface snow mass budget.

Another area for future research is to perform simulations on high grid resolutions as snow mass transport is negligible over large scale but may be important over small basin scales. Accurate simulation of snow budget over basin scale is important as accumulated snow mass determines the snow melt water fluxes in the springtime, an important parameter for fresh water resource management.

Finally, the model can easily be adapted to the studies of sandstorms. In northern China, wind driven sand storms can transport sand over long distances to affect the ecological and atmospheric environments. They affect agriculture productivity, reduce visibility, cause havoc in air traffic and road transportation, influence atmospheric radiation balance, and modify cloud formation. The accurate predictions of dust mass concentration, visibility and transport trajectories are very important to minimize the economical and ecological losses. This, in fact, was part of my original motivation for studying blowing snow.

References

- Alley, R. B., P. U. Clark, P. Huybrechts, and I. Joughin, 2005: Ice-sheet and sea-level changes. *Science*, **310**, 456-460.
- Andreas, E. L., 2002: Parameterizing scalar transfer over snow and ice: A review. *Journal of Hydrometeorology*, **3**, 417-432.
- Andreas, E. L., R. E. Jordan, and A. P. Makshtas, 2004: Simulations of snow, ice, and near-surface atmospheric processes on ice station Weddell. *Journal of Hydrometeorology*, **5**, 611-624.
- , 2005: Parameterizing turbulent exchange over sea ice: The ice station Weddell results. *Bound.-Layer Meteor.*, **114**, 439-460.
- Andreas, E. L., P. S. Guest, P. O. G. Persson, C. W. Fairall, T. W. Horst, R. E. Moritz, and S. R. Semmer, 2002: Near-surface water vapor over polar sea ice is always near ice saturation. *Journal of Geophysical Research*, **107(C10)**, 8045, doi: 10.1029/2000JC000705.
- Andreas, E. L., P. O. G. Persson, R. E. Jordan, T. W. Horst, P. S. Guest, A. A. Grachev, and C. W. Fairall, 2008: Parameterizing turbulent exchange at a snow-covered surface. Proceedings, 65th Eastern Snow Conference, Fairlee, VT, 28–30 May 2008, 65–72.
- Andreas, E. L., P. O. G. Persson, R. E. Jordan, T. W. Horst, P. S. Guest, A. A. Grachev, and C. W. Fairall, 2010: Parameterizing turbulent exchange over sea ice in winter. *Journal of Hydrometeorology*, **11**, 87-104.
- Bagnold, R. A., 1941: *The physics of blown sand and desert dunes*. Methuen, London, 265 pp.

-
- Benoit, R., J. Cote, and J. Mailhot, 1989: Inclusion of a TKE boundary-layer parameterization in the Canadian regional finite-element model. *Monthly Weather Review*, **117**, 1726-1750.
- Benoit, R., M. Desgagné, S. P. P. Pellerin, Y. Chartier, and S. Desjardins, 1997: The canadian MC2: A semi-lagrangian, semi-implicit wide-band atmospheric model suited for fine-scale process studies and simulation. *Monthly Weather Review*, **125**, 2382-2415.
- Berg, N. H., 1986: Blowing snow at a Colorado Alpine site: measurements and implications. *Arctic and Alpine Research*, **18**, 147-161.
- Bintanja, R., 1998: The contribution of snowdrift sublimation to the surface mass balance of Antarctica. *Annals of Glaciology*, **27**, 251-259.
- , 2000a: Snowdrift suspension and atmospheric turbulence. Part II: Results of model simulations. *Bound.-Layer Meteor.*, **95**, 369-395.
- , 2000b: Snowdrift suspension and atmospheric turbulence. Part I: Theoretical background and model description. *Bound.-Layer Meteor.*, **95**, 343-368.
- Black, R. X., and R. M. Dole, 1993: The dynamics of large-scale cyclogenesis over the north Pacific-Ocean. *Journal of the Atmospheric Sciences*, **50**, 421-442.
- Bodurtha, F. T., 1952: An investigation of anticyclogenesis in Alaska. *Journal of Meteorology*, **9**, 118-125.
- Bowling, S. A., T. Ohtake, and C. S. Benson, 1968: Winter pressure systems and ice fog in Fairbanks, Alaska. *Journal of Applied Meteorology*, **7**, 961-968.
- Box, J. E., and K. Steffen, 2001: Sublimation on the Greenland ice sheet from automated weather station observations. *Journal of Geophysical Research*, **106(D24)**, 33965-33981.

- Box, J. E., D. H. Bromwich, and L. S. Bai, 2004: Greenland ice sheet surface mass balance 1991-2000: Application of polar MM5 mesoscale model and in situ data. *Journal of Geophysical Research*, **109**, D16105, doi: 10.1029/2003JD004451.
- Boyle, J. S., and L. F. Bosart, 1983: A cyclone/anticyclone couplet over North America: an example of anticyclone evolution. *Monthly Weather Review*, **111**, 1025-1045.
- Budd, W. F., 1966: The drifting of non-uniform snow particles. *Studies in Antarctic Meteorology, Antarctic Research Series*, **9**, M. J. Rubin, Ed., American Geophysical Union, 59-70.
- Budd, W. F., W. R. J. Dingle, and U. Radoc, 1966: The Byrd snow drift project: outline and basic results. *Studies in Antarctic Meteorology, Antarctic Research Series*, **9**, M. J. Rubin, Ed., American Geophysical Union, 71-134.
- Charney, J. G., 1955: The use of primitive equations of motion in numerical prediction. *Tellus*, **7**, 22-26.
- Charney, J. G., and J. G. Devore, 1979: Multiple flow equilibria in the atmosphere and blocking. *Journal of the Atmospheric Sciences*, **36**, 1205-1216.
- Chen, G. T. J., C. C. Wang, and L. F. Lin, 2006: A diagnostic study of a retreating mei-yu front and the accompanying low-level jet formation and intensification. *Monthly Weather Review*, **134**, 874-896.
- Colucci, S. J., and L. F. Bosart, 1979: Surface anticyclone behavior in NMC prediction models. *Monthly Weather Review*, **107**, 377-394.
- Colucci, S. J., and J. C. Davenport, 1987: Rapid surface anticyclogenesis: synoptic climatology and attendant large-scale circulation changes. *Monthly Weather Review*, **115**, 822-836.
- Cuffey, K. M., and S. J. Marshall, 2000: Substantial contribution to sea-level rise during the last interglacial from the Greenland ice sheet. *Nature*, **404**, 591-594.

Curry, J., 1983: On the formation of continental polar air. *Journal of the Atmospheric Sciences*, **40**, 2278-2292.

——, 1987: The contribution of radiative cooling to the formation of cold-core anticyclones. *Journal of the Atmospheric Sciences*, **44**, 2575-2592.

Dallavalle, J. P., and L. F. Bosart, 1975: A synoptic investigation of anticyclogenesis accompanying North American polar air outbreaks. *Monthly Weather Review*, **103**, 941-957.

Davis, C. A., 1992: A potential vorticity diagnosis of the importance of initial structure and condensational heating in observed extratropical cyclogenesis. *Monthly Weather Review*, **120**, 2409-2428.

——, 1993: Decomposing the atmospheric flow using potential vorticity framework-comment. *Journal of the Atmospheric Sciences*, **50**, 2065-2067.

——, 1997: The modification of baroclinic waves by the Rocky Mountains. *Journal of the Atmospheric Sciences*, **54**, 848-868.

Davis, C. A., and K. A. Emanuel, 1991: Potential vorticity diagnostics of cyclogenesis. *Monthly Weather Review*, **119**, 1929-1953.

Davis, C. A., M. T. Stoelinga, and Y. H. Kuo, 1993: The integrated effect of condensation in numerical simulations of extratropical cyclogenesis. *Monthly Weather Review*, **121**, 2309-2330.

Deardorff, J. W., 1978: Efficient prediction of ground surface-temperature and moisture, with inclusion of a layer of vegetation. *Journal of Geophysical Research*, **83(C4)**, 1889-1903.

Delage, Y., 1997: Parameterizing sub-grid scale vertical transport in atmospheric models under statically stable conditions. *Bound.-Layer Meteor.*, **82**, 23-48.

-
- Déry, S. J., and M. K. Yau, 1999: A bulk blowing snow model. *Bound.-Layer Meteor.*, **93**, 237-251.
- , 2001a: Simulation of blowing snow in the Canadian Arctic using a double-moment model. *Bound.-Layer Meteor.*, **99**, 297-316.
- , 2001b: Simulation of an Arctic ground blizzard using a coupled blowing snow-atmosphere model. *Journal of Hydrometeorology*, **2**, 579-598.
- , 2002: Large-scale mass balance effects of blowing snow and surface sublimation. *Journal of Geophysical Research*, **107(D23)**, 4679, doi: 10.1029/2001JD001251.
- Déry, S. J., and M. Stieglitz, 2002: A note on surface humidity measurements in the cold Canadian environment. *Bound.-Layer Meteor.*, **102**, 491-497.
- Déry, S. J., P. A. Taylor, and J. B. Xiao, 1998: The thermodynamic effects of sublimating, blowing snow in the atmospheric boundary layer. *Bound.-Layer Meteor.*, **89**, 251-283.
- Dixon, M., R. M. Rasmussen, and S. Landolt, 2004: Short-term forecasting of airport surface visibility using radar and ASOS. In: *11th conference on Aviation, Range, and Aerospace*, Hyannis, MA, 4-7 Oct 2004.
- Dole, R. M., 1986a: The life-cycles of persistent anomalies and blocking over the North-Pacific. *Advances in Geophysics*, **29**, 31-69.
- , 1986b: Persistent anomalies of the extratropical Northern Hemisphere wintertime circulation: structure. *Monthly Weather Review*, **114**, 178-207.
- Dover, S. E., 1993: *Numerical modelling of blowing snow*. Ph.D. thesis, department of applied mathematics, University of Leeds, 233 pp.
- Dyunin, A. K., 1954: Vertical distribution of solid flux in a snow-wind flow. *National Research Council of Canada, Technical Translation 999*.

-
- , 1967: Fundamental of the mechanics of snow storms. *Physics of snow and ice*, **1(2)**, 1065-1073.
- Ebert, E. E., and J. A. Curry, 1993: An intermediate one-dimensional thermodynamic sea-ice model for investigating ice-atmosphere interactions. *Journal of Geophysical Research*, **98(C6)**, 10085-10109.
- Ertel, H., 1942: Ein neuer hydrodynamischer Wirbelsatz. *Meteor. Z.*, **59**, 271-281.
- Fang, X., and J. W. Pomeroy, 2009: Modelling blowing snow redistribution to prairie wetlands. *Hydrological Processes*, **23**, 2557-2569, doi: 10.1002/Hyp.7348.
- Fleagle, R. G., 1947: The fields of temperature, pressure, and three-dimensional motion in selected weather situations. *Journal of Meteorology*, **4**, 165-185.
- Fouquart, Y., and B. Bonnel, 1980: Computation of solar heating of the earth's atmosphere: A new parameterization. *Beitr. Phys. Atmos.*, **53**, 35-62.
- Garand, L., 1983: Some improvements and complements to the infrared emissivity algorithm including a parameterization of the absorption in the continuum region. *Journal of the Atmospheric Sciences*, **40**, 230-244.
- Garratt, J. R., 1992: *The atmospheric boundary layer*. Cambridge University Press, New York, 316 pp.
- Goodison, B. E., P. Y. T. Louie, and D. Yang, 1998: *WMO solid precipitation measurement intercomparison*, final report, WMO/TD-No.872. WMO, Geneva, 212 pp.
- Gordon, M., K. Simon, and P. A. Taylor, 2006: On snow depth predictions with the Canadian land surface scheme including a parameterization of blowing snow sublimation. *Atmosphere-Ocean*, **44**, 239-255.

- Grachev, A. A., E. L. Andreas, C. W. Fairall, P. S. Guest, and P. O. G. Persson, 2007: SHEBA flux-profile relationships in the stable atmospheric boundary layer. *Bound.-Layer Meteor.*, **124**, 315-333.
- Groisman, P. Y., V. V. Koknaeva, T. A. Belokrylova, and T. R. Karl, 1991: Overcoming biases of precipitation measurement: A history of the USSR experience. *Bulletin of the American Meteorological Society*, **72**, 1725-1733.
- Grumm, R. H., and J. R. Gyakum, 1986: Systematic surface anticyclone errors in NMC's limited area fine mesh and spectral models during the winter of 1981/82. *Monthly Weather Review*, **114**, 2329-2343.
- Guichard, F., D. B. Parsons, J. Dudhia, and J. Bresch, 2003: Evaluating mesoscale model predictions of clouds and radiation with SGP ARM data over a seasonal timescale. *Monthly Weather Review*, **131**, 926-944.
- Hakim, G. J., D. Keyser, and L. F. Bosart, 1996: The Ohio valley wave-merger cyclogenesis event of 25-26 January 1978. Part II: Diagnosis using quasigeostrophic potential vorticity inversion. *Monthly Weather Review*, **124**, 2176-2205.
- Hanesiak, J. M., R. L. Raddatz, and S. Lobban, 2004: Local initiation of deep convection on the Canadian prairie provinces. *Bound.-Layer Meteor.*, **110**, 455-470.
- Harrington, J. Y., M. P. Meyers, R. L. Walko, and W. R. Cotton, 1995: Parameterization of ice crystal conversion processes due to vapor deposition for mesoscale models using double-moment basis functions. Part I: Basic formulation and parcel model results. *Journal of the Atmospheric Sciences*, **52(23)**, 4344-4366.
- Holtslag, A. A. M., and H. A. R. de Bruin, 1988: Applied modeling of the nighttime surface-energy balance over land. *Journal of Applied Meteorology*, **27**, 689-704.
- Hood, E., M. Williams, and D. Cline, 1999: Sublimation from a seasonal snowpack at a continental, mid-latitude alpine site. *Hydrological Processes*, **13**, 1781-1797.

- Hoskins, B. J., M. E. McIntyre, and A. W. Robertson, 1985: on the use and significance of isentropic potential vorticity maps. *Quarterly Journal of the Royal Meteorological Society*, **111**, 877-946.
- Intrieri, J. M., and M. D. Shupe, 2004: Characteristics and radiative effects of diamond dust over the western Arctic Ocean region. *Journal of Climate*, **17**, 2953-2960.
- Ioannidou, L., and M. K. Yau, 2008: A climatology of the Northern Hemisphere winter anticyclones. *Journal of Geophysical Research*, **113**, D08119, doi: 10.1029/2007JD008409.
- Jordan, R. E., E. L. Andreas, and A. P. Makshtas, 1999: Heat budget of snow-covered sea ice at North Pole 4. *Journal of Geophysical Research*, **104(C4)**, 7785-7806.
- Kameda, T., N. Azuma, T. Furukawa, Y. Ageta, and S. Takahashi, 1997: Surface mass balance, sublimation and snow temperatures at dome Fuji Station, Antarctica, in 1995. *Proceedings of the NIPR symposium on polar meteorology and glaciology*, **11**, 24-34.
- King, J. C., 1989: Low-level wind profiles at an Antarctic coastal station. *Antarctic Science*, **1**, 169-178.
- King, J. C., and J. Turner, 1997: *Antarctic meteorology and climatology*. Cambridge University Press, United Kingdom, 409 pp.
- King, J. C., P. S. Anderson, and G. W. Mann, 2001: The seasonal cycle of sublimation at Halley, Antarctica. *Journal of Glaciology*, **47**, 1-8.
- King, J. C., P. S. Anderson, M. C. Smith, and S. D. Mobbs, 1996: The surface energy and mass balance at Halley, Antarctica during winter. *Journal of Geophysical Research*, **101(D14)**, 19119-19128.
- Kobayashi, D., 1972: Studies of snow transport in low-level drifting snow. *Contributions from the institute for low temperature science*, **24**, 1-58.

-
- Kong, F. Y., and M. K. Yau, 1997: An explicit approach to microphysics in MC2. *Atmosphere-Ocean*, **35**, 257-291.
- Launiainen, J., 1995: Derivation of the relationship between the Obukhov stability parameter and the bulk Richardson number for flux-profile studies. *Bound.-Layer Meteor.*, **76**, 165-179.
- Lettau, H. H., 1979: Wind and temperature profile prediction for diabatic surface-layers including strong inversion cases. *Bound.-Layer Meteor.*, **17**, 443-464.
- Li, L., and J. W. Pomeroy, 1997: Estimates of threshold wind speeds for snow transport using meteorological data. *Journal of Applied Meteorology*, **36**, 205-213.
- Lin, C. A., and Coauthors, 2010: Real-time forecast of the 2005 and 2007 summer severe floods in the Huaihe river basin of China. *Journal of Hydrology*, **381**, 33-41.
- Lindsay, R. W., 1998: Temporal variability of the energy balance of thick Arctic pack ice. *Journal of Climate*, **11**, 313-333.
- Liston, G. E., and M. Sturm, 1998: A snow-transport model for complex terrain. *Journal of Glaciology*, **44**, 498-516.
- Liston, G. E., R. L. Brown, and J. D. Dent, 1993: A two-dimensional computational model of turbulent atmospheric surface flows with drifting snow. *Annals of Glaciology*, **18**, 281-286.
- Loewe, F., 1956: *Etudes de glaciologie en terre adelie*, 1951-52. Paris, Hermann, 159pp.
- MacDonald, J., and J. W. Pomeroy, 2008: Gauge undercatch of two common snowfall gauges in a prairie environment. *Eastern Snow Conference 64*, 119-126.
- Mailhot, J., and R. Benoit, 1982: A finite-element model of the atmospheric boundary-layer suitable for use with numerical weather prediction models. *Journal of the Atmospheric Sciences*, **39**, 2249-2266.

- Mailhot, J., and C. Chouinard, 1989: Numerical forecasts of explosive winter storms: sensitivity experiments with a meso- α scale model. *Monthly Weather Review*, **117**, 1311-1343.
- Mailhot, J., and Coauthors, 1998: Scientific description of the RPN physics library-version 3.6. Recherche en Prévision Numérique. Atmospheric Environment Service, Dorval, Quebec, Canada, 188 pp.
- Male, D. H., 1980: The seasonal snowcover. *Dynamics of snow and ice masses*, S. C. Colbeck, Ed., Academic Press, NY, 305-395.
- Male, D. H., and R. J. Granger, 1979: Energy mass fluxes at the snow surface in a prairie environment. *Proceedings of the modelling of snow cover runoff*, S. C. Colbeck, and M. Ray, Eds., US Army Cold Reg. Res. and Eng. Lab., Hanover, New Hampshire, 101-124.
- Mann, G. W., 1998: Surface heat and water vapor budgets over Antarctica, The environment center, University of Leeds, 279 pp.
- Mann, G. W., P. S. Anderson, and S. D. Mobbs, 2000: Profile measurements of blowing snow at Halley, Antarctica. *Journal of Geophysical Research*, **105(D19)**, 24491-24508.
- Matsuzawa, M., Y. Kajiya, and M. Takeuchi, 2005: The development and validation of a method to estimate visibility during snowfall and blowing snow. *Cold Regions Science and Technology*, **41**, 91-109.
- Maxwell, J. B., 1982: Climate of the Canadian Arctic islands and adjacent water. *Climatol. Stud.*, **30**, 34-52.
- Maykut, G. A., 1982: Large-scale heat-exchange and ice production in the central Arctic. *Journal of Geophysical Research*, **87(C10)**, 7971-7984.
- Middleton, W. E. K., 1958: *Vision through the atmosphere*. Toronto, University of Toronto Press.

Milbrandt, J. A., and M. K. Yau, 2005: A multimoment bulk microphysics parameterization. Part I: Analysis of the role of the spectral shape parameter. *Journal of the Atmospheric Sciences*, **62**, 3051-3064.

—, 2006: A multimoment bulk microphysics parameterization. Part III: Control simulation of a hailstorm. *Journal of the Atmospheric Sciences*, **63**, 3114-3136.

Misra, V., and M. K. Yau, 2001: An ensemble strategy for high-resolution regional model forecasts. *Meteorology and Atmospheric Physics*, **78**, 61-74.

Misra, V., M. K. Yau, and N. Badrinath, 2000: Atmospheric water species budget in mesoscale simulations of lee cyclones over the Mackenzie River Basin. *Tellus*, **52A**, 140-161.

Mobbs, S., and S. E. Dover, 1993: Numerical modeling of blowing snow. *Antarctic Special Topic*, 55-63.

Muench, H. S., and H. A. Brown, 1977: Measurement of visibility and radar reflectivity during snowstorms in the AFGL Mesonet. Project 8628, Met Division, Air Force Geophysics Laboratory, Hanscom AFB, Massachusetts, AGFL-TR-77-0148.

Murray, F. W., 1967: On the computation of saturation vapor pressure. *J. Appl. Meteorol.*, **6**, 203-204.

Nagarajan, B., M. K. Yau, and D. L. Zhang, 2001: A numerical study of a mesoscale convective system during TOGA COARE. Part I: Model description and verification. *Monthly Weather Review*, **129(10)**, 2501-2520.

—, 2004: A numerical study of a mesoscale convective system during TOGA COARE. Part II: Organization. *Monthly Weather Review*, **132**, 1000-1017.

Persson, P. O. G., C. W. Fairall, E. L. Andreas, P. S. Guest, and D. K. Perovich, 2002: Measurements near the atmospheric surface flux group tower at SHEBA: Near-surface

conditions and surface energy budget. *Journal of Geophysical Research*, **107 (C10)**, 8045, doi: 10.1029/2000JC000705.

Pomeroy, J. W., 1988: Wind transport of snow. Ph.D. thesis, Division of Hydrology, University of Saskatchewan, 226 pp.

Pomeroy, J. W., and D. H. Male, 1988: Optical-properties of blowing snow. *Journal of Glaciology*, **34**, 3-10.

Pomeroy, J. W., and D. M. Gray, 1990: Saltation of snow. *Water Resources Research*, **26**, 1583-1594.

Pomeroy, J. W., and D. H. Male, 1992: Steady-state suspension of snow. *Journal of Hydrology*, **136**, 275-301.

Pomeroy, J. W., and D. M. Gray, 1995: Snowcover accumulation, relocation and management. *NHRI Science Rep. No. 7*, Saskatoon, 144 pp.

Pomeroy, J. W., and B. E. Goodison, 1997: Winter and snow. *Surface climates of Canada*, W. G. Bailey, T. R. Oke, and W. R. Rouse, Eds., McGill Queen's University Press, Canada, 68-100.

Pomeroy, J. W., and R. L. H. Essery, 1999: Turbulent fluxes during blowing snow: field tests of model sublimation predictions. *Hydrological Processes*, **13**, 2963-2975.

Pomeroy, J. W., and L. Li, 2000: Prairie and arctic areal snow cover mass balance using a blowing snow model. *Journal of Geophysical Research*, **105(D21)**, 26619-26634.

Pomeroy, J. W., D. M. Gray, and P. G. Landine, 1993: The prairie blowing snow model - characteristics, validation, operation. *Journal of Hydrology*, **144**, 165-192.

Pomeroy, J. W., P. Marsh, and D. M. Gray, 1997: Application of a distributed blowing snow model to the arctic. *Hydrological Processes*, **11**, 1451-1464.

- Pomeroy, J. W., N. Hedstrom, and J. Parviainen, 1999: The snow mass balance of Wolf Creek, Yukon: effects of snow, sublimation and redistribution. *Wolf Creek Research Basin: Hydrology, Ecology, Environment*, J. W. Pomeroy, and G. R. J., Eds., 15-30.
- Ramage, C. S., 1971: Monsoon meteorology. New York, Academic Press. International geophysics series, **15**, 27-33.
- Robinson, W. A., 1989: On the structure of potential vorticity in baroclinic instability. *Tellus*, **41A**, 275-284.
- Rossby, C. G., 1940: planetary flow patterns in the atmosphere. *Quarterly Journal of the Royal Meteorological Society*, **66**, 68-87.
- Schmidt, R. A., 1972: Sublimation of wind-transported snow—a model. *USDA Res. Paper RM-90, USDA Forestry Service, Rocky Mountain Forest and Range Experimental Station, Fort Collins, Colorado*, 24pp.
- , 1982: Vertical profiles of wind-speed, snow concentration, and humidity in blowing snow. *Bound.-Layer Meteor.*, **23**, 223-246.
- Shiotani, M., and H. Arai, 1953: A short note on the snow-storm. *Proceedings of second Japanese National congress for applied mechanics*, 217-218.
- Sommerfeld, R., and J. A. Businger, 1965: Density profile of blown snow. *Journal of Geophysical Research*, **70(14)**, 3303-3306.
- Sperenza, A., 1986: Deterministic and statistical properties of Northern Hemisphere middle latitude circulation. *Adv. Geophys.*, **29**, 199-226.
- Stewart, R. E., and Coauthors, 1995: Winter storms over Canada. *Atmosphere-Ocean*, **33**, 223-247.
- Sugiura, K., and T. Ohata, 2008: Large-scale characteristics of the distribution of blowing-snow sublimation. *Annals of Glaciology*, **49**, 11-16.

Tabler, R. D., 1975: Estimating the transport and evaporation of blowing snow. Great Plains Agricultural Council Publication, **73**, University of Nebraska, Lincoln, NE, 85-105.

Tabler, 1986: Snow fence handbook, Release 1.0. Tabler & Associates, Laramie, WY.

Takeuchi, M., 1984: Occurrence mechanics of blowing snow and snow drift (in Japanese), *Tetsudou Doboku*, 26, 12, 41-44.

Tan, Y. C., and J. A. Curry, 1993: A diagnostic study of the evolution of an intense North American anticyclone during winter 1989. *Monthly Weather Review*, **121**, 961-975.

Tanguay, M., A. Robert, and R. Laprise, 1990: A semi-implicit semi-lagrangian fully compressible regional forecast model. *Monthly Weather Review*, **118**, 1970-1980.

Thomas, S. J., C. Girard, R. Benoit, M. Desgagne, and P. Pellerin, 1998: A new adiabatic kernel for the MC2 model. *Atmosphere-Ocean*, **36**, 241-270.

Thorpe, A. D., and B. J. Mason, 1966: Evaporation of ice spheres and ice crystals. *British Journal of Applied Physics*, **17**, 541-548.

Thorpe, A. J., 1986: Synoptic scale disturbances with circular symmetry. *Monthly Weather Review*, **114**, 1384-1389.

van den Broeke, M. R., 1997: Spatial and temporal variation of sublimation on Antarctica: Results of a high-resolution general circulation model. *Journal of Geophysical Research*, **102(D25)**, 29765-29777.

Verseghy, D. L., 2000: The Canadian land surface scheme (CLASS): Its history and future. *Atmosphere-Ocean*, **38(1)**, 1-13.

-
- Vihma, T., 1995: Subgrid parameterization of surface heat and momentum fluxes over polar oceans. *Journal of Geophysical Research*, **100(C11)**, 22625-22646.
- Webb, E. K., 1970: Profile relationships: Log-linear range, and extension to strong stability. *Quarterly Journal of the Royal Meteorological Society*, **96**, 67-90.
- Wexler, H., 1951: Anticyclones. *Compendium of Meteorology*, Malone, T. F., Ed., Amer. Meteor. Soc., 621-628.
- Xiao, J. B., R. Bintanja, S. J. Déry, G. W. Mann, and P. A. Taylor, 2000: An intercomparison among four models of blowing snow. *Bound.-Layer Meteor.*, **97**, 109-135.
- Yang, J., and M. K. Yau, 2008: A new triple-moment blowing snow model. *Bound.-Layer Meteor.*, **126**, 137-155, doi: 10.1007/s10546-007-9215-4.
- Yang, J., M. K. Yau, X. Fang, and J. W. Pomeroy, 2010: A triple-moment blowing snow-atmospheric model and its application in computing the seasonal wintertime snow mass budget. *Hydrol. Earth Syst. Sci. Discuss.*, **7**, 929-970.